# Interactions of Halogens and Formic Acid, the Simplest Carboxylic Acid

Christian Haakansson

*Supervisor*: Dr Duncan Wild

Honours Thesis submitted as part of the B. Sc. (Hons) degree

The School of Molecular Sciences

The University of Western Australia

Date of Submission: 03/11/2017

# Declaration

I certify that the material within this thesis has not been submitted for any other degree or award at any institution.

To the best of my knowledge, any sources used as part of the thesis and any help received have been acknowledged in the thesis.

_____

Christian Haakansson, November 2017

# Summary

The gas-phase anion complexes of formic acid and the halogens have been investigated from both an experimental and a theoretical standpoint. High level *ab initio* methods and photoelectron spectroscopy were utilised. The complexes of halides and formic acid are of interest with respect to the chemistry of the atmosphere and furthering understanding of intermolecular interactions.

Mass spectra were collected for chloride, bromide and iodide complexes with formic acid. However, the binding energy of the chloride-formic acid complex meant that photoelectron spectra were only reported for bromide-formic acid and iodide-formic acid. The experimental data was used in conjunction with the computational results in order to create a regime where experiment was rationalised by theory.

The calculation of energies allowed prediction of parameters such as the electron affinity and vertical detachment energy as well as the dissociation energy associated with both the anion and neutral formic acid-halide complexes. As a general trend, it was observed that the complex dissociation energy decreased with halide size with regard to the anion complexes and increased with halogen size with regard to the neutral complexes.

# Acknowledgements

Firstly, I would like to thank my supervisor Duncan Wild, for the guidance and help throughout the year. The year as a whole was a great experience and a large part of this is down to your ability to make a stressful year seem fun and interesting.

I would also like to thank Amir Karton for the help received with regard to complete basis set extrapolations and Matthew Piggott for kindly supplying formic acid for use in experiment as well as helpful discussions on the nomenclature of formic acid.

I would like to acknowledge Tim Corkish and Peter Watson. Your continuing help with both experimental and theoretical work as well as understanding the many new computer programs was greatly appreciated. Hannah Adam, it was great to have a fellow honours student to 'endure' the year with, and chat to about the honours work. All three of you helped ease the stresses of the year through our 'Dirty Burger Fridays'.

My sincere gratitude goes to the Bayliss Workshop for the fast work completed when we needed the permanent magnet switched with the electromagnet.

To my partner and love, Elham Eshragian, thank you for your continuous support and encouragement throughout the year, you made it possible for me to complete this thesis.

Finally, I would like to thank my family and friends, your patience and moral support brought me through to the end of this year (and thesis).

This research was undertaken with the assistance of computational resources from the Pople high-performance computing cluster of the Faculty of Science at the University of Western Australia.

# Contents


**1 Introduction** **1**

1.1 Atmospheric Chemistry . . . . . 1

1.1.1 Formic Acid . . . . . 2

1.2 Van der Waals Clusters . . . . . 3

1.3 Previous Research . . . . . 3

1.4 Computational Chemistry . . . . . 6

1.5 Experimental Techniques . . . . . 8

1.5.1 Mass Spectrometry . . . . . 8

1.5.2 Anion Photoelectron Spectroscopy . . . . . 9

1.6 Project Aims . . . . . 10

**2 Materials and Methods** **12**

2.1 Overview of Experimental Apparatus . . . . . 12

2.1.1 Gas Mixture Formation . . . . . 14

2.1.2 Ion Production and Extraction . . . . . 15

2.1.3 Ion Flight Tube . . . . . 17

2.1.4 Photodetachment and Photoelectron Detection . . . . . 18

2.2 Analysis of Experimental Data . . . . . 20

2.2.1 Mass Spectrum Analysis . . . . . 20

2.2.2 Photoelectron Spectrum Analysis . . . . . 21

2.2.2.1 Jacobi Transform . . . . . 22

2.3 Computational Methods . . . . . 24

2.3.1 Basis Set Explanation . . . 25
2.3.2 Complete Basis Set Limit . . . 26

**3 Results and Discussion** **29**

3.1 Experimental Results . . . 29
3.1.1 Mass Spectra . . . 29
3.1.2 Photoelectron Spectra . . . 33
3.2 Computational Results . . . 36
3.2.1 Formic Acid Interacting with a Point Charge . . . 36
3.2.2 Formic Acid Halide Complexes . . . 39
3.2.2.1 *anti*-Formic Acid Halide Minima . . . 40
3.2.2.2 *syn*-Formic Acid Halide Minima . . . 41
3.2.2.3 Fluoride: The Special Case . . . 44
3.2.2.4 Anion Minima Summary and Experimental Comparison . . 46
3.2.3 Formic Acid Halogen Complexes . . . 47
3.2.3.1 In plane Formic Acid Potential Energy Scan . . . 48
3.2.3.2 *anti*-Formic Acid Halogen Minima . . . 49
3.2.3.3 *syn*-Formic Acid Halogen Minima . . . 55
3.2.3.4 Neutral Minima Summary and Comparison with Experiment 61
3.2.4 Literature Comparison . . . 63

**4 Conclusions and Future Work** **66**

**References** **68**

**Appendix A Data and Tables** **i**

**Appendix B Timing Diagram** **xxxiii**

**Appendix C Formic Acid Multipole Expansion Data** **xxxv**

# List of Abbreviations

BE - Binding Energy

CBS - Complete Basis Set limit

CCSD(T) - Coupled Cluster theory with Singlets, Doublets and perturbative inclusion of Triplets

CFC - Chlorofluorocarbons

DFT - Density Functional Theory

EA - Electron Affinity

HF - Hartree-Fock

MP2 - Møller-Plesset second order perturbation theory

Nd:YAG - Neodymium doped yttrium aluminium garnet

SAPT - Symmetry Adapted Perturbation Theory

TOF - time-of-flight

TOF-PES - time-of-flight photoelectron spectrometer

VDE - Vertical Detachment Energy

VOC - Volatile Organic Compound

W1w - Weizmann-1 w protocol

# Chapter 1

# Introduction

Intermolecular interactions are a central part of chemistry. The primary concern of this research is the investigation of intermolecular interactions between formic acid and the halogens. Through a combination of experimental and theoretical investigation, namely photoelectron spectroscopy and computational studies, the forces underpinning the formic acid halogen interactions will be investigated. A main aim of the research is to contribute to the furthering of understanding of intermolecular interactions. The following chapter will outline the motivation of the research as well as the associated background and theory.

## 1.1 Atmospheric Chemistry

Halogens are present in our atmosphere in both the troposphere and stratosphere, they play an active and not fully understood role in the chemistry of the atmosphere.[1] Halogens enter the atmosphere through natural and anthropogenic pathways, they can enter the atmosphere as a result of anthropogenic emissions such as chlorofluorocarbons (CFCs) and as a result of sea spray.[2] A very well-known atmospheric process in which halogens play a part is the degradation of stratospheric ozone, halogen radicals in the stratosphere catalyse the destruction of ozone by way of the reactions displayed in equations 1.1 and 1.2. Leading to a net loss of an ozone molecule as displayed in equation 1.3.

$$\cdot \mathrm{X} + \mathrm{O_3} \longrightarrow \cdot \mathrm{XO} + \mathrm{O_2} \tag{1.1}$$

$$\cdot \mathrm{XO} + \mathrm{O} \longrightarrow \cdot \mathrm{X} + \mathrm{O_2} \tag{1.2}$$

$$\mathrm{O_3} + \mathrm{O} \longrightarrow 2\,\mathrm{O_2} \tag{1.3}$$

### 1.1.1 Formic Acid

Much like the halogens, formic acid is present in the atmosphere in significant amounts. Formic acid is one of the most abundant carboxylic acids in the atmosphere and a dominant source of atmospheric acidity.[3] Similarly to the halogens, atmospheric formic acid has both anthropogenic and natural pathways by which it enters the atmosphere. The main anthropogenic sources are biomass burning and fossil fuels burning, and the main natural source is the oxidation of non-methane volatile organic compounds (VOCs).[4] The main sinks of atmospheric formic acid is reaction with hydroxyl radicals and dissolution in rain and cloud water.[4]

The reaction of formic acid with a hydroxyl radical proceeds predominantly via two different mechanisms, namely the abstraction of the formyl hydrogen or the abstraction of the acidic hydrogen. These two reactions can be seen in equations 1.4 and 1.5.

$$\mathrm{HCOOH} + \cdot \mathrm{OH} \longrightarrow \cdot \mathrm{HCOO} + \mathrm{H_2O} \tag{1.4}$$

$$\mathrm{HCOOH} + \cdot \mathrm{OH} \longrightarrow \cdot \mathrm{HOCO} + \mathrm{H_2O} \tag{1.5}$$

An extensive computational study found that the reaction preferentially proceeded via the abstraction of the acidic hydrogen.[5] It was found that the abstraction of the acidic hydrogen possessed a lower activation energy.[5] Upon investigation, it was determined that acidic hydrogen abstraction had lower activation energy due to the formation of a pre-reaction complex (a van der Waals complex) where the hydroxyl radical interacts with the acidic hydrogen as well as the carbonyl oxygen.[5]

In marine areas, the impact associated with chlorine radicals rivals that of hydroxyl radicals.[6] An investigation of the reaction between a chlorine radical and a formic acid molecule

showed that again the predominant mechanism of reaction was hydrogen abstraction,[7] however unlike the reaction with a hydroxyl radical, the main mechanism was the abstraction of the formyl hydrogen.[7] A major aim of this research project is to create, and experimentally study, gas phase complexes of formic acid and chlorine. The structures of the complexes may be akin to important points on the potential energy surface of the reaction between formic acid and a chlorine radical. Theoretical predictions based on computational investigation of the important reaction points, will allow the rationalisation of the experimental results.

## 1.2 Van der Waals Clusters

A chemical reaction is the conversion of one species, the reactant, to another form, the product. However, the potential energy surface on which the reactants and products are minima, also features additional points of interest. Specifically, the path leading from reactants to products contains the transition state, and may contain reaction adducts (pre- and post-). The transition state is an extremely short-lived state that serves as a 'mapping' from the reactants to the products of the reaction.[8] The adducts are essentially van der Waals clusters, which are molecular systems held together by intermolecular forces.[9] The clusters of concern in this study, namely formic acid halide clusters, are indeed van der Waals clusters.

With modern computational power and *ab initio* methods, the pathway of a reaction and the associated adducts and transition state can be modelled. However, in addition to being accessible through computer modelling, van der Waals clusters can also be studied experimentally. A number of experimental studies of van der Waals complexes will be outlined in the next section.

## 1.3 Previous Research

Many complexes formed from molecules and halogens have been studied, using a number of techniques relating to both experimental and theoretical methods. Examples of common methods through which molecular complexes are studied are: mass spectrometry, photo-

electron spectroscopy and *ab initio* calculations. The computational theory as well as the experimental techniques will be discussed in detail in Sections 1.5 and 1.6. Mass spectrometry has been used to investigate numerous gas-phase complexes,[10–12] including the formic acid-halide complexes and clusters,[11] which allows for the determination of thermochemical properties of the complex such as cluster dissociation energies.

Numerous studies involving the use of anion photoelectron spectroscopy have been undertaken, such as those done by the groups of Neumark[13] and Lineberger,[14,15] additionally, the water solvation shells of the halides ($Cl^-$, $Br^-$ and $I^-$) have been investigated by Markovich.[16] Up until this point, there has been no research carried out on the photoelectron spectra associated with formic acid-halide complexes and as such, the experimental results of this project will be novel.

The Wild group at UWA has carried out experimental and theoretical work on halide-molecule clusters.[17–19] Photoelectron spectroscopy experiments have been carried out on complexes, and currently, there is a push to move towards slow electron velocity imaging as the primary source of experimental data. However, for this project, all photoelectron spectroscopy was carried out using the existing time-of-flight photoelectron spectrometer.

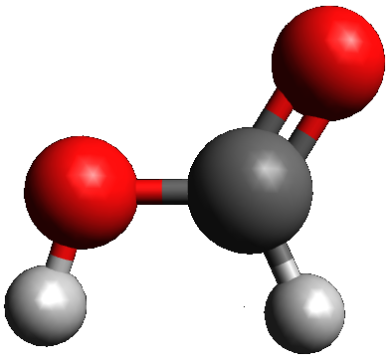

Figure 1.1: The *anti*-formic acid conformer

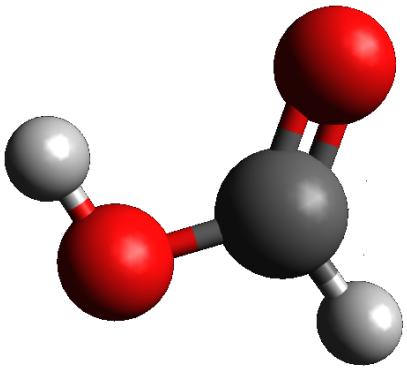

Figure 1.2: The *syn*-formic acid conformer

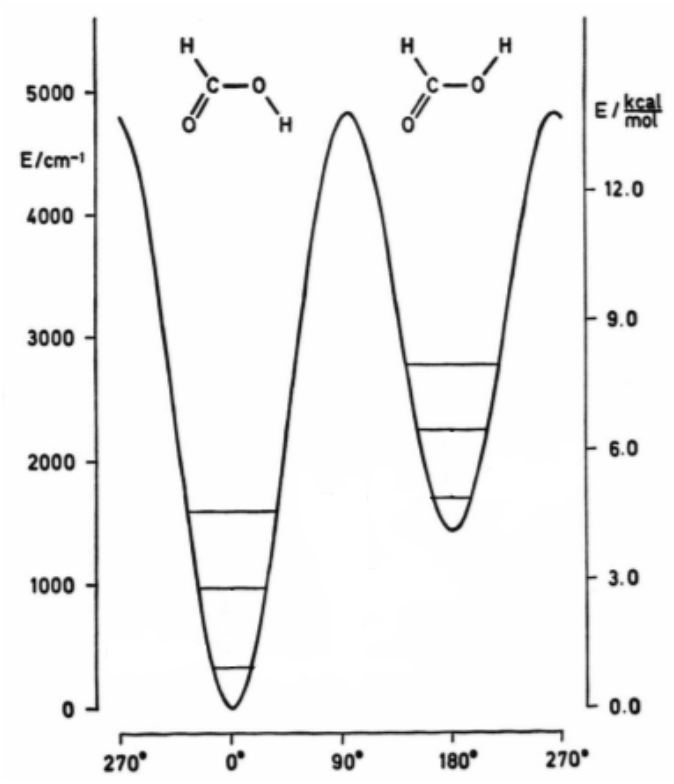


Figure 1.3: Potential energy curve associated with rotation from the *syn*-conformer to the *anti*-conformer.[24]

The molecules studied in the Wild group thus far have associated with them only one conformer, however, there exists two conformers of the formic acid molecule, namely the *anti*-conformer and the *syn*-conformer. The respective structures of the two conformers can be seen in Figure 1.1 and 1.2. The *syn*-conformer is more stable than the *anti*-conformer, with an energy difference between the two of approximately 20 kJ/mol.[20] The energy barrier between the two conformers is relatively high, lying approximately 60 kJ/mol above the *syn*-conformer.[20] The potential energy curve associated with transitioning from the *syn*- to the *anti*-conformer can be seen in Figure 1.3. Quantum mechanical tunnelling allows the *anti*-conformer to convert to the *syn*-conformer resulting in the *anti*-conformer being unstable with a half-life on the order of several minutes.[21] However, it has been found that the higher energy *anti*-conformer of formic acid stabilises when it forms van der Waals complexes with other species. Specifically, argon matrix studies of the complexes of formic acid with water and nitrogen found that the higher energy conformer appeared to be stabilised indefinitely once in a van der Waals complex.[22,23]

Only a limited number of studies have been undertaken on complexes of formic acid halides, namely the mass spectrometry study mentioned earlier as well as an infrared spectrum characterisation of the formic acid iodide complex.[11,25] The infrared spectroscopic study of the iodide-formic acid complex also included a low level theoretical study (*ab initio* calculations were carried out at B3LYP/LANL2DZ level of theory).[25] Vibrational modes were assigned to

the spectrum based on the theoretical calculations, the reliability of these assignments should however be questioned as density functional theory (DFT) methods such as B3LYP have been found unreliable for use in studies pertaining to loosely-bound complexes.[26] Additionally, the infrared study of the iodide-formic acid complex only considered the presence of the *anti*-conformer of formic acid in the results and no results associated with the (more populous) *syn*-conformer were reported.

Numerous techniques are used in the study of van der Waals complexes. The theory associated with both the computational and experimental methods will be outlined in the following sections.

## 1.4 Computational Chemistry

Computational chemistry is used to provide theoretical data associated with a chemical system, and can be used in a predictive sense for smaller systems due to the highly accurate nature of the calculations. Computational studies will be utilised in this project in addition to experimental studies, to allow for an interplay between experiment and theory, where experimental results can be rationalised by theoretical predictions.

*Ab initio* ('from first principles') calculations can be used to describe the behaviour of a molecular system, whereby these calculations provide approximate solutions to the many-body, time-independent, Born-Oppenheimer approximated Schrödinger equation, the non-relativistic version of which can be seen in equation 1.6. The Born-Oppenheimer approximation states that the electrons can be regarded as moving through a field generated by stationary nuclei, due to the extreme difference in mass between electrons and nuclear particles.[27,28]

$$\hat{H}\left|\Psi\right\rangle = E\left|\Psi\right\rangle \tag{1.6}$$

In equation 1.6, $\hat{H}$ is the Hamiltonian operator, which consists of both the potential energy

operator and the kinetic energy operator, and $\Psi$ is the wavefunction, which when acted upon by the Hamiltonian operator yields an energy eigenvalue (E). Essentially, all physical properties stem from the complete wavefunction. Therefore, when the approximate wavefunction has been determined, numerous properties associated with the system flow, in relation to van der Waals complexes, examples of important properties are the binding energy of the complex and the location in space of the constituent molecules of the complex.

The quantum chemical calculations conducted during the course of this project will be Hartree-Fock (HF), Møller-Plesset pertubation theory (MP2) and coupled-cluster theory with singlets, doublets and pertubative inclusion of triplets (CCSD(T)). The HF approach is one of the earliest approaches used to solve the Schrödinger equation for a multi-electron system. In essence, the method works by approximating each electron as existing in a field of the nuclei and other electrons.[29] The major deficiency of the HF method is the fact that electron spin correlation is not accounted for in the method.[30] Electron spin correlation refers to the effect of spin on the motion of electrons, specifically the spin of other electrons around the electron of interest. A multitude of methods were developed to build on the HF theory in an attempt to increase the accuracy of the calculated energies.

MP2 calculations essentially treat the system Hamiltonian in a series of parts, the unperturbed part as well as a series of perturbations (in the case of MP2, two pertubations).[29,31] It has been shown previously that MP2 calculations account for $(92.4 \pm 4.6)\%$ of the correlation energy associated with the investigated system.[32] The main disadvantages associated with MP2 calculations is the tendency to underestimate the ground state energy as a result of the second-order correction and the requirement of relatively large basis sets in order to achieve accurate results.[32,33]

CCSD(T) incorporates creation and annihilation operators to virtually excite electrons and thereby account for the electron spin correlation energy.[34,35] This project will aim to perform calculations at the CCSD(T) level of theory, since CCSD(T) has emerged as the 'golden stan-

dard'[36] in computational chemistry. The method used for quantum chemical calculations is only half the story, the other half is the basis set used to approximate the atomic orbitals and then used in linear combinations of these atomic orbitals to form molecular orbitals. The basis sets to be used as part of this project will be outlined in the Materials and Methods Chapter (Chapter 2).

## 1.5 Experimental Techniques

Van der Waals clusters have been investigated by a number of experimental techniques, the techniques focussed on as part of this review are: mass spectrometry and photoelectron spectroscopy (specifically anion photoelectron spectroscopy). Anion photoelectron spectroscopy and mass spectrometry are routinely utilised techniques as part of the study of van der Waals complexes, with the first implementation of anion photoelectron spectroscopy in 1967.[37]

### 1.5.1 Mass Spectrometry

Mass spectrometry has two main uses in the study of van der Waals complexes, namely, mass spectrometry can be utilised directly to elucidate properties of the complexes or it can be used as a mass 'recognition' and selection setup to ensure only one cluster type at a time is investigated by other techniques (e.g., anion photoelectron spectroscopy). For the specific setup of this project, mass spectrometry (time-of-flight) will be used as a mass selection device rather than directly used to investigate properties of complexes.

Van der Waals complexes can, however be directly studied by mass spectrometry. Mass spectrometry allows the experimental determination of thermochemical properties of the complexes of interest. Properties such as the enthalpy, entropy and Gibbs free energy of complex formation can be determined.[38] Spectroscopic investigation is an advancement on the mass spectrometry techniques as spectroscopy allows the determination of structural parameters associated with the complex.

### 1.5.2 Anion Photoelectron Spectroscopy

The technique of anion photoelectron spectroscopy will be employed in this project as part of the experimental investigation, in order to obtain photoelectron spectra of the formic acid-halide complexes. The overarching goal of photoelectron spectroscopy is "the attainment of an electron-centred view of chemical bonding and reactivity"[39]. Photoelectron spectroscopy of ion complexes allows elucidation of the neutral potential energy surface.[40] A potential energy surface can be thought of as a visual representation of the potential energy of the molecular (or cluster) system with respect to the position of the individual nuclei associated with the system. In other words, energetic properties associated with the neutral complex can be obtained by way of photoelectron spectroscopy of the anion complex.

Anion photoelectron spectroscopy is, essentially, based on the photoelectric effect where radiation above a certain threshold energy (wavelength) ejects electrons from an atom or molecule (in this case, van der Waals complexes). The resultant kinetic energy of the ejected photoelectrons is related to the photon energy of the ionising radiation and the binding energy of the ejected electron by way of equation 1.7. Different photon energies are used depending on the nature of the target orbital from which electrons are to be ejected, X-rays are used in the case of core-shell electrons and ultraviolet radiation is used in the case of valence electrons.[41]

$$E_{KE} = h\nu - E_{BE} \tag{1.7}$$

From inspection of equation 1.7, the binding energy of the system can be determined if both the photon energy and the photoelectron kinetic energy are known, this binding energy corresponds to the electron affinity of the neutral species.[42] Interestingly, the determination of the electron affinity of helium was among the first studies to make use of the anion photoelectron spectroscopic technique.[43]

A graphical representation of anion photoelectron spectroscopy can be seen in Figure 1.4. An

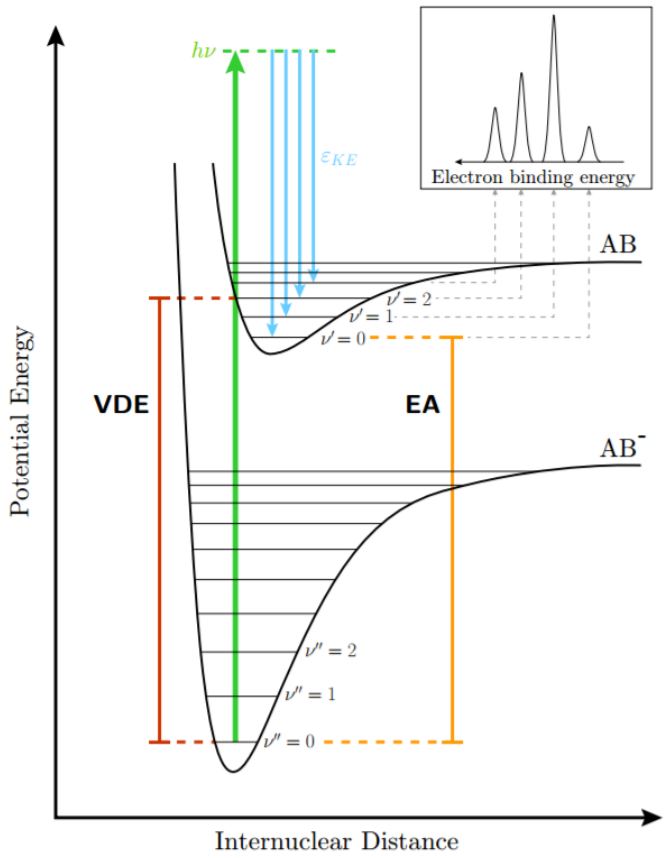


Figure 1.4: Underlying process associated with anion photoelectron spectroscopy.[41]

electron is ejected from the anion complex, forcing the complex to transition from the anion potential energy surface to the neutral potential energy surface. The resultant photoelectron spectrum exhibits peaks corresponding to the vibrational energy levels of the neutral complex, the intensities of which follow from the Frank-Condon principle. The experimental parameters relevant for this project are the electron affinity (EA in Figure 1.4 ) and the vertical detachment energy (VDE in Figure 1.4 ). The electron affinity is the ground state to ground state transition and the vertical detachment energy is the energy associated with the most likely transition based on the Frank-Condon principle.

## 1.6 Project Aims

The overall aims of this research project can be distilled into three main points:

1. Creation of gas phase anion clusters of formic acid and halides ($Cl^-$, $Br^-$ and $I^-$).
2. Study the intermolecular interactions of these clusters by making use of photoelectron spectroscopy.
3. Use computational studies of the above-mentioned clusters in conjunction with the experimental data, in order to rationalise the experimental data and complement the results.

The main outcomes of the project are linked with the above aims. Namely, the experimental anion photoelectron spectroscopic study of the formic acid-halide complexes will yield information relevant to the neutral complexes such as the electron affinity. The combination of the experimental data with the computational modelling will allow experimental data rationalisation as well as allowing the formulation of a complete picture of the intermolecular interactions underpinning the formic acid-halide complexes. Additionally, the study will further understanding of the intermolecular interactions between carboxylic acids and halides more broadly, such as for example, the solvation of halogens by carboxylic acid species.

# Chapter 2

# Materials and Methods

This chapter will outline the experimental techniques associated with this study as well as the computational methods. The gas mixture preparation, the time-of-flight photoelectron spectrometer (TOF-PES) and the experimental results analysis will be outlined. Additionally, the specific computational methods used as part of this study will be outlined followed by the computational data analysis.

## 2.1 Overview of Experimental Apparatus

The cornerstone of the experimental study is the Wiley-McLaren[44] style mass spectrometer coupled with a photoelectron spectrometer, which was used to record experimental photoelectron spectra of the formic acid halide complexes. The Wild group TOF-PES was constructed in 2008 by LaMacchia,[45] a schematic of the TOF-PES apparatus can be seen in Figure 2.1. The cluster ions of interest (and a multitude of other species) are formed in the ion source chamber, the negative ions are then selectively diverted down the time-of-flight axis of the Wiley-McLaren[44] style mass spectrometer. The anions then pass through a series of ion optics as they move towards the ion detector (in the case of mass spectra collection) or are intersected by a laser pulse (in the case of photoelectron spectra collection). The following sections will elaborate on the ion production, the TOF-PES components as well as the laser-ion interaction and the photoelectron collection.

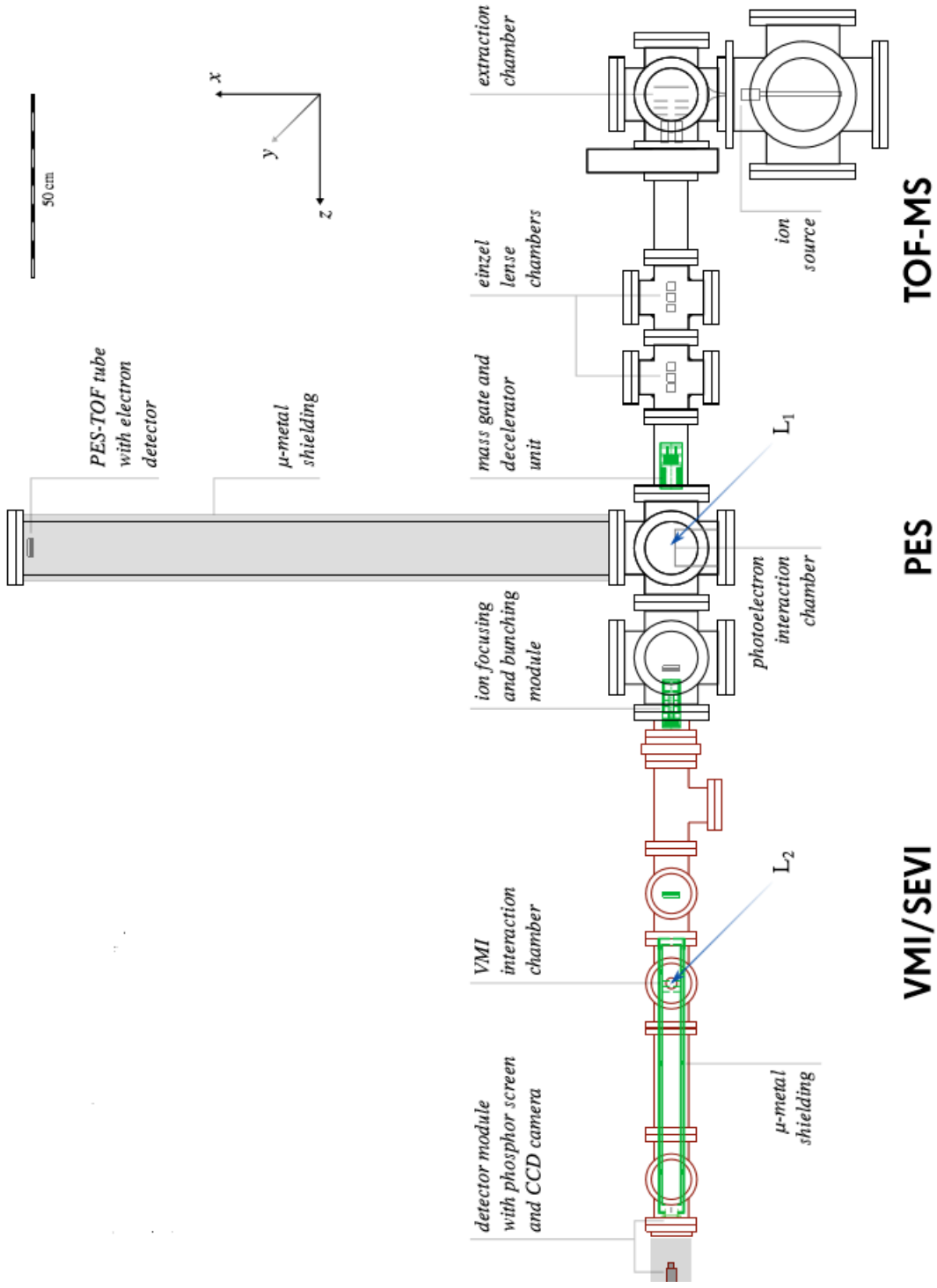


Figure 2.1: Birds-eye view of the TOF-PES experimental apparatus.[46]

### 2.1.1 Gas Mixture Formation

In order to form the formic acid halide ion complexes, an appropriate gas mixture must be prepared for subsequent pulsed release into the ion source chamber. The gas mixture is prepared and stored in the gas mixing station, a stainless steel compartment sealed until experimentation commences. The successful creation of a gas mixture requires three components: the halide donor species, the solvating species and argon which serves as the major component of the mixture. The halide donor species routinely used in the Wild group are iodomethane, dibromomethane and tetrachloromethane, the solvating species in this study is formic acid and argon is the buffer gas and acts to cause vibrational cooling of the ion complexes.

In order to ensure minimal contamination of the gas mixture, the gas mixing station is evacuated between each usage. The evacuation procedure consists of cycles of flushing with argon and pumping with a liquid nitrogen assisted rotary pump. After a number of such evacuations (at least three), the new gas mixture is created. The liquid halide source and formic acid are placed in glass vials and connected to the gas mixing station. The liquids are subjected to freeze-pump-thaw cycles in order to encourage degassing of the liquids, thus ensuring high purity of the resulting gas mixture. The liquids are frozen using liquid nitrogen and then the head space is evacuated followed by thawing of the liquid.

Following the freeze-pump-thaw procedure, the liquid species are allowed to enter the gas mix. This is done by cooling the halide donor and the formic acid using a salt-water-ice bath and allowing the species to escape into the gas mix over a nominal period of a few seconds owing to their vapour pressure. Following the addition of the halide donor and formic acid, the gas mixture is made up to approximately $400$ kPa using argon. At the point of production, the gas 'mixture' in the gas vessel is poorly mixed with stratification of the different gaseous species occurring in the vessel. Therefore, the gas mixture is then allowed to equilibrate and mix thoroughly, following which, the mixture is ready for experimentation.

### 2.1.2 Ion Production and Extraction

The equilibrated gas mixture is pulsed into the source chamber through a solenoid nozzle. The solenoid nozzle allows gas to pass through when a current is applied to the solenoid and at the point in time where the current is removed, the solenoid acts to block the flow of gas. As the flow of gas passes through the solenoid nozzle, a supersonic expansion is formed, which allows cooling and collimation of the gas pulse. The cooling occurring in the supersonic expansion is more effective for translational cooling than vibrational cooling,[47] and for this reason, the argon carrier gas is added to allow for vibrational cooling as well.[46]

The expanding gas column is intersected by a pulsed electron beam from an adjacent heated rhenium filament. The current and pulse width of the rhenium filament is controlled and an einzel lens allows focussing of the electron beam. The application of a pulsed negative potential on a Wehnelt shield located behind the filament accelerates the electrons towards the expanding gas beam. The bombardment of electrons incites dissociative electron attachment reactions promoting the formation of anion complexes, amongst which are halide-formic acid complexes, a series of such reactions can be seen in equations 2.1, 2.2 and 2.3.

$$\mathrm{Ar} + \mathrm{e}^-_{\mathrm{fast}} \longrightarrow \mathrm{Ar}^+ + \mathrm{e}^-_{\mathrm{slow}} + \mathrm{e}^-_{\mathrm{fast}} \tag{2.1}$$

$$\mathrm{e}^-_{\mathrm{slow}} + \mathrm{CH_2Br_2} \longrightarrow [\mathrm{CH_2Br_2}]^{*-} \longrightarrow \mathrm{CH_2Br} + \mathrm{Br}^- \tag{2.2}$$

$$\mathrm{Br}^- + \mathrm{HCOOH} \longrightarrow \mathrm{HCOOH} \cdot \cdot \cdot \mathrm{Br}^- \tag{2.3}$$

Subsequent to the electron bombardment, the gas mixture contains anionic, cationic and neutral molecules and complexes (i.e., a plasma). As part of this project, it was observed that the mass spectrum signal of the complex of interest was heavily dependent on the rhenium filament current and timing. A portion of the plasma beam then passes through a skimmer forming a collimated plasma beam. A schematic of the skimmer assembly can be seen in Figure 2.2. The now collimated plasma beam then enters the ion extraction chamber.

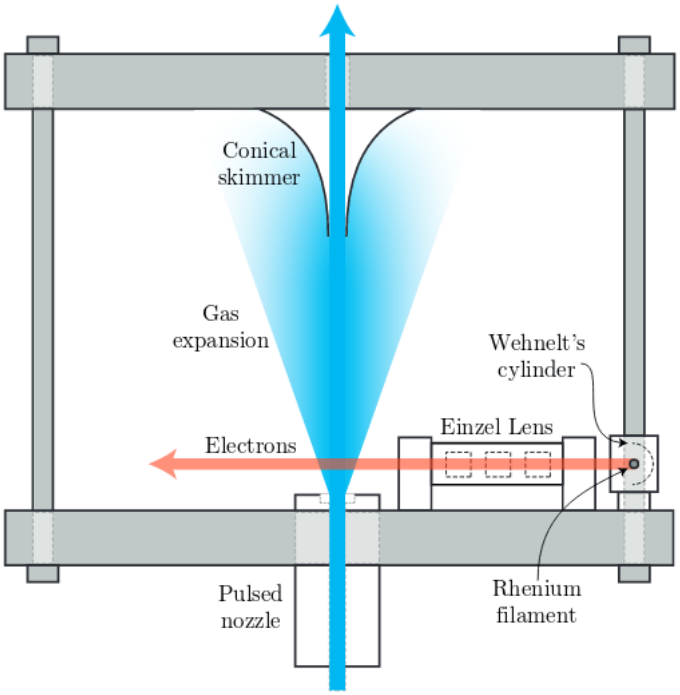


Figure 2.2: Skimmer assembly schematic, showing the expanding gas intersecting the electron beam and the collimation associated with the skimmer.[41]

The extraction chamber contains the time-of-flight (TOF) plates, which are three metal plates: two plates are used for the extraction of the anions and the third plate is held at ground potential to create a field-free region in the ion flight tube. The first plate is pulsed to a high negative potential (-1500 V) as the plasma beam arrives, simultaneously the second plate is pulsed to a slightly smaller potential (approximately -1350 V). This application of voltages deviates the anions along the flight axis of the ion flight tube, the cations collide with the more negatively charged plate and the neutrals are unaffected and collide with the chamber walls. Only one negatively (or positively) charged plate would be required to separate the various charged species, the second TOF plate is used in order to allow space focussing of the anion beam as it travels through the flight tube. Previous studies making use of the extraction chamber have used TOF plate settings of -1000 V and -910 V respectively. The TOF plates and the ion extraction chamber and ion flight tube were thoroughly cleaned. However, even after cleaning, the TOF plates still required voltages in the region -1500 V in order to produce an appreciable ion signal at the detector.

### 2.1.3 Ion Flight Tube

The third metal plate in the extraction chamber, which is held at ground potential, isolates the ion flight tube from the extraction chamber to ensure no electric fields apply further acceleration to the ion beam. Upon entry into the flight tube, the ion beam passes a set of X-Y deflection plates (voltage range $\pm 100\,\mathrm{V}$), which allow the application of ion trajectory corrections. As the ions travel through the flight tube, inter-ionic repulsion between the anions forces the ion beam apart resulting in expansion of the beam. To combat this, the ion beam travels through two einzel lens assemblies, which (in a similar manner to light travelling through a convex lens) refocusses the ion beam.[46] A second set of X-Y deflection plates are located after the einzel lenses, which again allows adjustment of the ion beam trajectory. Initially, significant deflection of the ion beam was observed, this was attributed to a loose cable hanging across the ion flight path.

Every anion in the beam has approximately the same amount of kinetic energy (the acceleration applied by the TOF plates). The anions therefore separate along the flight-axis in the time domain. This has been shown mathematically in equation 2.4:

$$\begin{aligned} E_{KE} &= \frac{1}{2}mv^2 \\ \implies v &= \sqrt{\frac{2E_{KE}}{m}} \\ \implies \frac{d}{t} &= \sqrt{\frac{2E_{KE}}{m}} \\ \therefore t &\propto \sqrt{m} \end{aligned} \tag{2.4}$$

Essentially, the ion kinetic energy is constant, which implies that the velocity of the individual anions only depends on their respective masses. In other words, the velocity is inversely proportional to the square-root of the mass and since the velocity is inversely proportional to the time taken by the anions to traverse the ion flight tube, the time-of-flight of the anions is directly proportional to the square-root of the mass of the anions. In the case of mass

spectrum acquisition, the ions arrive and are detected by a microchannel plate detector. The microchannel plate detector allows detection of relatively weak signals as it creates a cascade of electrons subsequent to initial collision with the incoming anion. Alternatively, the anion beam is overlapped with a laser pulse in order to detach electrons.

### 2.1.4 Photodetachment and Photoelectron Detection

The laser beam is overlapped in time and space with the anion mass of interest to detach and thus produce photoelectrons. The laser source is a Spectra-Physics Quanta-Ray Pro-230, which is a 10 Hz pulsed neodymium doped yttrium aluminium garnet (Nd:YAG) laser. A Nd:YAG laser produces a fundamental frequency of $1064\,\text{nm}$, which is then frequency quadrupled to produce ultraviolet photons of $266\,\text{nm}$. The Nd:YAG laser system is a four-level system, which means population inversion is achieved with relative ease in comparison to three-level laser systems such as a Ruby laser.

At the point of intersection of the laser and anion complex ($L_1$ in Figure 2.1), photoelectrons are detached, and directed along the photoelectron flight tube time-of-flight axis by way of a bottleneck-shaped magnetic field.[48,49] The magnetic field shape at the laser interaction point can be seen in Figure 2.3. With reference to Figure 2.3, $B_1$ is the strong magnetic field, $B_2$ is the weak magnetic field and the velocity vector diagrams display the increasing x-component as the electron travels along the field.[46] Essentially, a large, diverging magnetic field in superposition with a weaker solenoid magnetic field generate an environment where almost the entire $4\pi$ steradians distribution of detached electrons are captured and parallelised as they travel along the solenoid magnetic field lines.[48] The solenoid magnetic field is generated by applying a constant current to a copper wire wrapped around a cylinder, which has been shielded with $\mu$-metal to allow attenuation of any stray magnetic fields. The strongly diverging magnetic field in the electron detachment region is generated by way of an electromagnet. A permanent magnet was initially in use, but was however, swapped out for the electromagnet in a attempt to determine the root cause of problems with the photoelectron flight times.

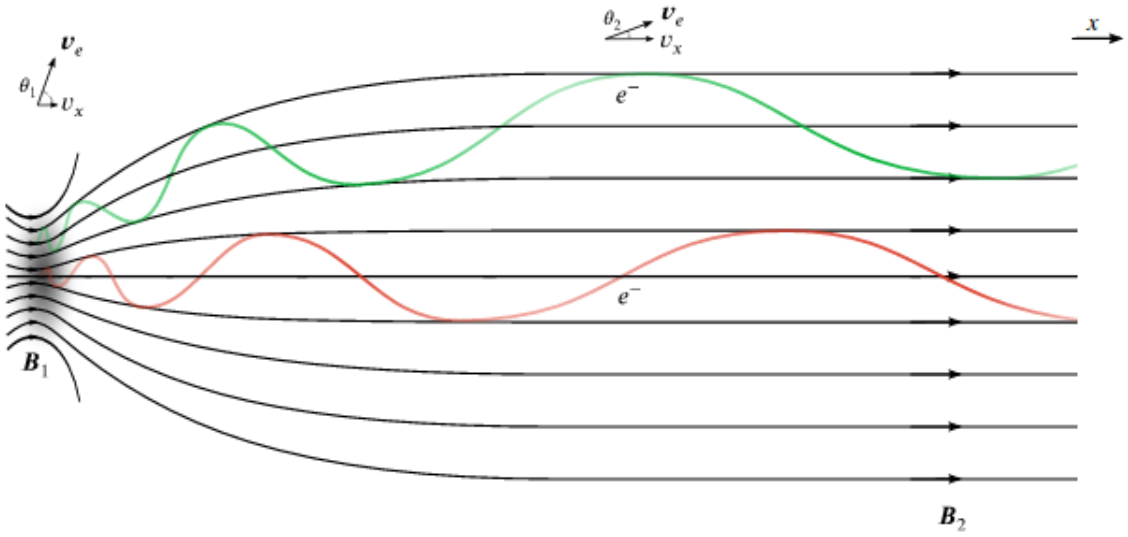


Figure 2.3: Bottle-neck shaped magnetic field used for electron capture.[46]

During initial photoelectron spectrum acquisition, it was observed that photoelectrons appeared to decrease flight times during the course of a day. Initially, this was attributed to the permanent magnet assembly and, as such, the permanent magnet was replaced with an electro-magnet. The problem was later found to be a possible stray connection in the microchannel plate detector assembly used to detect the photoelectrons. It is thought that a stray connection produced an electric field, which applied an acceleration to the electrons towards the detector and thus the photoelectron flight times were observed to decrease.

The laser beam properties, the anion beam properties and the magnetic field strength are all adjusted in order to achieve an optimised photoelectron signal arriving at the detector. In general, the experiment is adjusted in a way as to maintain a low rate of photodetachment. This is done in order to ensure the detector does not become saturated. Similarly to the anion detection associated with the mass spectrum acquisition, a microchannel plate detector is used to detect the inbound photoelectrons. In contrast to the anions, the photoelectrons have comparatively little energy when they hit the detector, as such, a grounded mesh is located immediately in front of the microchannel plate detector, which accelerates the incoming electrons directly before the detector. The fact that the mesh is located very close to the detector

and relatively far from the detachment point of the photoelectrons, means that the electron flight times are minimally affected.

All of the experimental results hinge on the recording of photoelectron time-of-flight data. If temporal data is to be collected accurately, then the timing associated with the equipment used to collect the data has to be well controlled. In the experimental setup used as part of this project, the timing associated with all the equipment is controlled by two pulse generators (SRS, DG535, Four channel digital delay/pulse generator). A timing diagram describing the relative timing of the various experimental components with respect to one another can be seen in Appendix B.

## 2.2 Analysis of Experimental Data

The experimental data are all collected in terms of time-of-flight. However, the desired form of the data for mass spectrometry and photoelectron spectroscopy is mass to charge ratio and electron binding energy respectively. The data analysis employed to transform the collected raw data from time-of-flight to m/z and binding energy (eV) will be outlined in the following sections.

### 2.2.1 Mass Spectrum Analysis

The mass spectrum data are collected in the time-of-flight domain by a digital oscilloscope (Agilent Technologies, DSO6032a) coupled with the microchannel plate detector. The oscilloscope averages multiple mass spectra (generally 256 averages) and the resultant average time-of-flight mass spectrum is then analysed using a computer. The analysis utilises the proportionality relationship between mass/charge and the square-root of time-of-flight (the derivation of which can be seen in equation 2.4) to convert from the temporal to the mass-to-charge domain.

Easily identifiable mass peaks are used to calibrate the spectrum. In particular, the isotopic

abundances associated with chlorine (namely, $^{35}$Cl and $^{37}$Cl) and bromine (namely, $^{79}$Br and $^{81}$Br) are used in order to calibrate the spectrum. Following the calibration, the various mass peaks can be identified and the experimental parameters can be optimised with an aim at maximising the intensity of the mass peak of interest.

### 2.2.2 Photoelectron Spectrum Analysis

The photoelectrons are detected (in a similar fashion to the anions) by a microchannel plate. The signal is then digitised (P7888 Fast Comtec GmbH, 2 ns) and assigned to individual time bins, the timing pulse that starts the digitisation and signal collection is the laser impacting a photodiode located below the laser interaction point. Essentially, each detected electron is registered as one event and counted, the event is then associated with a 2 ns wide time bin. The bin number can be converted to time-of-flight by way of equation 2.5.

$$TOF = (16(Delay) + 2(Bin - 1)) * 10^{-9} \tag{2.5}$$

The delay term present in equation 2.5 corresponds to any delay imposed between the photodiode laser pulse detection and timing commencement, the delay was routinely set to zero during the course of this project. The data treatment allowing for conversion from time-of-flight to electron binding energy and the background subtraction from the spectral data was performed in Origin, which is a data analysis program.

In order to convert the time-of-flight data to electron kinetic energy, a calibration is used, which utilises known electron energies associated with the $^2P_{3/2}$ and $^2P_{1/2}$ peaks of iodide and bromide. Electron kinetic energy is directly proportional to the reciprocal of time-of-flight squared, which has been shown in equation 2.6:

$$
\begin{aligned}
E_{KE} &= \frac{1}{2}mv^2 \\
\implies KE &= \frac{1}{2}m(\frac{d}{TOF})^2 \\
\implies KE &= \frac{md^2}{2}\frac{1}{TOF^2} \\
\therefore KE &\propto \frac{1}{TOF^2}
\end{aligned} \tag{2.6}
$$

Therefore, the time-of-flight associated with the iodide and bromide peaks can be graphically determined and the reciprocal square of these values can then be plotted against the known electron kinetic energy values (sourced from NIST[50]) to produce a line of best fit. The line of best fit is then used to transform the experimental time-of-flight data to the kinetic energy domain. The kinetic energy values can then be converted to electron binding energy by way of equation 1.7 (essentially, the kinetic energy is subtracted from the laser energy of $4.661$ eV, yielding the binding energy).

Essentially, the photoelectron data is collected in data bins with a width of $2$ ns, so the domain can be trivially converted from bin number to time-of-flight. The proportionality relationship between kinetic energy and reciprocal time-of-flight squared can then be utilised in order to calibrate the domain to kinetic energy by making use of known photoelectron kinetic energies. Following which, the kinetic energy can be converted to binding energy. However, the transformations so far have only been applied to the x-axis variables (i.e bin number, time-of-flight, kinetic energy and binding energy). In order to ensure correct spectroscopic intensities the y-axis data are transformed making use of a Jacobi transform.

#### 2.2.2.1 Jacobi Transform

Essentially, the integral of the experimental data (i.e., the area under the experimental data) is required to remain constant independent of transformation.[51] In other words, the integral over the transformed data should be identical to the integral over the original data. The intensity associated with the time-of-flight data can be thought of as being time-dependent (i.e., I(t))

and the intensity associated with energy can be thought of as energy-dependent (i.e., I(E)).

$$\begin{aligned} \int I(t)dt &= \int I(E)dE \\ \implies I(t)dt &= I(E)dE \\ I(E) &= I(t)\frac{dt}{dE} \end{aligned} \tag{2.7}$$

The $\frac{dt}{dE}$ term can be found with relative ease by inverting the derivative of binding energy (BE) with respect to time:

$$\begin{aligned} BE &= 4.661 - KE \\ BE &= 4.661 - \frac{1}{2}m_e(\frac{d}{t})^2 \\ \implies \frac{dBE}{dt} &= \frac{m_e d^2}{t^3} \\ \therefore \frac{dt}{dBE} &= \frac{t^3}{m_e d^2} \end{aligned} \tag{2.8}$$

Combining equation 2.7 and equation 2.8, results in a conversion factor to convert the time-of-flight intensities to binding energy intensities:

$$I(E) = I(t)\frac{t^3}{m_e d^2} \tag{2.9}$$

The electron mass ($m_e$) as well as the electron flight distance ($d$) parameters which are present in equation 2.9 are constants and as such can be disregarded for use in conversion. Therefore, the Jacobi conversion factor is time-of-flight cubed. Simply put, the experimental data intensities are all multiplied by the time-of-flight cubed.

## 2.3 Computational Methods

*Ab inito* calculations were performed on the halide-formic acid anion and neutral complexes in order to complement the experimental data. The calculations were performed using Gaussian 09.[52] The types of calculations undertaken were: van der Waals complex and formic acid molecule geometry optimisations, frequency calculations on the optimised geometries as well as single point energy determinations associated with the bare halides. In each case, the frequency analysis associated with the optimised geometries were carried out in order to confirm the identity of the geometry as a potential energy surface minimum. It is the case that a minimum geometry has associated with it all real frequencies, while non-minimum geometries (e.g., transition states and higher order saddle points) have associated with them at least one imaginary vibrational mode.

The level of theory approached as part of this project was CCSD(T) with respect to the fluoride and chloride van der Waals complexes and MP2 in the case of both the bromide and iodide van der Waals complexes. In each case, Dunning's[53–57] augmented, correlation consistent basis sets up to quintuple zeta (i.e., aug-cc-pVXZ where X is D, T, Q, 5) were used. Initially, calculations were carried out at MP2/aug-cc-pVDZ (aug-cc-pVDZ-PP for bromine and iodine) level of theory to determine the approximate van der Waals geometries corresponding to potential energy minima. Subsequently, the resultant minimum geometries were optimised further using MP2/aug-cc-pVQZ (aug-cc-pV(Q+d)Z for chlorine and aug-cc-pVQZ-PP for bromine and iodine) level of theory. The basis sets making use of additional diffuse functions (aug-cc-pV(X+d)Z) and pseudopotentials (aug-cc-pVXZ-PP) were sourced from the EMSL basis set exchange[58,59].

Subsequent to the geometry optimisations, frequency analyses were carried out on all the anion and neutral structures. The flourine van-der-Waals frequency analysis was carried out at the MP2/aug-cc-pVQZ level of theory, the chlorine van-der-Waals frequency analysis was carried out at the MP2/aug-cc-pV(Q+d)Z level of theory. In the case of both the bromine and iodine van-der-Waals complexes, the anion frequency analyses were done at the MP2/aug-

cc-pVQZ-PP level of theory while the neutral frequency analyses were done at the MP2/aug-cc-pVTZ-PP level of theory. The use of the triple zeta basis set for use in frequency analysis of the neutral complexes of bromine and iodine stems from the large amount of time required to run such calculations.

In the case of the fluorine and chlorine van der Waals anion and neutral complexes, the MP2 quadruple zeta optimised structure was used in single point energy calculations at CCSD(T) using triple and quadruple zeta basis sets in order to allow extrapolation of the determined energy to the complete basis set (CBS) limit. In the case of the bromine and iodine van der Waals anion and neutral complexes, the MP2 quadruple zeta optimised structure was used in subsequent single point energy determinations at quintuple zeta (still using the MP2 method) to again allow extrapolation to the CBS limit. The CBS extrapolation will be explored further in Section 2.3.2. The bromide and iodide complexes were also calculated at CCSD(T)/aug-ccpVTZ-PP to serve as a point of comparison.

### 2.3.1 Basis Set Explanation

The general form of basis sets used as part of this project for the computational investigation of the formic acid-halide van der Waals complexes is:

$$\text{aug-cc-pVXZ} \quad \text{where} \quad \text{X} = \text{D, T, Q, 5}$$

The full name of these types of basis sets is, augmented, correlation consistent, polarised valence X zeta. *Augmented* refers to the addition of extra diffuse functions in order to allow a more accurate description of the long-range behaviour associated with the system.[55] *Correlation consistent* refers to the addition of atomic orbital functions in shells, which allows smooth convergence to the CBS limit.[53] *Polarised valence* refers to the addition of mixing orbitals to allow the atomic orbitals to polarise (shift direction of electron density).[53] The *X zeta* (where X is double, triple, quadruple or quintuple) refers to the number of gaussian functions used in the basis set to provide the approximate atomic orbital description. The pseudopo-

tential (PP) refers to the replacement of core-shell electrons with a potential,[57] because the core-shell electrons do not take part in bonding. Additionally, the use of pseudopotentials increases the computational speed.

### 2.3.2 Complete Basis Set Limit

A CBS extrapolation is done in an attempt to circumvent (at least in part) the fact that the basis set used for calculation is incomplete and only serves as an approximation. There exists a multitude of different methods for extrapolation to the complete basis set limit.[60] The methods have varying levels of accuracy and time-consumption, but central to all the CBS methods, is the result of highly accurate energies from extrapolation of calculated energies. Two different extrapolation methods were used as part of this project. Namely, a modified version of the Weizmann-1 w (W1w) protocol was used in the case of flourine and chlorine where CCSD(T) energies were available. Traditionally, the W1w protocol relies on a B3LYP/cc-pV(T+d)Z optimised geometry from which, CCSD(T) single point energies are determined.[61] However, as part of this project, a MP2/aug-cc-pVQZ reference geometry was used due to the fact that B3LYP has been shown to be unreliable in the case of loosely-bound complexes.[26] A CBS extrapolation was also performed in the case of complexes associated with all four halides (fluorine, chlorine, bromine and iodine), using the MP2 quadruple zeta and quintuple zeta energies. This was done in order to serve as a comparison between MP2 and CCSD(T) results and since, CCSD(T) extrapolations could not be completed for the bromine and iodine complexes.

A CBS extrapolation is carried out by separately extrapolating the Hartree-Fock (HF) energy and the correlation energy (MP2, CCSD and CCSD(T) energies). Following the separate extrapolations, the extrapolated HF energy is summed together with the extrapolated correlation energy. This can be seen in equation 2.10 where $E^{\infty}$ is the extrapolated energy.

$$E^{\infty}_{Total} = E^{\infty}_{HF} + E^{\infty}_{Corr} \tag{2.10}$$

The HF energy extrapolation formula is slightly different depending on whether the extrapolation is done using quadruple and quintuple zeta energies or triple and quadruple zeta energies. The HF extrapolation for use with the MP2 quadruple and quintuple zeta energies can be seen in equation 2.11.[62] The HF extrapolation for use with the CCSD(T) triple and quadruple zeta energies can be seen in equation 2.12.

$$E_{HF}^{\infty} = E_{HF}^{L} + \frac{E_{HF}^{L} - E_{HF}^{L-1}}{\frac{L\exp\left(9(\sqrt{L}-\sqrt{L-1})\right)}{L+1} - 1} \tag{2.11}$$

$$E_{HF}^{\infty} = E_{HF}^{L} + \frac{E_{HF}^{L} - E_{HF}^{L-1}}{(\frac{L}{L-1})^{\alpha} - 1} \tag{2.12}$$

The $\alpha$ in equation 2.12 is equal to 5 as per the W1w protocol.[61] The extrapolation formula associated with correlation energy is almost identical to equation 2.12 in the case of both the MP2 and the CCSD(T) CBS extrapolation. The form of the correlation extrapolation can be seen in equation 2.13.

$$E_{Corr}^{\infty} = E_{Corr}^{L} + \frac{E_{Corr}^{L} - E_{Corr}^{L-1}}{(\frac{L}{L-1})^{\beta} - 1} \tag{2.13}$$

In the case of the MP2 extrapolation, $\beta = 3$[63] and in the case of the CCSD(T) extrapolation, $\beta = 3.22$.[61] Interestingly, in keeping with the W1w protocol, when determining the perturbative triplet correlation energy, the extrapolation is performed using CCSD(T) double and triple zeta energies rather than the CCSD(T) triple and quadruple zeta energies.[61]

Following the culmination of the CBS extrapolations, a number of properties can be determined. These properties include the dissociation energy ($D_e$ and $D_0$), which is the difference in energy between the complex and the individual components. The vertical detachment energy (VDE), which is the difference in energy between the anion and neutral complex with the same geometry. Essentially, this simulates the process associated with anion photoelectron spectroscopy, since the electron would detach and only after detachment would the geometry

rearrange to a new optimum structure. The electron affinity (EA) can also be determined, which is the difference in energy between the anion and neutral complex. Finally, the stabilisation energy ($E_{stab}$) can be determined by calculating the difference in dissociation energy of the anion and neutral complexes.

# Chapter 3

# Results and Discussion

This chapter contains all the experimental and computational results. Initially, mass spectra associated with each halide-formic acid mixture are reported. Following the mass spectra, the photoelectron spectra associated with formic acid-bromide and formic acid-iodide will be reported. The formic acid-chloride photoelectron spectra will be discussed, however, the laser energy was found to be insufficient to detach an electron. After the experimental data, a multipole expansion of a formic acid molecule interacting with a negative charge will be presented followed by the computationally determined anion and neutral complex geometries and energetics.

## 3.1 Experimental Results

### 3.1.1 Mass Spectra

The mass spectra associated with the formic acid-chloride, bromide and iodide gas mixture are presented below. In each case, the main peaks of interest as well as notable peaks are discussed here. In the case of all three mass spectra, the peak(s) associated with the formic acid-halide complex can be seen, showing that the complexes of interest were produced.

The mass spectrum associated with the tetrachloromethane and formic acid gas mixture can be seen in Figure 3.1. The characteristic natural abundance of the $^{35}$Cl and $^{37}$Cl isotopes leads to the splitting pattern of approximately 3:1, allowing chloride mass peaks to be identified with relative ease. The mass peaks appearing at $34.91$ m/z and $36.87$ m/z correspond to the two chloride isotopes, noting that these peaks do display the characteristic splitting pattern as shown in the inset graph of Figure 3.1. A preliminary calibration of the spectrum was carried out using these peaks, allowing approximate assignment of additional peaks such as the chloride-argon complex peaks located at $74.95$ m/z and $76.92$ m/z respectively. The inclusion of additional peaks in the calibration increased the accuracy, thus allowing the main peaks of interest to be identified. Namely, the chloride-formic acid peaks found to be located at $80.96$ m/z and $83.01$ m/z respectively. Upon close inspection, the residual peak of $^{79}$Br was assigned to the $78.93$ m/z peak. The fact that bromine-79 was present, suggested that bromine-81 would also be present and convoluted with the $^{35}\mathrm{Cl}\cdots\mathrm{HCOOH}$ mass peak. For the purpose of photoelectron spectroscopy, the $^{37}\mathrm{Cl}\cdots\mathrm{HCOOH}$ peak should be used in order to eliminate the possibility of photoelectrons appearing in the spectrum originating from a $^{81}$Br anion.

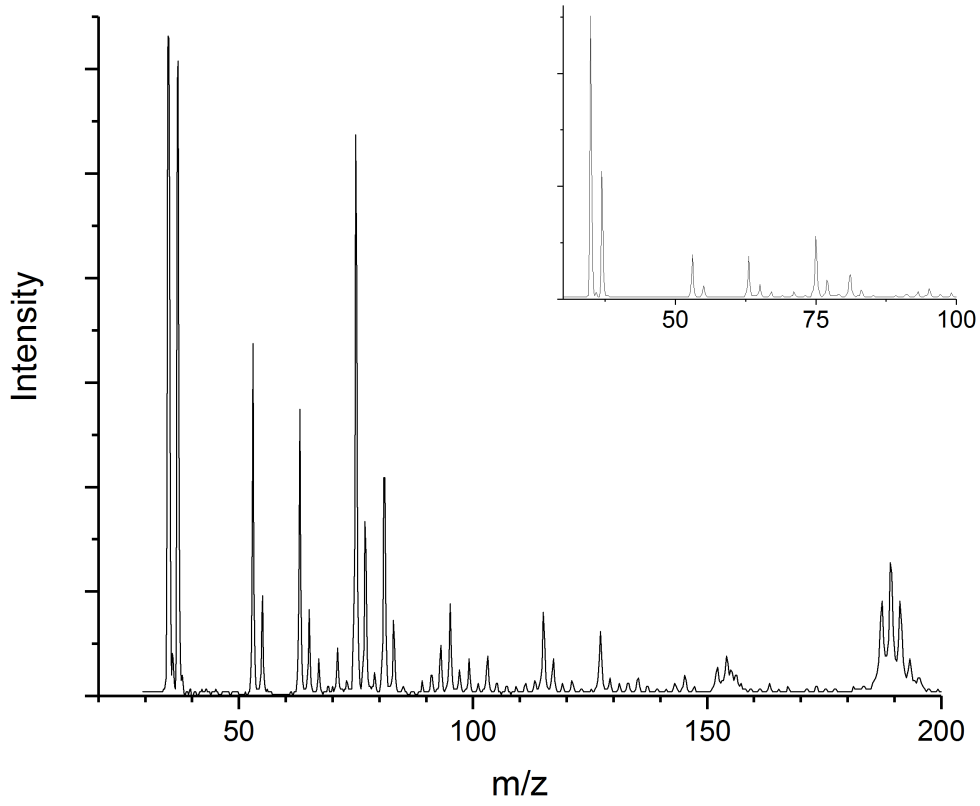


Figure 3.1: Time-of-flight mass spectrum of the $CCl_4$, HCOOH and Ar mixture.

The mass spectrum for the dibromomethane and formic acid gas mixture can be seen in Figure 3.2. The bromide peaks (i.e., bromide-79 and bromide-81) were used for calibration and can be seen in the spectrum to be the two most intense mass peaks at $78.92$ m/z and $81.04$ m/z respectively. The other intense peak, with a mass peak of $126.9$ m/z, was found to be iodide. Interestingly, the mass of iodide and the formic acid-bromine-81 cluster is approximately the same explaining why only one peak associated with the formic acid-bromine complex is observed in the spectrum located at $125.0$ m/z. Similarly to the formic acid-chloride peaks, photoelectron spectroscopy was carried out using the $125$ m/z mass peak in order to eliminate the significant iodide photoelectron signal that one would observe had the $126.9$ m/z peak been used.

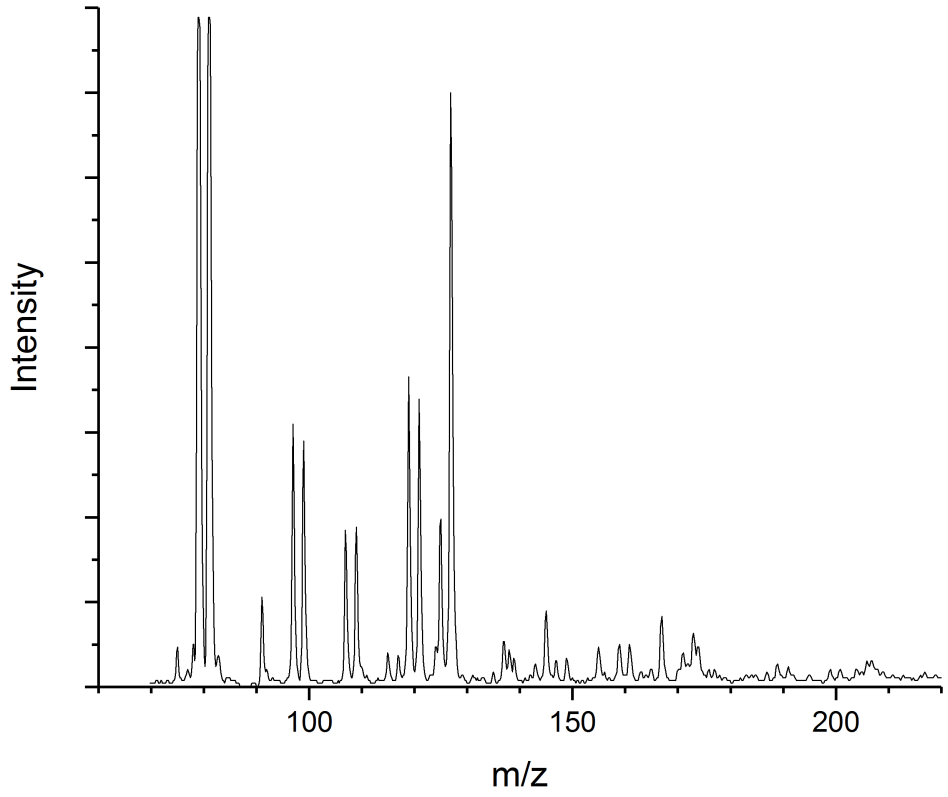


Figure 3.2: Time-of-flight mass spectrum of the $CH_2Br_2$, HCOOH and Ar mixture.

The mass spectrum associated with the iodomethane and formic acid gas mixture can be seen in Figure 3.3. The most intense peak corresponds to iodide located at $126.9$ m/z. With the next most intense peak located at $166.8$ m/z associated with the iodide-argon complex. These two peaks were used in the initial calibration of the spectrum. Subsequent to calibration, the iodide-formic acid peak was found to be located at $172.8$ m/z.

As an aside, the iodide mass spectrum in Figure 3.3 has a relatively large peak located at $138.1$ m/z and a smaller peak located at $184$ m/z. It is thought that these are the peaks of $(HCOOH)_3^-$ and $(HCOOH)_4^-$ respectively. These types of anion clusters are commonly referred to as dipole-bound states,[64] where a relatively large dipole on the molecule or cluster in question allows the binding of an electron resulting in an anion. The formic acid dimer anion has been studied previously,[65] however, it was found not to be a dipole-bound anion, since the

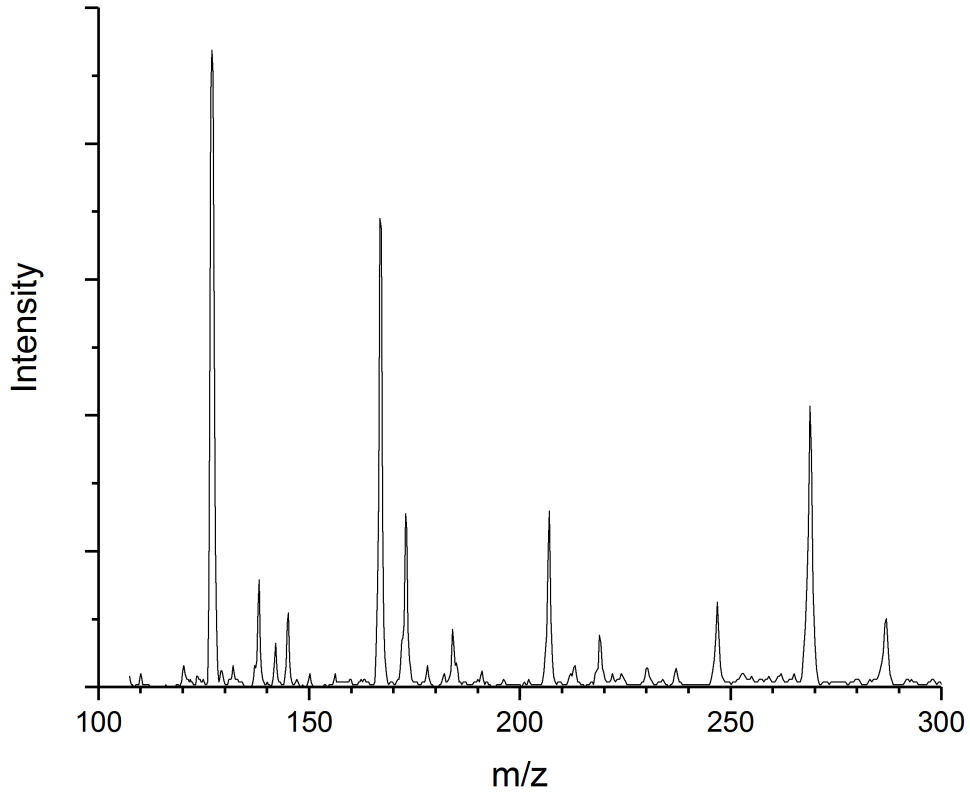


Figure 3.3: Time-of-flight mass spectrum of the $CH_3I$, HCOOH and Ar mixture.

formic acid dimer has no dipole. The mass peak at $138.1$ m/z was also present in the bromide mass spectrum (Figure 3.2), but it is anticipated that the iodide spectrum was collected under experimental conditions better suited for the formation of these types of clusters.

### 3.1.2 Photoelectron Spectra

The experimental photoelectron spectra associated with formic acid-iodide and bromide can be seen in Figures 3.4 and 3.5. Traditionally, two peaks with the ratio 2:1 would be observed in the photoelectron spectrum of a halide containing species, since subsequent to electron detachment, the halogen system is left in either the $^2P_{3/2}$ or the $^2P_{1/2}$ energy state. However, in spectra collected as part of this project, only one peak (the $^2P_{3/2}$ peak) was observed in each case due to the fact that the $^2P_{1/2}$ peak had an energy larger than the laser detachment

energy ($4.661$ eV).

An attempt was made to collect the formic acid-chloride photoelectron spectrum. However, the VDE associated with the formic acid-chloride complex was found to be too large to probe with a $4.661$ eV laser. Additionally, problems associated with the magnetic field plagued the entirety of photoelectron spectra collection. Specifically, drift associated with the photoelectron flight times was observed, which was thought to be due to poor overlap of the magnetic fields forming the bottle-neck magnetic field. This drift in flight times meant that calibration of the spectra in order to convert from the time-of-flight to binding energy became impossible to carry out with an acceptable level of accuracy. The peak assignments associated with the spectra can be seen in Table 3.1.

Table 3.1: Experimental energies associated with the investigated formic acid-halide complexes. (Note: N/A refers to values too large to observe with the $4.661$ eV laser.)

| | $Br^-$ (eV) | | $I^-$ (eV) | |
|---|---|---|---|---|
| | $^2P_{3/2}$ | $^2P_{1/2}$ | $^2P_{3/2}$ | $^2P_{1/2}$ |
| Bare halide | 3.380 | 3.813 | 3.114 | 4.003 |
| Complex | 4.191 | N/A | 3.874 | N/A |
| $E_{stab}$ | 0.811 | | 0.760 | |

The single peak observed in the formic acid-bromide spectrum (Figure 3.4) was thought to be a $^2P_{3/2}$ peak. The peak position as well as the experimental peak positions associated with bromide have been reported in Table 3.1.

The formic acid-iodide photoelectron spectrum is presented in Figure 3.5. Similarly to the formic acid-bromide spectrum, only the $^2P_{3/2}$ peak is observed. However, there is an additional peak located at approximately $4.213$ eV. This additional peak could possibly be due to a vibrational excitation of the neutral complex and will be discussed further in part 3.2.3.4.

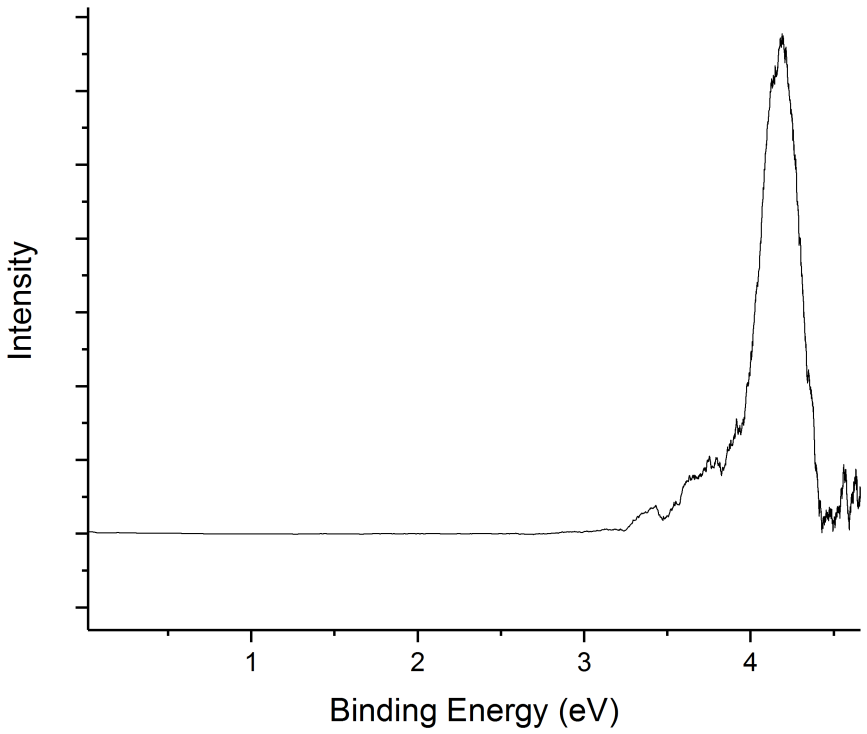


Figure 3.4: Photoelectron spectrum of the HCOOH $\cdots$ $Br^-$ complex.

The stabilisation energy ($E_{stab}$) is calculated slightly differently experimentally compared to theoretically. Experimentally, the stabilisation energy is the difference in energy between the bare halide and the complex. However, the computational stabilisation energy is calculated as the difference between the dissociation of the anion complex and the neutral complex. The stabilisation energies presented in Table 3.1, show a clear trend in that stabilisation energy decreases as the halide size increases.

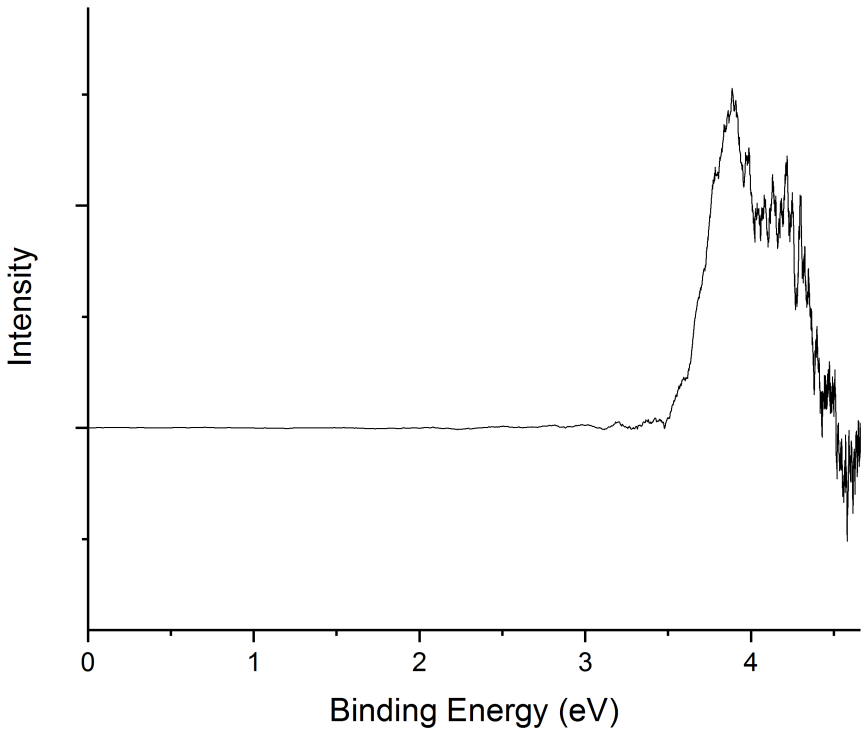


Figure 3.5: Photoelectron spectrum of the HCOOH $\cdots$ $I^-$ complex.

## 3.2 Computational Results

Before 'jumping' head-first into high level *ab initio* calculations, it can be instructive to first consider the system using a more basic method of analysis. Specifically, the system can be analysed using a multipole expansion to determine the likely points of interaction between a charge and the solvating species of interest. This is precisely what was initially carried out and can be seen in the case of formic acid interacting with a point negative charge in the next section.

### 3.2.1 Formic Acid Interacting with a Point Charge

An electrostatic analysis consisting of a multipole expansion was carried out for the *anti*- and *syn*-formic acid molecules interacting with a point charge (modelling the halide anions). The expansion was approximated and as such, the major interactions included were:

charge-dipole, charge-quadrupole and charge-octupole for the electrostatic interactions and charge-induced dipole for the induction interaction. The analysis was carried out based on the equations presented by Buckingham.[66] The potential energy contribution associated with the electrostatic interaction and induction interaction can be seen in equations 3.1 and 3.2

$$U_{elec} \approx T_i q\mu_i + \frac{1}{3}T_{ij}q\Theta_{ij} + \frac{1}{15}T_{ijk}q\Omega_{ijk} \tag{3.1}$$

$$U_{ind} \approx -\frac{1}{2}q^2\alpha_{ij}T_iT_j \tag{3.2}$$

The definitions of the parameters are as follows: q is electronic charge, $\mu_i$ is the dipole tensor, $\Theta_{ij}$ is the quadrupole tensor, $\Omega_{ijk}$ is the octupole tensor and $\alpha_{ij}$ is the polarizability tensor. The T tensors in equation 3.1 and 3.2 are presented below:

$$T_i = -R_iR^{-3}$$

$$T_{ij} = (3R_iR_j - R^2\delta_{ij})R^{-5}$$

$$T_{ijk} = -3(5R_iR_jR_k - R^2(R_i\delta_{jk} + R_j\delta_{ki} + R_k\delta_{ij}))R^{-7}$$

In the case of both conformers of formic acid, their respective dipole, quadrupole and octupole moments and polarizability were determined computationally by way of MP2/aug-cc-pVQZ calculations of the molecular geometries and can be found in Appendix C.

The potential energy associated with *anti*-formic acid interacting with a point charge has been shown in Figure 3.6. Importantly, it can be seen that the point charge has an attractive interaction with both the acidic and formyl hydrogens (stronger for the acidic hydrogen), whereas a repulsive interaction is observed with regard to the oxygen atoms. The result is an attractive interaction on the hydrogen side and a repulsive interaction on the oxygen side of the formic acid molecule. This agrees well with the *ab inito* results presented in subsequent sections. However, the description is only qualitative, since the halide anions are modelled by a point charge, meaning results cannot be used in a description of the differences in interaction associated with the different halides.

The potential energy associated with *syn*-formic acid interacting with a point charge can be

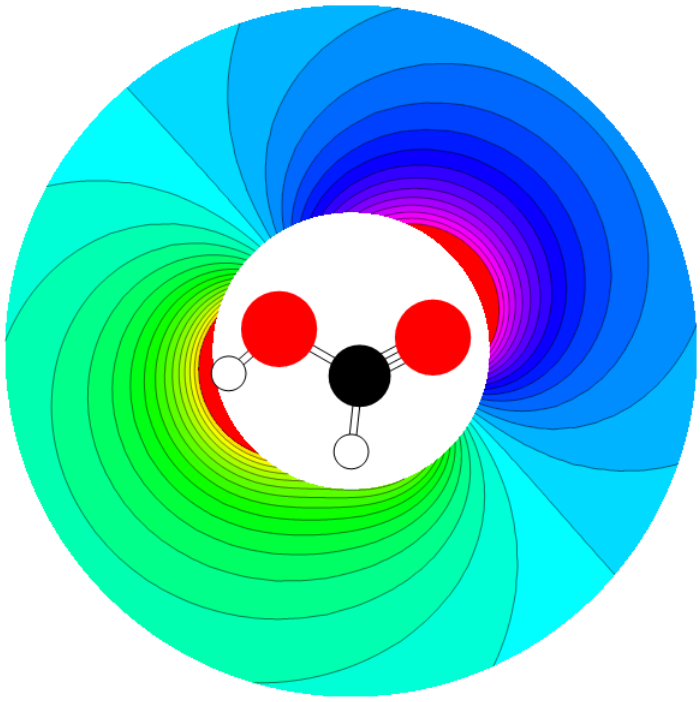

Figure 3.6: Potential energy of *anti*-formic acid interacting with a point charge. (Note: Blue indicates repulsion and green indicates attraction)

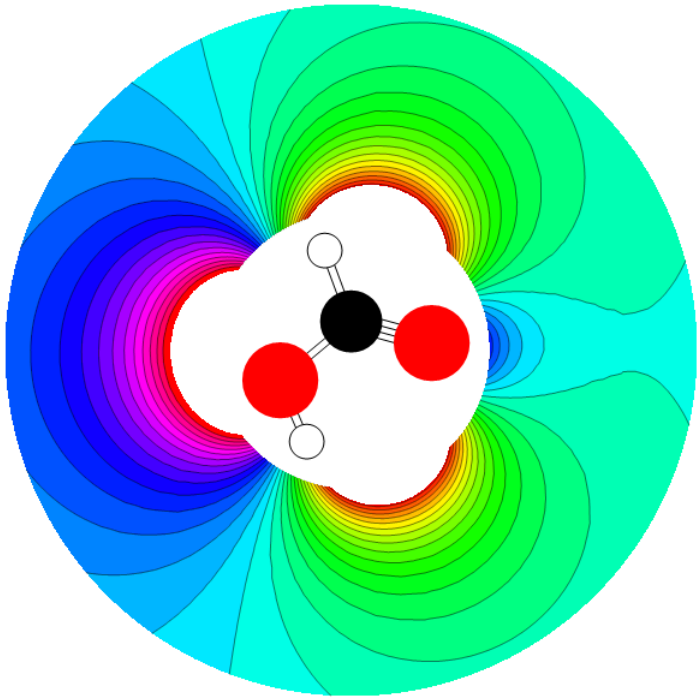

Figure 3.7: Potential energy of *syn*-formic acid interacting with a point charge. (Note: Blue indicates repulsion and green indicates attraction)

seen in Figure 3.7. Similarly to the alternative conformer, the point charge has attractive interactions with the two hydrogen atoms and repulsive interactions with the two oxygen atoms. Qualitatively, the multipole expansion appears to agree with the *ab initio* calculations to be presented. However, the relative strength of the interaction of the point charge with the acidic hydrogen and the point charge with formyl hydrogen appears to be similar, which was found not to be the case when the system was treated with *ab initio* methods.

The multipole expansion yielded qualitative results which aided in determining the approximate location of potential energy minima with regard to halide-formic acid complexes.

### 3.2.2 Formic Acid Halide Complexes

A number of different potential energy minima were discovered associated with the formic acid-halogen complex. Each anion and neutral geometry was optimised at the MP2/aug-cc-pVQZ (aug-cc-pV(Q+d)Z for Cl and aug-cc-pVQZ-PP for Br and I) level of theory. Single point energy calculations were then carried out as per the Computational Methods, which allowed parameters such as the dissociation energy and the vertical detachment energy (VDE) to be determined. The full set of computational results can be found in Appendix A, with important results being highlighted in this section. It should be noted that where structures are presented, the chlorine/chloride formic acid complex structure is presented, with structural parameters associated with the other halogens present.

The halides all behave in a relatively similar manner when interacting with a formic acid molecule, since the major interaction is the halide charge interacting with the formic acid moiety. As such, it was determined that there exists one minimum with regard to a halide interacting with the *anti*-formic acid conformer and two minima with regard to a halide interacting with the *syn*-formic acid conformer. This trend was observed for chloride, bromide and iodide, with fluoride acting differently in that the proton affinity of fluoride is higher than that of the formate anion.

#### 3.2.2.1 *anti*-Formic Acid Halide Minima

The *ab initio* calculations were found to be in agreement with the multipole expansion, since the halide- formic acid van der Waals complex minimum geometry was found to be one where the halide interacts with the acidic hydrogen of the formic acid. The geometry can be seen in Figure 3.8, no structural parameters have been reported for fluoride with regard to this geometry since fluoride did not possess this minimum geometry. In the case of the three halides, the geometry was found to be of $C_s$ symmetry. The distance from the acidic hydrogen to the halide increased with increasing halide size with the H$-$Cl$^-$ distance being $1.882$ Å and increasing to $2.305$ Å for iodide. The $\angle$O$-$H$-$Cl$^-$ angle was found to be $172.3°$ decreasing as the halide size increases. The fact that the halide is on the inside of the $\angle$O$-$H$-$Cl$^-$ angle suggests that there exists a slight attractive interaction between the halide and the formyl hydrogen.

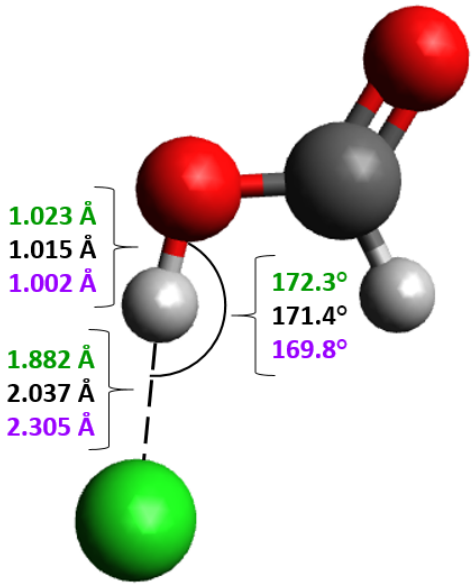


Figure 3.8: *anti*-Formic acid interacting with a halide. (Note: for all molecular geometry figures, blue values refer to F$^-$, green values refer to Cl$^-$, black values refer to Br$^-$ and purple values refer to I$^-$)

The O$-$H distance of bare formic acid was found to be approximately $0.963$ Å. From Figure 3.8, it can be seen that for all three halides, the O$-$H distance has increased as the bond elongates in order to move the hydrogen closer to the interacting halide. The energetics asso-

ciated with these three complexes have been summarised in Table 3.2. The chloride complex was found to be the most stable with a CCSD(T)/CBS dissociation energy of $130.2$ kJ/mol, the dissociation energy decreases as the halide size increases. This trend can be rationalised by the charge density of the halide decreasing as the atomic radius increases, the decreasing charge density implies a diminished binding ability to the formic acid.

Table 3.2: Summary of energetics of the *anti*-formic acid halide complex.

| Complex | MP2 | | | CCSD(T) | | |
|---|---|---|---|---|---|---|
| | $D_0$ | VDE (eV) | | $D_0$ | VDE (eV) | |
| | (kJ/mol) | $^2P_{3/2}$ | $^2P_{1/2}$ | (kJ/mol) | $^2P_{3/2}$ | $^2P_{1/2}$ |
| HCOOH $\cdots$ $Cl^-$ | 133.9 | 5.17 | 5.28 | 130.2 | 5.16 | 5.27 |
| HCOOH $\cdots$ $Br^-$ | 123.6 | 4.91 | 5.37 | 121.2 | 4.73 | 5.19 |
| HCOOH $\cdots$ $I^-$ | 111.2 | 4.11 | 5.06 | 105.2 | 4.11 | 5.05 |

The bromide and iodide CCSD(T) energies are aug-cc-pVTZ-PP energies rather than CBS energies.

#### 3.2.2.2 *syn*-Formic Acid Halide Minima

*syn*-Formic acid was found to exhibit two minimum geometries when interacting with a halide. One was similar to the acidic hydrogen appended minimum associated with the *anti*-formic acid molecule while the other minimum was found to consist of the halide appending to the formyl hydrogen. The acidic appended minimum does not exist for fluoride, while the formyl appended minimum does exist for fluoride.

The acidic hydrogen appended geometry is presented in Figure 3.9, which exhibited $C_s$ symmetry in the case of the three halides. The structure displays similarities with the *anti*-formic acid complex, but the halide is situated away from the carbonyl-oxygen. The halide-hydrogen distance was found to increase with increasing halide size and the O$-$H bond was found to be elongated (from a value of $0.969$ Å), with a decreasing degree of elongation with increasing halide size. The energetics associated with the *syn*-formic acid acidic hydrogen appended

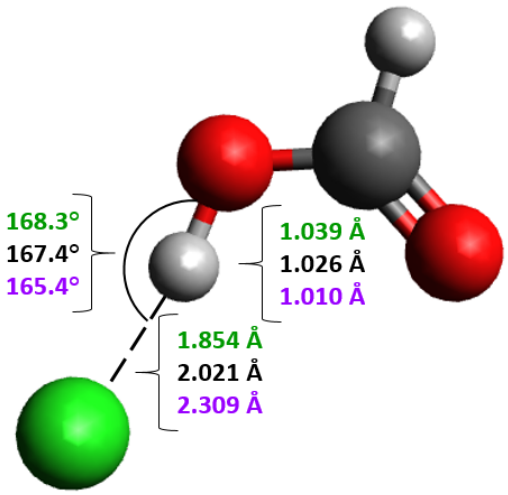


Figure 3.9: *syn*-Formic acid interacting with a halide, acidic hydrogen appended minimum.

halide complexes can be seen in Table 3.3. In a similar fashion to the *anti*-formic acid halide complex, the dissociation energy decreases with increasing halide size.

Table 3.3: Summary of energetics of the *syn*-formic acid halide acidic hydrogen appended complex.

| Complex | MP2 | | | CCSD(T) | | |
|---|---|---|---|---|---|---|
| | $D_0$ | VDE (eV) | | $D_0$ | VDE (eV) | |
| | (kJ/mol) | $^2P_{\frac{3}{2}}$ | $^2P_{\frac{1}{2}}$ | (kJ/mol) | $^2P_{\frac{3}{2}}$ | $^2P_{\frac{1}{2}}$ |
| $HCOOH \cdots Cl^-$ | 96.0 | 4.83 | 4.94 | 91.9 | 4.82 | 4.92 |
| $HCOOH \cdots Br^-$ | 85.6 | 4.56 | 5.01 | 83.1 | 4.52 | 4.98 |
| $HCOOH \cdots I^-$ | 74.7 | 3.75 | 4.69 | 68.1 | 3.75 | 4.67 |

The bromide and iodide CCSD(T) energies are aug-cc-pVTZ-PP energies rather than CBS energies.

The formyl hydrogen appended geometry can be seen in Figure 3.10, this is the only one of the three formic acid-halide geometries that allowed fluoride appending. Similarities are present between this minimum and that of the acidic hydrogen appended minimum. The halide forces an elongation of the C−H bond and the halide-hydrogen distance increases with the size of the halide.

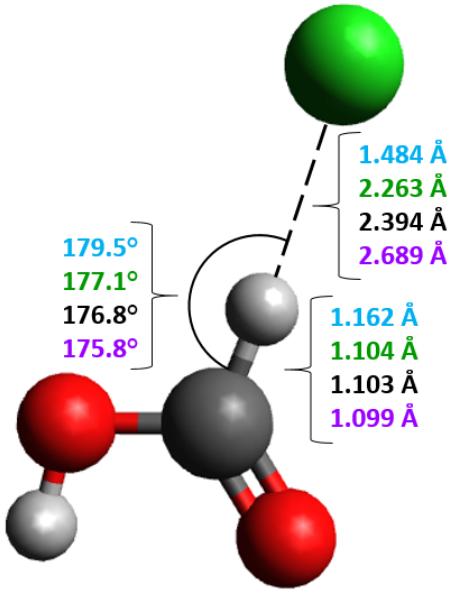


Figure 3.10: *syn*-Formic acid interacting with a halide, formyl hydrogen appended minimum.

Interestingly, the fluoride structure contains an almost linear interaction (i.e., $180°$) between the fluoride, hydrogen and carbon and the fluoride is significantly closer to the hydrogen compared to chloride (the difference is $0.779\,\text{Å}$). This suggests the fluoride interacts almost solely with the hydrogen and is not repelled significantly by the carbonyl-oxygen. The other three halides do appear to be repelled slightly by the electron density on the carbon and oxygen, shown by their non-straight $\angle \text{C}-\text{H}-\text{X}^-$ angle.

A summary of the energetics associated with the formyl hydrogen appended minimum are found in Table 3.4. The trends observed in both the dissociation energy and the VDE is very similar to the two other anion complexes. Specifically, both the dissociation energy and VDE decrease with halide size. The fluoride dissociation energy is significantly higher than the rest, it is approximately double that of the corresponding chloride complex. This is likely due to the fact that fluoride has an ionic radius much smaller than that of chloride and the other halides, meaning that fluoride can approach closer to the formic acid (as observed) forming a stronger interaction.

Table 3.4: Summary of energetics of the *syn*-formic acid halide formyl hydrogen appended complex.

| Complex | MP2 | | | CCSD(T) | | |
|---|---|---|---|---|---|---|
| | $D_0$ | VDE (eV) | | $D_0$ | VDE (eV) | |
| | (kJ/mol) | $^2P_{3/2}$ | $^2P_{1/2}$ | (kJ/mol) | $^2P_{3/2}$ | $^2P_{1/2}$ |
| HCOOH $\cdots$ $F^-$ | 90.2 | 4.67 | 4.72 | 95.6 | 4.50 | 4.55 |
| HCOOH $\cdots$ $Cl^-$ | 45.9 | 4.17 | 4.28 | 46.2 | 4.17 | 4.28 |
| HCOOH $\cdots$ $Br^-$ | 42.0 | 3.85 | 4.31 | 44.7 | 3.85 | 4.30 |
| HCOOH $\cdots$ $I^-$ | 37.5 | 3.42 | 4.35 | 37.6 | 3.42 | 4.36 |

The bromide and iodide CCSD(T) energies are aug-cc-pVTZ-PP energies rather than CBS energies.

#### 3.2.2.3 Fluoride: The Special Case

The fluoride anion is a special case, as was seen previously, fluoride does not form the acidic hydrogen appended minima associated with both the *anti*- and *syn*-formic acid conformers. Instead of appending to the acidic hydrogen, fluoride abstracts the hydrogen and forms a complex consisting of hydrogen fluoride and a formate anion. The case of abstraction from both the *anti* and *syn* conformer can be seen in Figures 3.11 and 3.12. Fluoride abstracts the hydrogen due to the proton affinity of the fluoride anion being larger than that of the formate anion, with the fluoride proton affinity being approximately $1555$ kJ/mol and the formate anion proton affinity being approximately $1449$ kJ/mol.[50]

These complexes are structurally very similar to the acidic hydrogen appended minima found for the other halides. Instead of the fluoride appending to the hydrogen, the hydrogen is abstracted and then appends to the oxygen from where it originated forming a van der Waals complex. By inspection of the two structures (Figures 3.11 and 3.12), it can be seen that the formate anion internal structure is almost identical in both cases. In each instance, the two C$-$O bonds are not the same length, the longer C$-$O bond belongs to the oxygen appending to the HF molecule. A 'free' formate anion has identical C$-$O bond lengths (approximately

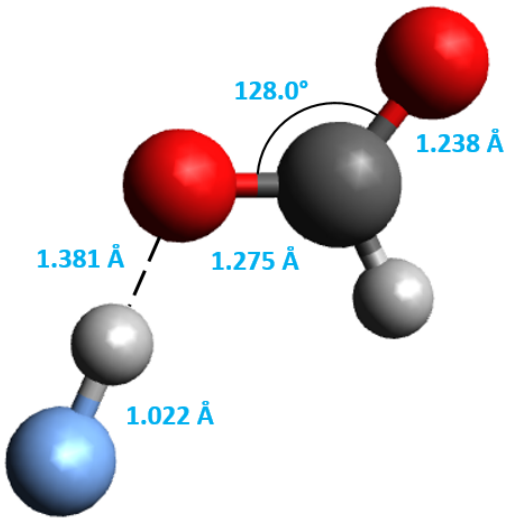


Figure 3.11: HF · · · HCOO⁻ complex resulting from hydrogen abstraction from the *anti*-formic acid conformer.

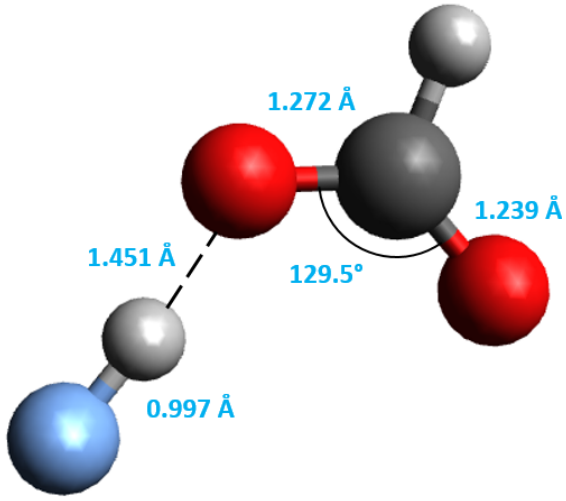


Figure 3.12: HF · · · HCOO⁻ complex resulting from hydrogen abstraction from the *syn*-formic acid conformer.

1.255 Å), since the negative charge is delocalised across both oxygen atoms. The fact that the complexes presented here do not have identical C−O bond lengths, and the fact that the longer C−O bond is the one to which the HF molecule appends, suggests that the charge is localised on the appending oxygen as opposed to both oxygens.

Table 3.5: Summary of energetics of the HF · · · HCOO⁻ complexes.

| | MP2 | CCSD(T) |
|---|---|---|
| Complex | $D_0$ (kJ/mol) ) | $D_0$ (kJ/mol) |
| *anti* HF · · · HCOO⁻ | 110.4 | 111.3 |
| *syn* HF · · · HCOO⁻ | 103.6 | 105.1 |

The dissociation energy determined for both complexes is presented in Table 3.5. The dissociation energy of both forms of the complex are relatively similar, deviating by approximately 6.8 kJ/mol at MP2/CBS and even less at CCSD(T)/CBS (decreasing to 6.2 kJ/mol). The slight difference in dissociation energy between the two complexes is likely due to the location of

the non-appending oxygen. That is, the oxygen not involved in the binding of the complex can either be on the same side of the complex as the HF molecule or the opposite side.

#### 3.2.2.4 Anion Minima Summary and Experimental Comparison

Chloride, bromide and iodide were found to behave similarly when forming complexes with formic acid, three minima were located for each halide. Fluoride was found to be the 'odd one out' abstracting the acidic hydrogen from the formic acid as opposed to appending to it. This behaviour was rationalised as being due to the difference in proton affinity between the formate anion and the fluoride anion.

The three minima found for the halides were: the acidic hydrogen appended minimum, existing for both the *anti*- and *syn*-formic acid conformers, and the formyl hydrogen appended minimum, which only existed for the *syn*-formic acid conformer. In comparing the chloride, bromide and iodide complexes, chloride-formic acid complexes featured the largest dissociation energy of the three halides, while the *anti*-formic acid acidic hydrogen appended minimum had the overall largest dissociation energy.

A Boltzmann distribution was used in order to determine which of the three anion complexes would be the more populous and the likely candidate to appear in the experimental study. The Boltzmann distribution was carried out by taking into account both the relative energy of the complexes and the relative energy of the *anti*- and *syn*-formic acid conformers. The result was that the *syn*-formic acid acidic hydrogen appended anion complex was by far the most populous in the case of all three considered halides, with a population percentage on the order of 99.9%. As such, it was assumed that the anion complex observed during experiment was the acidic hydrogen appended *syn*-formic acid complex.

The $^2P_{3/2}$ peak was located at approximately $4.191$ eV in the case of the formic acid-bromide experimental spectrum and at $3.874$ eV in the case of the formic acid-iodide spectrum. The acidic hydrogen appended minimum was found to have the $^2P_{3/2}$ peak at approximately

$4.56$ eV in the case of bromide and $3.75$ eV in the case of iodide (these are MP2/CBS values). Comparison of the experimental and computational values shows that the iodide values are relatively close to one another while the bromide values are far apart from one another. In terms of whether the experimental peak could be due to one of the other formic acid bromide complexes, this was thought to be unlikely since the respective energies of the other bromide complexes are $4.91$ eV and $3.85$ eV with regard to the remaining *anti* and *syn* complexes respectively.

The iodide values agree relatively well with one another, while the bromide values do not appear to be in agreement. However, due to the issues associated with calibration and drift of the experimental data, it is suggested that the computational results are more accurate than the experimental results.

### 3.2.3 Formic Acid Halogen Complexes

The halogens all behave in a similar fashion when interacting with formic acid, now that fluorine has no charge and hence there is no longer a large proton affinity, it follows the same bonding motifs as for the other halogens. The major interaction between the neutral halogen and formic acid is in the form of dispersion interactions. Even so, it was still found that some of the minima to be discussed did not exist for all four halides, which may be attributable to their polarisabilities and relative atomic sizes. For both the *anti*- and *syn*-formic acid conformer, complexes with chlorine were found to be most numerous with four chlorine-formic acid complexes associated with both conformers. As such, the structures presented are those with chlorine, where parameters associated with all four halides have been reported. Additionally, the calculated stabilisation energy ($E_{stab}$) has only been computed associated with the most populous anion complex (i.e., the acidic hydrogen appended *syn*-formic acid-halide complex) and the most stable neutral complex (which will be shown to be the double appended *syn*-formic acid minimum where the halide appends to both the acidic hydrogen and the carbonyl-oxygen).

#### 3.2.3.1 In plane Formic Acid Potential Energy Scan

Initially, a low level (MP2/aug-cc-pV(D+d)Z) scan was performed where a chlorine atom was revolved around a formic acid molecule. This was done both for *anti*- and *syn*-formic acid in order to produce a 'map' of the potential energy space associated with van der Waals complex formation. The two scans and there associated minima structures are presented in Figures 3.13 and 3.14.

In the case of both scans, three possible minima were located. With regard to the *anti*-formic acid scan, two of the three minima featured the chlorine appending to the carbonyl-oxygen (either side of the oxygen) and the third minimum was found to be appended to the acidic hydrogen. Similarly, the *syn*-formic acid scan resulted in two minima where the chlorine again appeared to be appended to the carbonyl oxygen and one minimum where the chlorine was appended to the hydroxyl-oxygen.

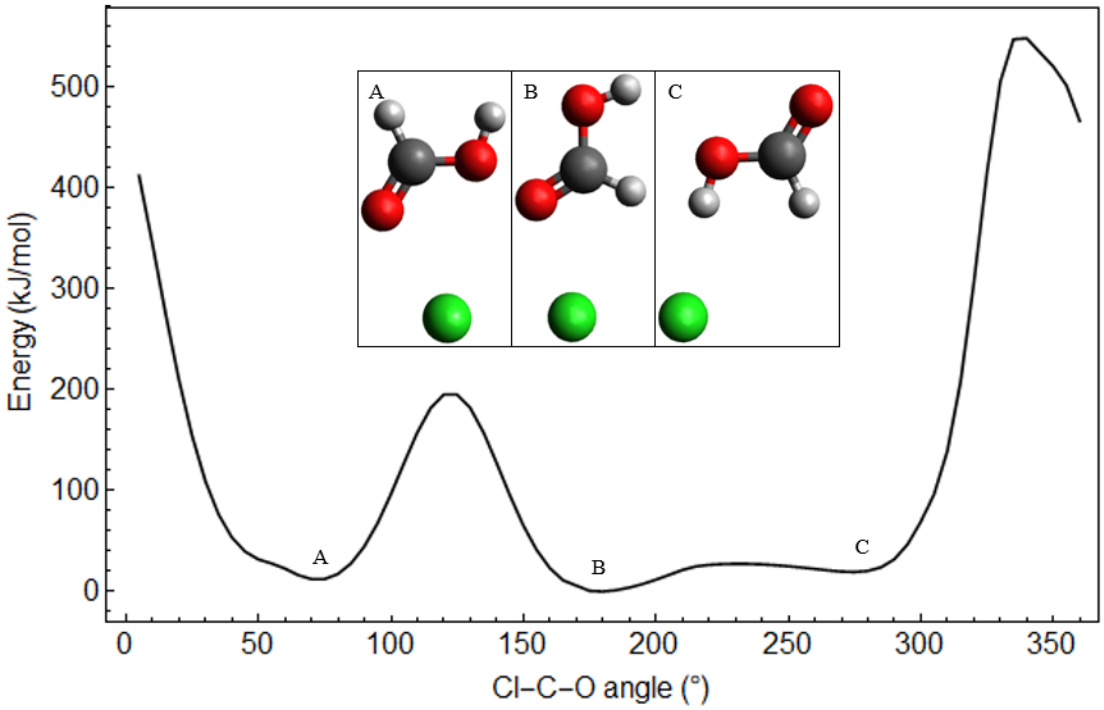


Figure 3.13: Potential energy scan of chlorine revolving around *anti*-formic acid.

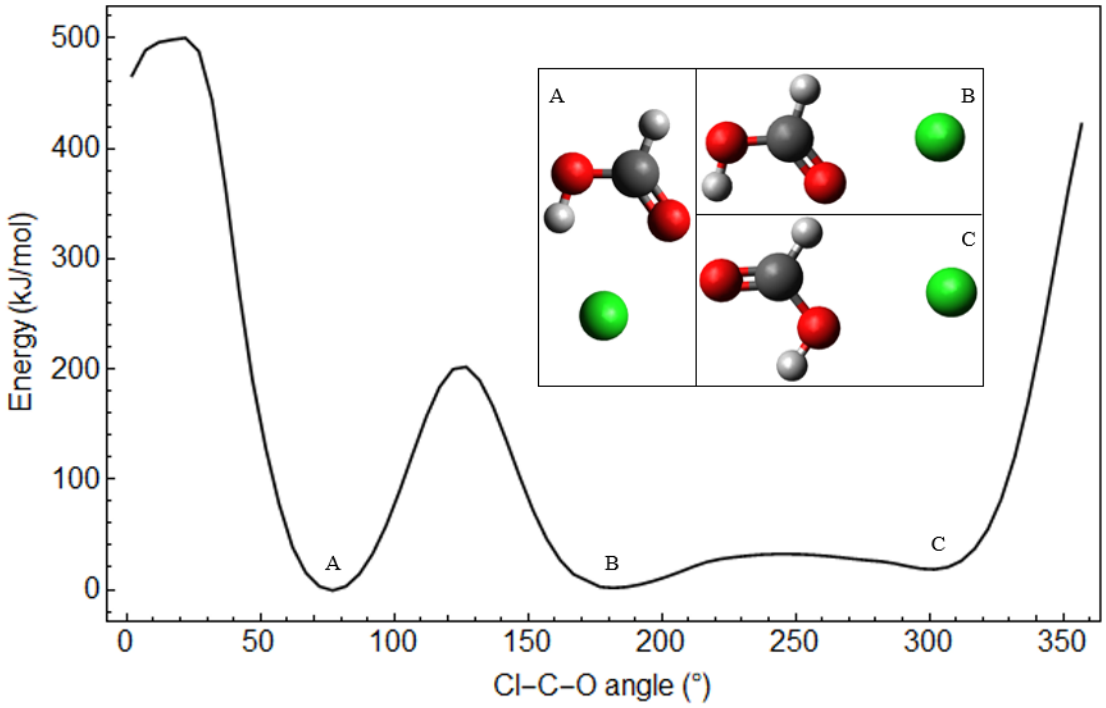


Figure 3.14: Potential energy scan of chlorine revolving around *syn*-formic acid.

#### 3.2.3.2 *anti*-Formic Acid Halogen Minima

The scan suggested three possible minimum energy geometries associated with chlorine interacting with *anti*-formic acid. A fourth minimum was later uncovered where by the chlorine was located out of the molecular plane (i.e., $C_1$ symmetry) and appended to the hydroxyl-oxygen. The electron affinity (EA) reported in the case of each neutral complex was determined by calculating the difference in energy between the anion and neutral complex. The electron affinities associated with fluorine complexes have not been reported since there exists no *anti*-formic acid complex with fluoride to which the neutral complexes can be compared. It was observed that the fluorine complex dissociation energies were markedly different when moving from MP2 to CCSD(T), the exact reason for this is unknown, however it could be due to the fact that the CCSD(T) energy is calculated using the MP2 structures such that the CCSD(T) energy is not associated with an optimised CCSD(T) geometry.

The carbonyl-oxygen appended structure with the halogen on the hydroxyl side can be seen in Figure 3.15. The halogen is appended to the carbonyl-oxygen, with the possibility of

slight interaction with the hydroxyl-oxygen. The halogen-oxygen distance increases with the halogen size, while the $\angle$C$-$O$-$X angle appears initially to decrease with halogen size. However, the angle then increases when moving from bromine to iodine, which could stem from the iodine size, which being the largest of the four halogens, may not be able to fit in the minimum energy pocket, forcing the increase in angle.

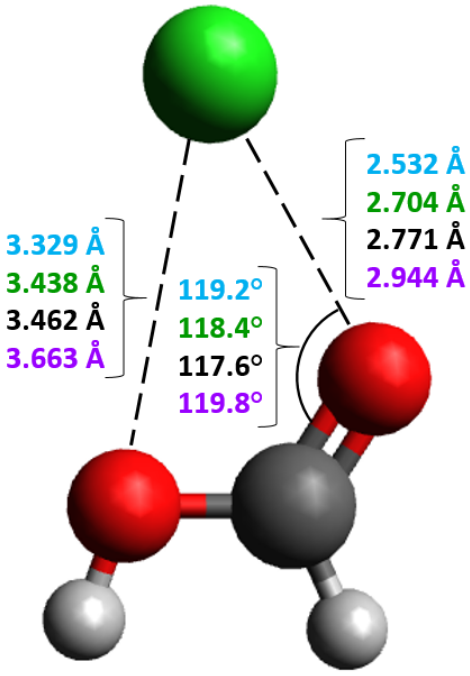


Figure 3.15: *anti*-Formic acid interacting with a halogen, carbonyl-oxygen appended minimum.

The dissociation energy and electron affinities have been summarised in Table 3.6. In general, the dissociation energy increases with halogen size, which can be rationalised by the magnitude of dispersion interaction increasing as the number of electrons associated with the halogen increases. The MP2 and CCSD(T) EA values are in relatively good agreement with the MP2 prediction appearing to slightly overestimate the respective electron affinities.

Table 3.6: Summary of energetics of the *anti*-formic acid halogen carbonyl-oxygen appended complex.

| Complex | MP2 | | | CCSD(T) | | |
|---|---|---|---|---|---|---|
| | $D_0$ | EA (eV) | | $D_0$ | EA (eV) | |
| | (kJ/mol) | $^2P_{\frac{3}{2}}$ | $^2P_{\frac{1}{2}}$ | (kJ/mol) | $^2P_{\frac{3}{2}}$ | $^2P_{\frac{1}{2}}$ |
| HCOOH $\cdots$ F | 4.7 | - | - | 7.5 | - | - |
| HCOOH $\cdots$ Cl | 11.4 | 4.88 | 4.99 | 12.1 | 4.84 | 4.95 |
| HCOOH $\cdots$ Br | 14.6 | 4.49 | 4.95 | 15.1 | 4.46 | 4.92 |
| HCOOH $\cdots$ I | 19.0 | 4.01 | 4.96 | 15.7 | 3.99 | 4.93 |

The bromine and iodine CCSD(T) energies are aug-cc-pVTZ-PP energies rather than CBS energies.

The carbonyl-oxygen appended structure featuring the halogen on the non-hydroxyl side is shown in Figure 3.16. The halogen-oxygen distance increases with halogen size, as does the angle made by the halogen with the carbonyl double bond. This geometry is very similar to the halogen-formaldehyde neutral complex, studied previously in the Wild group.[67] The similarity is not surprising as the carbonyl side of the formic acid molecule resembles that of formaldehyde with a carbonyl group and a hydrogen bonded to the carbon. As an example, the formaldehyde-halogen study found the formaldehyde-chlorine complex to display an angle to the carbonyl bond of $106.3^\circ$ and an oxygen-chlorine distance of $2.550$ Å.[67]

The energetics associated with the complex are provided in Table 3.7. Similarly, to the previous complex, the dissociation energy increases with halogen size, since the dispersion interaction increases as the electron number on the halogen increases. Relating this back to the formaldehyde-halogen study, the formaldehyde-chlorine complex was reported to have an MP2/CBS dissociation energy of $9.9$ kJ/mol,[67] compared with $10.8$ kJ/mol found in the current study associated with formic acid. The striking similarity seen both in terms of geometry and dissociation energy suggests that the carbonyl section of the formic acid molecule is similar to a formaldehyde molecule.

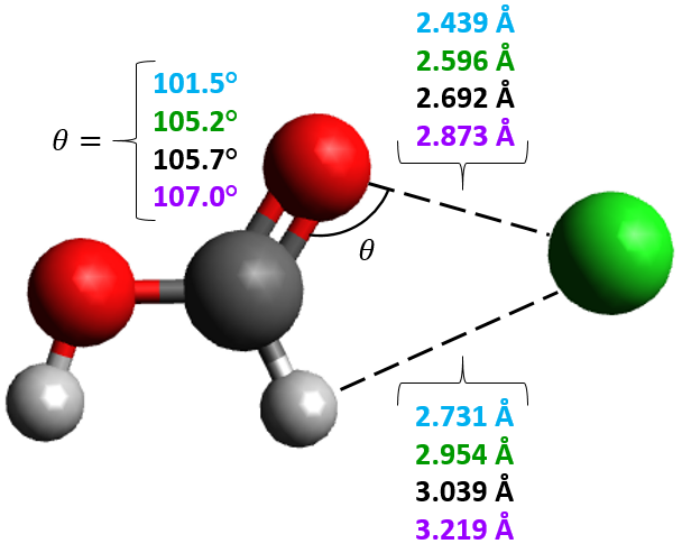


Figure 3.16: *anti*-Formic acid interacting with a halogen, carbonyl-oxygen appended minimum.

Table 3.7: Summary of energetics of the *anti*-formic acid halogen carbonyl-oxygen appended complex.

| Complex | MP2 | | | CCSD(T) | | |
|---|---|---|---|---|---|---|
| | $D_0$ | EA (eV) | | $D_0$ | EA (eV) | |
| | (kJ/mol) | $^2P_{3/2}$ | $^2P_{1/2}$ | (kJ/mol) | $^2P_{3/2}$ | $^2P_{1/2}$ |
| HCOOH · · · F | 5.7 | - | - | 10.5 | - | - |
| HCOOH · · · Cl | 10.8 | 4.86 | 4.97 | 14.8 | 4.81 | 4.92 |
| HCOOH · · · Br | 16.7 | 4.47 | 4.93 | 17.4 | 4.44 | 4.90 |
| HCOOH · · · I | 20.9 | 3.99 | 4.94 | 17.5 | 3.97 | 4.91 |

The bromine and iodine CCSD(T) energies are aug-cc-pVTZ-PP energies rather than CBS energies.

The ability of a halogen to append to the acidic hydrogen is thought to stem from the ability of the polar O−H bond to polarise the halogen electron cloud, thus forming a dipole-induced dipole interaction. Such a structure can be seen in Figure 3.17, this minimum was only observed associated with chlorine and iodine. The halogen-hydrogen distance is larger than the

distance associated with the corresponding anion minimum, which had a H $\cdots$ Cl distance of 1.882 Å.

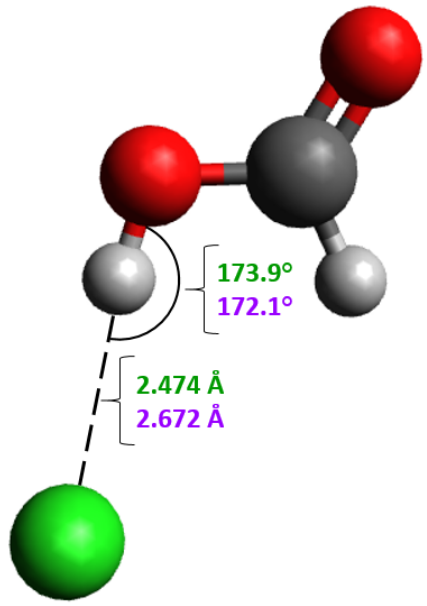


Figure 3.17: *anti*-Formic acid interacting with a halogen, acidic hydrogen appended minimum.

Attempts were made to optimise this geometry with regard to both fluorine and bromine however, both displayed a single imaginary vibrational mode when optimised, which for fluorine was a vibrational mode corresponding to out of plane motion, while for bromine was a vibrational mode in the formic acid molecular plane. Essentially, it appears that fluorine and bromine did not have a favourable interaction with the acidic hydrogen. Polarisability increases with increasing electron number, so bromine should be more polarisable than chlorine. However, polarisation is only one factor determining the interaction, the other being the halogen size. In particular, if the halogen is too large (less dense electron cloud) the interaction may not be strong enough to form a stable complex. From this point of view then, one explanation of the halogen behaviour could be that fluorine is not polarisable enough to interact favourably, chlorine is polarisable enough and also small enough to approach closer to the hydrogen, bromine is more polarisable than chlorine and so should be able to interact, however may be too large an atom and finally, iodine is larger than bromine, but also has more electrons so has a larger polarisability.

Table 3.8: Summary of energetics of the *anti*-formic acid halogen acidic hydrogen appended complex.

| Complex | MP2 | | | CCSD(T) | | |
|---|---|---|---|---|---|---|
| | $D_0$ | EA (eV) | | $D_0$ | EA (eV) | |
| | (kJ/mol) | $^2P_{3/2}$ | $^2P_{1/2}$ | (kJ/mol) | $^2P_{3/2}$ | $^2P_{1/2}$ |
| HCOOH $\cdots$ Cl | 7.7 | 4.92 | 5.03 | 7.4 | 4.89 | 5.00 |
| HCOOH $\cdots$ I | 15.8 | 4.05 | 4.99 | 14.7 | 4.00 | 4.94 |

The iodine CCSD(T) energies are aug-cc-pVTZ-PP rather than CBS energies.

The dissociation energies listed in Table 3.8 show the previously observed trend of increasing dissociation energy with increasing halogen size. By comparison of the dissociation energies associated with the acidic hydrogen appended complex and the two carbonyl-oxygen appended complexes, it can be seen that this complex (the acidic hydrogen appended complex) is the least stable with a dissociation energy approximately $3$ kJ/mol less than the other two.

The fourth and final complex geometry associated with *anti*-formic acid was a $C_1$ symmetry geometry displayed in Figure 3.18. This structure was found to only exist for chlorine, with fluorine, bromine and iodine unable to optimise to yield the structure. It is anticipated that (much like with the acidic hydrogen appended geometry) the interaction is again largely due to halogen polarisability and the discriminating factor is the halogen atomic radius. Culminating in only chlorine appearing to meet the criteria allowing for a favourable interaction.

The dissociation energy (seen in Table 3.9) is comparable to that of the chlorine acidic hydrogen appended geometry. The chlorine-oxygen distance associated with this geometry is larger than the other three presented geometries, possibly explaining why the dissociation energy is less than the carbonyl-oxygen appended minima.

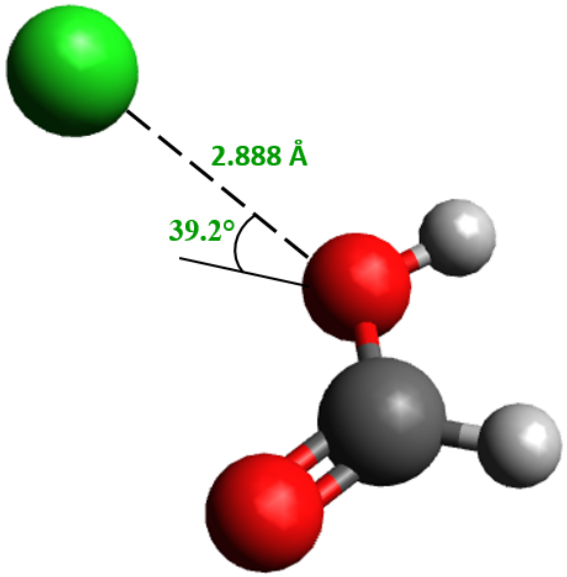


Figure 3.18: *anti*-Formic acid interacting with chlorine, out-of-plane minimum.

Table 3.9: Summary of energetics of the *anti*-formic chlorine out-of-plane complex.

| Complex | MP2 | | | CCSD(T) | | |
|---|---|---|---|---|---|---|
| | $D_0$ (kJ/mol) | EA (eV) $^2P_{3/2}$ | $^2P_{1/2}$ | $D_0$ (kJ/mol) | EA (eV) $^2P_{3/2}$ | $^2P_{1/2}$ |
| HCOOH $\cdots$ Cl | 7.5 | 4.92 | 5.03 | 7.6 | 4.88 | 4.99 |

#### 3.2.3.3 *syn*-Formic Acid Halogen Minima

The initial potential energy scan located three possible geometries with regard to the *syn*-formic acid-chlorine complex. A fourth minimum was subsequently found with a geometry so as to append to the acidic hydrogen. The complex with double appended halogen on both the carbonyl-oxygen and the acidic hydrogen was found to be the most stable neutral complex. As such, the stabilisation energy has been reported only for this complex calculated with respect to the acidic hydrogen appended *syn*-formic acid anion complex (which was shown earlier to be by far the most populous). Electron affinities have been reported with reference to the anion acidic hydrogen appended complex in the case of each halide. Therefore, electron affinities have not been reported for the fluorine containing complexes as the acidic

hydrogen appended anion geometry does not exist.

The neutral complex with the largest dissociation energy with respect to all four halides was found to be a double appended complex with the halogen appended to the carbonyl-oxygen and the acidic hydrogen simultaneously. The geometry is shown in Figure 3.19, in the case of each halogen, the distance to the hydrogen and the distance to the oxygen is the shortest such distance when compared to the other neutral complexes for both formic acid conformers. This suggests that the halogen is relatively strongly bound. The halogen formic acid distance follows the standard observed trend whereby the distance increases with halogen size. It could be hypothesised that the binding strength of the complex arises from the O−H bond resulting in a slightly positive hydrogen while the C=O bond results in a relatively negative oxygen. This together could mean that the halogen is polarised and has a slight increase in electron density near the hydrogen and a slight decrease in electron density near the oxygen, leading to favourable interactions with both atoms.

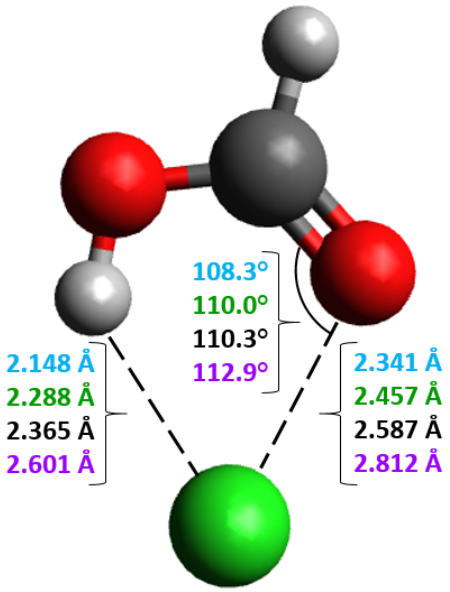


Figure 3.19: *syn*-Formic acid interacting with a halogen, carbonyl-oxygen and acidic hydrogen double appended complex.

The (relatively) large dissociation energies have been summarised in Table 3.10. A large

Table 3.10: Summary of energetics of the *syn*-formic double appended halogen complex.

| Complex | MP2 | | | | CCSD(T) | | | |
|---|---|---|---|---|---|---|---|---|
| | $D_0$ (kJ/mol) | EA (eV) $^2P_{3/2}$ | EA (eV) $^2P_{1/2}$ | $E_{stab}$ (eV) | $D_0$ (kJ/mol) | EA (eV) $^2P_{3/2}$ | EA (eV) $^2P_{1/2}$ | $E_{stab}$ (eV) |
| HCOOH $\cdots$ F | 7.1 | - | - | 0.86 | 17.3 | - | - | 0.81 |
| HCOOH $\cdots$ Cl | 19.1 | 4.41 | 4.52 | 0.80 | 22.6 | 4.33 | 4.44 | 0.72 |
| HCOOH $\cdots$ Br | 23.1 | 4.01 | 4.47 | 0.65 | 24.6 | 3.97 | 4.43 | 0.61 |
| HCOOH $\cdots$ I | 26.7 | 3.55 | 4.49 | 0.49 | 22.5 | 3.53 | 4.47 | 0.47 |

The bromine and iodine CCSD(T) energies are aug-cc-pVTZ-PP energies rather than CBS energies.

deviation (on the order of $10.2$ kJ/mol) can be seen for the fluorine complex between MP2 and CCSD(T). The difference between MP2 and CCSD(T) with regard to fluorine was highlighted earlier, and may be an artefact of the CCSD(T) energy being based on an optimised MP2 geometry. The fact that the CCSD(T)/aug-cc-pVTZ-PP dissociation energy of the iodine complex is less than that of the bromine complex appears nonsensical and could also be an artefact of the calculations. These issues aside, this geometry was found to be the most stable formic acid-halogen complex and for this reason has stabilisation energies with reference to the anion complex reported. The computational $E_{stab}$ values decrease with increasing halogen size, this can be understood by the dissociation energy of the anion complex decreasing with increasing halide size while the neutral complex dissociation energy increases with increasing halogen size. The result is a decrease in $E_{stab}$, since it represents the difference in dissociation energy of the neutral and anion complexes.

The second carbonyl-oxygen appended structure is presented in Figure 3.20, this geometry was found to be very similar to the carbonyl-oxygen appended minimum associated with *anti*-formic acid with the halogen on the non-hydroxyl side of the carbonyl. The carbonyl-halogen angle and the halogen-oxygen distance were found to be analogous to the complex discussed earlier, and again the geometry is very similar to that of formaldehyde interacting

with a halogen.[67]

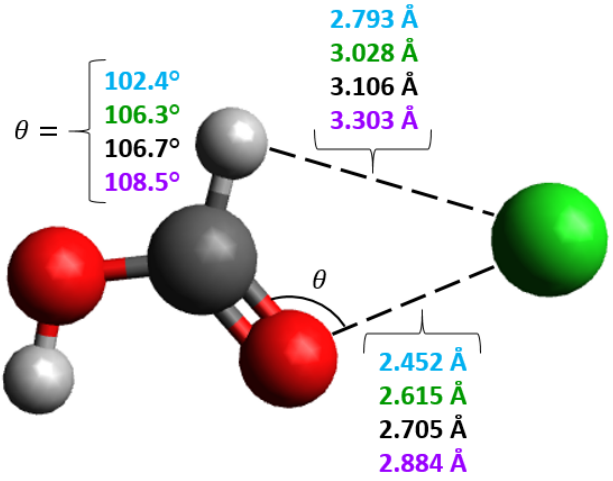


Figure 3.20: *syn*-Formic acid interacting with a halogen, carbonyl-oxygen appended complex.

The dissociation energies and electron affinities have been summarised in Table 3.11. The dissociation energies associated with this geometry were found to be remarkably similar to the analogous geometry optimised for the *anti*-formic acid conformer (e.g., the CCSD(T)/CBS dissociation energy associted with the *anti*-formic acid-chlorine complex was 14.8 kJ/mol, and the same energy with regard to the current geometry is 14.1 kJ/mol).

Table 3.11: Summary of energetics of the *syn*-formic acid halogen carbonyl-oxygen appended complex.

| Complex | MP2 | | | CCSD(T) | | |
|---|---|---|---|---|---|---|
| | $D_0$ | EA (eV) | | $D_0$ | EA (eV) | |
| | (kJ/mol) | $^2P_{3/2}$ | $^2P_{1/2}$ | (kJ/mol) | $^2P_{3/2}$ | $^2P_{1/2}$ |
| HCOOH · · · F | 5.5 | - | - | 9.9 | - | - |
| HCOOH · · · Cl | 13.0 | 4.47 | 4.58 | 14.1 | 4.20 | 4.53 |
| HCOOH · · · Br | 15.9 | 4.09 | 4.54 | 16.5 | 4.05 | 4.51 |
| HCOOH · · · I | 19.7 | 3.62 | 4.56 | 16.4 | 3.59 | 4.54 |

The bromine and iodine CCSD(T) energies are aug-cc-pVTZ-PP energies rather than CBS energies.

The hydroxyl-oxygen appended complex can be seen in Figure 3.21. This geometry is similar to that displayed by *anti*-formic acid with the halogen appending to the hydroxyl-oxygen out of the plane, with the chlorine-oxygen distances being very similar (2.880 Å for the $C_1$ symmetry complex). Unlike the out of plane geometry, this complex was found to occur for all four halogens.

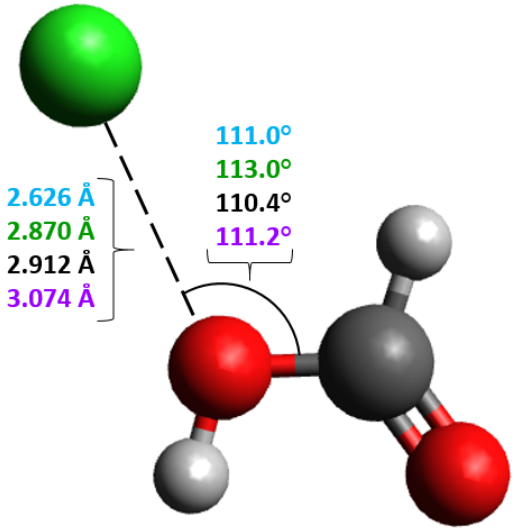


Figure 3.21: *syn*-Formic acid interacting with a halogen, hydroxyl-oxygen appended complex.

The energetics associated with the in-plane hydroxyl-oxygen appended complex can be seen in Table 3.12. Unlike, other geometries, the CCSD(T) energies were only calculated using a triple zeta basis set, since the quadruple zeta energies required to extrapolate to the CBS limit did not converge. Comparing the chlorine complex dissociation energy to the out-of-plane geometry, the two are very close (identical CCSD(T)/CBS dissociation energies). However, the respective electron affinities are different (out of plane: 4.88 eV and 4.99 eV for $^2P_{3/2}$ and $^2P_{1/2}$ respectively).

Table 3.12: Summary of energetics of the *syn*-formic acid halogen hydroxyl-oxygen appended complex.

| Complex | MP2 | | | CCSD(T)/aug-cc-pVTZ | | |
|---|---|---|---|---|---|---|
| | $D_0$ (kJ/mol) | EA (eV) $^2P_{3/2}$ | EA (eV) $^2P_{1/2}$ | $D_0$ (kJ/mol) | EA (eV) $^2P_{3/2}$ | EA (eV) $^2P_{1/2}$ |
| HCOOH $\cdots$ F | 3.4 | - | - | 5.3 | - | - |
| HCOOH $\cdots$ Cl | 7.4 | 4.53 | 4.64 | 7.6 | 4.34 | 4.44 |
| HCOOH $\cdots$ Br | 9.9 | 4.15 | 4.61 | 10.7 | 4.12 | 4.57 |
| HCOOH $\cdots$ I | 13.5 | 3.68 | 4.63 | 11.1 | 3.65 | 4.59 |

Similarly to *anti*-formic acid, a geometry where the halogen appears appended to the acidic hydrogen was optimised with regard to *syn*-formic acid. This geometry is presented in Figure 3.22, where it also becomes apparent that the structure was found to exist only in the case of chlorine and iodine. This is reminiscent to the *anti*-formic acid acidic hydrogen appended neutral structure, which was also found only to exist in the case of chlorine and iodine. Again, attempts were made to optimise the geometry in relation to both fluorine and bromine, with both cases proving to be unsuccessful. This led to the conclusion that fluorine and bromine were unable to interact favourably with the acidic hydrogen, leading to the same conclusion as with the similar *anti*-formic acid geometry, namely that the interaction is driven by both polarisability and halogen size. As discussed previously, as the halogens increase in size their polarisability also increases.

The dissociation energies and electron affinities associated with the acidic hydrogen appended minimum can be found in Table 3.13. Comparing these dissociation energies with those of the other three *syn*-formic acid minima, it becomes clear that the acidic hydrogen minimum is the least tightly held (lowest dissociation energy) complex. Comparing the *anti*- and *syn*-formic acid acidic hydrogen appended minima, it can be seen that the *syn* minimum has the lower dissociation energy (7.7 kJ/mol compared to 5.9 kJ/mol). This could be due to slight repulsion between the carbonyl-oxygen and the halogen atom.

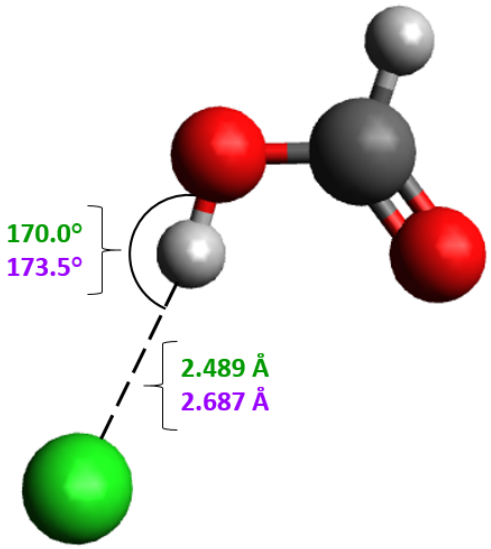


Figure 3.22: *syn*-Formic acid interacting with a halogen, acidic-hydrogen appended complex.

Table 3.13: Summary of energetics of the *syn*-formic acid halogen acidic hydrogen appended complex.

| Complex | MP2 | | | CCSD(T) | | |
|---|---|---|---|---|---|---|
| | $D_0$ | EA (eV) | | $D_0$ | EA (eV) | |
| | (kJ/mol) | $^2P_{3/2}$ | $^2P_{1/2}$ | (kJ/mol) | $^2P_{3/2}$ | $^2P_{1/2}$ |
| HCOOH $\cdots$ Cl | 5.9 | 4.55 | 4.66 | 5.6 | 4.51 | 4.62 |
| HCOOH $\cdots$ I | 12.4 | 3.69 | 4.64 | 11.7 | 3.64 | 4.59 |

The iodine CCSD(T) energies are aug-cc-pVTZ-PP energies rather than CBS energies.

#### 3.2.3.4 Neutral Minima Summary and Comparison with Experiment

In general, fluorine, chlorine, bromine and iodine were found to behave in a similar manner when interacting with formic acid. Four minimum geometries were located in the case of each formic acid conformer.

With regard to *anti*-formic acid, two carbonyl-oxygen appended minima were located as well

as a hydroxyl-oxygen appended minimum and an acidic hydrogen appended minimum. The out-of-plane hydroxyl-oxygen appended minimum was found to only exist for chlorine while the acidic hydrogen appended minimum was found only for chlorine and iodine. With regard to *syn*-formic acid, again two carbonyl-oxygen appended minima were localised, one of these was a double appended structure which also interacted favourably with the acidic hydrogen. The two remaining geometries were an acidic hydrogen appended minimum and an in-plane hydroxyl-oxygen appended structure.

In the case of both formic acid conformers, one of the carbonyl-appended minima was very similar to the formaldehyde-halogen minimum with the corresponding dissociation energies very close to one another. This is suggestive that the O−C−H side of the formic acid molecule can be approximated as formaldehyde when considering loosely-bound complexes. Both conformers also displayed an acidic hydrogen appended minimum, found to only exist for chlorine and iodine. The discriminating factor determining which halogen was able to interact was thought to be the polarisability and atomic radius. Specifically, the polar O−H bond can polarise the halogen forming a dipole-induced dipole interaction.

The stabilisation energies found by way of experiment and computation do not agree with one another. However, the relative trend is conserved in both sets of results. That is, as the halogen size increases, the stabilisation energy decreases, since the dissociation energy of the anion complex decreases with halide size while the neutral complex dissociation energy increases with halogen size.

In the experimental iodide-formic acid photoelectron spectrum (see Figure 3.5) a second peak was observed located approximately $0.339\,\text{eV}$ ($\approx 2700\,\text{cm}^{-1}$) higher than the main $^2P_{3/2}$ peak. It is possible that this peak may be due to excitation to a higher vibrational level of the neutral complex. The iodide double appended (carbonyl-oxygen and acidic hydrogen) *syn*-formic acid complex was found to have C−H and O−H stretch frequencies at $3128\,\text{cm}^{-1}$ and $3602\,\text{cm}^{-1}$ respectively (calculated at MP2/aug-cc-pVTZ-PP). Since these frequencies were

calculated using a harmonic approximation, the 'actual' frequencies would be lower.

### 3.2.4 Literature Comparison

The dissociation energies associated with the chloride, bromide and iodide formic acid complexes have been determined previously by way of experiment. For comparison, the literature results were assumed to be associated with the *syn*-formic acid acidic hydrogen appended geometry, and the comparison with literature values can be seen in Table 3.14, where a note should be made that the literature experimental method required calculation of the vibrational frequencies of the complex. The vibrational frequencies were computed using a semi-empirical method,[11] which may impact the accuracy of their results slightly. The dissociation energies do not appear to be very close to the literature values. However, the trend has been predicted correctly and they appear to be on the same scale.

Table 3.14: Formic acid-halide dissociation energy comparison

| | Computational $D_0$ (kJ/mol) | Literature[11] $D_0$ (kJ/mol) | |
|---|---|---|---|
| | | 0 K | 298 K |
| $HCOOH \cdots Cl^-$ | 96.0 | 114±9 | 116±9 |
| $HCOOH \cdots Br^-$ | 85.6 | 70±7 | 72±7 |
| $HCOOH \cdots I^-$ | 74.7 | 52±9 | 54±9 |

The MP2/CBS energies were used in each case for consistency.

A final point of comparison has been done with regard to other halide complexes. Specifically, the dissociation and stabilisation energy of the complex of chloride with *syn*-formic acid has been compared with previously studied chloride-complexes. The chloride complexes chosen for comparison are those of: acetylene, carbon-monoxide, formaldehyde, acetone and water. The comparison can be seen in Table 3.15, with acetylene, carbon-monoxide, acetone

and water having experimental stabilisation energies and computational dissociation energies. In contrast, both the dissociation energy and stabilisation energy are computational (CCSD(T)/CBS) with regard to formic acid and formaldehyde.

Table 3.15: Comparison of $HCOOH \cdots Cl^-$ with other chloride complexes.

| | $D_0$ (kJ/mol) | $E_{stab}$ (eV) |
|---|---|---|
| $HCCH \cdots Cl^-$ [18] | 16.5 | 0.50 |
| $CO \cdots Cl^-$ [17] | 16.8 | 0.16 |
| $CH_2O \cdots Cl^-$ [67] | 49.6 | 0.358 |
| $CH_3COCH_3 \cdots Cl^-$ [67] | 59.2 | 0.683 |
| $H_2O \cdots Cl^-$ [16,50] | 60.0 | 0.76 |
| $HCOOH \cdots Cl^-$ | 91.9 | 0.80 |

Comparing the dissociation and stabilisation energies of different complexes, it becomes apparent that, generally, as the dipole moment increases, so too does the strength of the interaction. Although, the formic acid-chloride complex dissociation energy appears much larger than that of water, it does appear that formic acid is comparable to water when considering halide complexes.

In Chapter 1, a computational study of the chlorine radical reaction with formic acid was presented. The main conclusion of the study is that the predominant reaction pathway was abstraction of the formyl hydrogen.[7] Focussing on the dominant form of formic acid (i.e., *syn*-formic acid), the study located two of the four minima located as part of this thesis. Namely, the carbonyl-oxygen appended minimum presented in Figure 3.20 and the acidic hydrogen appended minimum presented in Figure 3.22.[7] With the carbonyl-oxygen appended structure suggested to be a pre-reaction adduct for formyl hydrogen abstraction and the acidic hydrogen appended structure suggested to be an acidic hydrogen abstraction pre-reaction adduct.[7] The double appended minimum found to be the most stable as part of this project does not

feature in the literature study and neither does the hydroxyl-oxygen appended minimum. A study of the reaction of formic acid with a hydroxyl radical was also presented in Chapter 1, this study found acidic hydrogen abstraction to occur preferentially due to the formation of a pre-reaction adduct which interacts with both the carbonyl-oxygen and the acidic hydrogen. This double appended hydroxyl radical minimum has a similar structure to the double appended minimum found with regard to the chlorine radical.

The chlorine radical reaction with formic acid has been experimentally investigated, and found to preferentially occur via formyl hydrogen abstraction.[68] Therefore, the conclusion of the theoretical study that formyl hydrogen abstraction is the dominant abstraction channel is not questioned. However, adding the double appended chlorine pre-reaction adduct 'into the mix' it would be interesting to determine the relative change (if any) in the importance of the acidic hydrogen abstraction channel.

# Chapter 4

# Conclusions and Future Work

The overarching aim of this work was to produce photoelectron spectra and computationally investigate the formic acid-halide complexes. In terms of phototelectron spectra, the bromide and iodide formic acid complexes were studied. However, as was pointed-out, the calibration had major issues associated with photoelectron drift and as such it is suggested that these spectra as well as the formic acid chloride spectrum should be re-taken.

The *ab initio* investigation was conducted for both anion and neutral complexes of formic acid with fluorine, chlorine, bromine and iodine in an attempt to produce a complete picture of the halide-formic acid interactions. These calculations allowed the determination of dissociation energies, etc. The geometries were optimised using the MP2 method with quadruple zeta basis sets. The next step is to optimise using the CCSD(T) method.

Visually inspecting an optimised geometry can provide a 'guess' as to the type interaction stabilising the complex. However, in future, the optimised complex geometries will be investigated using symmetry adapted perturbation theory (SAPT). SAPT decomposes the interaction energy (dissociation energy) into individual interaction components.[69] In other words, the amount of dispersion interaction, induction interaction, etc. can be determined.

As the slow electron velocity imaging setup is implemented in the Wild group, the formic

acid-halide complexes should be investigated to provide more accurate spectroscopic data. On a final note, this formic acid study can be thought of as the inception of a large-scale study investigating the interactions of larger carboxylic acid containing molecules with halogens.

# References


[1] Prather, M. J.; McElroy, M. B.; Wofsy, S. C. *Nature*. **1984**, *312*, 227-231.

[2] Wayne, R. P. *Chemistry of Atmospheres*, 3 rd Ed, Oxford University Press, New York, 2000.

[3] Chaliyakunnel, S.; Millet, D. B.; Wells, K. C.; Cady-Pereira, K. E.; Shepard, M. W. *Environ. Sci. Technol*. **2016**, *50*, 5631-5640.

[4] Stavrakou, T.; Mller, J-F.; Peeters, J.; Razavi, A.; Clarisee, L.; Clerbaux, C.; Coheur, P-F.; Hurtmans, D.; De Mazire, M.; Vigouroux, C.; Deutscher, N. M.; Griffith, D. W. T.; Jone, N.; Paton-Walsh, C. *Nat. Geosci*. **2012**, *5*, 26-30.

[5] Anglada, J. M. *J. Am. Chem. Soc*. **2004**, *126*, 9809-9820.

[6] Singh, H. B.; Kasting, J. F. *J. Atmos. Chem*. **1988**, *7*, 261-285.

[7] Ng, M.; Mok, D. K. W.; Lee, E. P. F.; Dyke, J. M. *Mol. Phys*. **2015**, *113*, 1511- 1533.

[8] Neumark, D. M. *Phys. Chem. Chem. Phys*. **2005**, *7*, 433-442.

[9] IUPAC, 1999, *71*, 1968 (van der Waals complexes (IUPAC Compendium of Chemical Terminology 2006)).

[10] French, M. A.; Ikuta, S.; Kebale, P. *Can. J. Chem*. **1982**, *60*, 1907-1918.

[11] Walker, B. W.; Sunderlin, L. S. *Int. J. Mass Spectrom*. **1999**, *184*, 183-199.

[12] Ziegler, B. E.; Gamble, T. N.; Li, C.; McMahon, T. B. *J. Phys. Chem. A*. **2013**, *117*, 5785-5793.

[13] Asmis, K. R.; Taylor, T. R.; Neumark, D. M. *Chem. Phys. Lett*. **1998**, *295*, 75-81.

[14] Vogelhuber, K. M; Wren, S. W.; Shaffer, C. J.; McMahon, R. J.; McCoy, A. B.; Lineberger, W. C. *J. Chem. Phys*. **2011**, *135*, 204307.

[15] Oliveira, A. M.; Lehman, J. H.; McCoy, A. B.; Lineberger, W. C. *J. Chem. Phys*. **2016**, *145*, 124317.

[16] Markovich, G.; Pollack, S. Giniger, R.; Cheschnovsky, O. *J. Chem. Phys*. **1994**, *101*, 9344-9353.

[17] Lapere, K. M.; LaMacchia, R. J.; Quak, L. H.; Kettner, M.; Gale, S. G.; McKinley, A. J.; Wild, D. A. *J. Phys. Chem. A*. **2012**, *116*, 3577-3584.

[18] Beckham, D. A. R.; Conran, S.; Lapere, K. M.; Kettner, M.; McKinley, A. J.; Wild, D. A. *Chem. Phys. Lett*. **2015**, *619*, 241-246.

[19] Lapere, K. M.; Kettner, M.; Watson, P. D.; McKinley, A. J.; Wild, D. A. *J. Phys. Chem. A*. **2015**, *119*, 9722-9728.

[20] Zirz, C.; Ahlrichs, R. *Theoret. Chim. Acta*. **1981**, *60*, 355-361.

[21] Mardyukov, A.; Quanz, H.; Schreiner, P. R. *Nat. Chem*. **2017**, *9*, 71-76.

[22] Marushkevich, K.; Khiachtchev, L.; Räsänen, M. *J. Phys. Chem. A. Lett*. **2007**, *111*, 2040-2042.

[23] Marushkevich, K.; Rsnen, M.; Khiachtchev, L. *J. Phys. Chem. A*. **2010**, *114*, 10584-10589.

[24] Hocking, W. H. Z. *Naturforsch*. **1976**, *31*, 1113-1121.

[25] Robertson, W. H.; Kelley, J. A.; Johnson, M. A. *J. Chem. Phys*. **2000**, *113*, 7879- 7884.

[26] Goerigk, L.; Grimme, S. *Phys. Chem. Chem. Phys*. **2011**, *13*, 6670-6688.

[27] Born, M.; Oppenheimer, R. *Ann. D. Phys*. **1927**, *84*, 457-484.

[28] Sutcliffe, B. T.; Woolley, R. G. *J. Chem. Phys*. **2012**, *137*, 22A544.

[29] Hasanein, A. A.; Evans, M. W. *Computational Methods in Quantum Chemistry: Quantum Chemistry Vol. 2*, World Scientific, Singapore, 1996.

[30] Lewars, E. G. *Computational Chemistry: Introduction to the Theory and Applications of Molecular and Quantum Mechanics*, $2^{nd}$ Ed, Springer, Dordrecht, 2011.

[31] Møller, C.; Plesset, M. S. *Phys. Rev*. **1934**, *46*, 618-622.

[32] Jung, Y.; Lochan, R. C.; Dutoi, A. D.; Head-Gordon, M. *J. Chem. Phys*. **2004**, *121*, 9793-9802.

[33] Foresman,J. B.; Firsch. *Æ. Exploring Chemistry with Electronic Structure Methods*, Gaussian Inc., U.S.A.

[34] Pople, J. A.; Krishnan, R.; Schlegel, H. B.; Binkley, J. S. *Int. J. Quantum Chem*. **1978**, *14*, 545-560.

[35] Bartlett, R. J.; Purvis, G. D. *Int. J. Quantum Chem*. **1978**, *14*, 561-581.

[36] Ramabhadran, R. O.; Raghavachari, K. *J. Chem. Theory Comput*. **2013**, *9*, 3986-3994.

[37] Neumark, D. M. *J. Phys. Chem. A*. **2008**, *112*, 13287-13301.

[38] Takashima, K.; Riveros, J. M. *Mass Spectrom. Rev*. **1998**, *17*, 409-430.

[39] Sanow, A.; Mabbs, R. *Int. Rev. Phys. Chem*. **2008**, *27*, 53-85.

[40] Wild, D. A.; Bieske, E. J. *Int. Rev. Phys. Chem*. **2003**, *22*, 129-151.

[41] Lapere, K. M. L. Anion Photoelectron Spectroscopy of Halide Complexes and Clusters. Ph.D. Thesis, University of Western Australia, August 2014.

[42] DePuy, C. H. *Int. J. Mass Spectrom*. **2000**, *200*, 79-96.

[43] Brehm, B.; Gusinow, M. A.; Hall, J. L. *Phys, Rev. Lett*. **1967**, *19*, 737-741.

[44] Wiley, W. C.; McLaren, I. H. *Rev. Sci. Instrum*. **1955**, *26*, 1150-1157.

[45] LaMacchia, R. Towards Anion Photoelectron Spectroscopy of Complexes and Clusters. B. Sc (Hons). Thesis, University of Western Australia, November 2008.

[46] Kettner, M. Aspects of Gas-Phase Anion Spectrosopy. Ph.D. Thesis, University of Western Australia, September 2015.

[47] Koperski, J.; Fry, E. S. *J. Phys. B: At. Mol. Opt. Phys*. **2006**, *39*, S1125-S1150.

[48] Kruit, P.; Read, F. H. *J. Phys. E: Sci. Instrum*. **1983**, *16*, 313-324.

[49] Cheshnovsky, O.; Yang, S. H.; Pettiette, C. L.; Craycraft, M. J.; Smalley, R. E. *Rev. Sci. Instrum*. **1987**, *58*, 2131-2137.

[50] Bartmess, J.E. "Negative Ion Energetics Data" in **NIST Chemistry WebBook, NIST Standard Reference Database Number 69**, Linstrom, P. J.; Mallard, W. G. Eds., National Institute of Standards and Technology, Gaithersburg MD, 20899.

[51] Mooney J.; Kambhampati, P. *J. Phys. Chem. Lett*. **2013**, *4*, 3316-3318.

[52] Gaussian 09, Revision D.01, Frisch, M. J.; Trucks, G. W.; Schlegel, H. B.; Scuseria, G. E.; Robb, M. A.; Cheeseman, J. R.; Scalmani, G.; Barone, V.; Mennucci, B.; 18Petersson, G. A.; Nakatsuji, H.; Caricato, M.; Li, X.; Hratchian, H. P.; Izmaylov, A. F.; Bloino, J.; Zheng, G.; Sonnenberg, J. L.; Hada, M.; Ehara, M.; Toyota, K.; Fukuda, R.; Hasegawa, J.; Ishida, M.; Nakajima, T.; Honda, Y.; Kitao, O.; Nakai, H.; Vreven, T.; Montgomery Jr., J. A.; Peralta, J. E.; Ogliaro, F.; Bearpark, M.; Heyd, J. J.; Brothers, E.; Kudin, K. N.; Staroverov, V. N.; Kobayashi, R.; Normand, J.; Raghavachari, K.; Rendell, A.; Burant, J. C.; Iyengar, S. S.; Tomasi, J.; Cossi, M.; Rega, N.; Millam, J. M.; Klene, M.; Knox, J. E.; Cross, J. B.; Bakken, V.; Adamo, C.; Jaramillo, J.; Gomperts, R.; Stratmann, R. E.; Yazyev, O.; Austin, A. J.; Cammi, R.; Pomelli, C.; Ochterski, J. W.; Martin, R. L.; Morokuma, K.; Zakrzewski, V. G.; Voth, G. A.; Salvador, P.; Dannenberg, J. J.; Dapprich, S.; Daniels, A. D.; Farkas, O.; Foresman, J. B.; Ortiz, J. V.; Cioslowski, J.; Fox, D. J. Gaussian, Inc., Wallingford CT, 2013.

[53] Dunning, Jr., T. H. *J. Chem. Phys*. **1989**, *90*, 1007-1023.

[54] Kendall, R. A.; Dunning, Jr., T. H.; Harrison, R. J. *J. Chem. Phys*. **1992**, *96*, 6796- 6806.

[55] Woon, D. E.; Dunning, Jr., T. H. *J. Chem. Phys*. **1993**, *98*, 1358-1371.

[56] Dunning, Jr., T. H.; Peterson, K. A.; Wilson, A. K. *J. Chem. Phys*. **2001**, *114*, 9244-9253.

[57] Peterson, K. A.; Figgen, D.; Goll, E.; Stoll, H.; Dolg, M. *J. Chem. Phys*. **2003**, *119*, 11113-11123.

[58] Feller D. *J. Comp. Chem*. **1996**, *17*, 1571-1586.

[59] Schuchardt, K. L.; Didier, B. T.; Elsethagen, T.; Sun, L.; Gurumoorthi, V.; Chase, J.; Li, J.; Windus, T. L. *J. Chem. Inf. Model*. **2007**, *47*, 1045-1052.

[60] Karton, A.; Rabinovich, E.; Martin, J. M. L.; Ruscic, B. *J. Chem. Phys*. **2006**, *125*, 144108.

[61] Karton, A.; Martin, J. M. L. *J. Chem. Phys*. **2012**, *136*, 124114.

[62] Karton, A.; Martin, J. M. L. *Theor. Chem. Acc*. **2006**, *115*, 330-333.

[63] Helgaker, T.; Klopper, W. *J. Chem. Phys*. **1997**, *106*, 9639-9646.

[64] Gutowski, M.; Jordan, K. D.; Skurski, P. *J. Phys. Chem. A*. **1998**, *102*, 2624-2633.

[65] Bachorz, R. A.; Haranczyk, M.; Dabkowska, I.; Rak, J.; Gutowski, M. *J. Chem. Phys*. **2005**, *122*, 204304.

[66] Buckingham, A. D. Permanent and Induced Molecular Moments and Long-Range Intermolecular Forces. In *Advances in Chemical Physics: Intermolecular Forces*, Hirschfelder, J. O, Eds.; John Wiley & Sons, Inc.:New Jersey, 1967; 12, 107-142.

[67] Corkish, T. R. Interactions Between Halogens and the Simplest Carbonyls, Formaldehyde and Acetone. B. Sc (Hons). Thesis, University of Western Australia, November 2016.

[68] Tyndall, G. S.; Wallington, T. J.; Potts, A. R. *Chem. Phys. Lett*. **1991**, *186*, 149-153.

[69] Heßelmann, A.; Korona. T. *J. Chem Phys*. **2014**, *141*, 094107.

# Appendix A

# Data and Tables

Table A.1: MP2/aug-cc-pVQZ geometry of the *anti*- and *syn*-formic acid molecules.

| Atom | *anti* | | | *syn* | | |
|---|---|---|---|---|---|---|
| | X | Y | Z | X | Y | Z |
| C | -0.130537 | 0.363252 | 0.000000 | 0.000000 | 0.421633 | 0.000000 |
| O | 1.055953 | -0.281231 | 0.000000 | -1.032152 | -0.437920 | 0.000000 |
| H | 1.767149 | 0.368380 | 0.000002 | -0.650154 | -1.327916 | 0.000000 |
| O | -1.174467 | -0.219402 | 0.000000 | 1.160152 | 0.106771 | 0.000000 |
| H | -0.035813 | 1.457169 | 0.000000 | -0.373845 | 1.447307 | 0.000000 |

Table A.2: Energies of the *anti*- and *syn*-formic acid molecules.

| | MP2 | | | CCSD(T) | | | |
|---|---|---|---|---|---|---|---|
| | Q | 5 | CBS | D | T | Q | CBS |
| *anti* | -189.533755 | -189.553244 | -189.571129 | -189.348753 | -189.511013 | -189.560949 | -189.589307 |
| *syn* | -189.540518 | -189.560031 | -189.577942 | -189.355475 | -189.517731 | -189.567679 | -189.596061 |

Table A.3: Vibrational frequencies of *anti*- and *syn*-formic acid calculated at MP2/aug-cc-pVQZ.

| *anti* | | *syn* | |
|---|---|---|---|
| Frequency ($cm^{-1}$) | Intensity (km/mol) | Frequency ($cm^{-1}$) | Intensity (km/mol) |
| 533 | 84.2 | 629 | 41.3 |
| 659 | 10.6 | 681 | 134.7 |
| 1038 | 0.1 | 1061 | 3.5 |
| 1120 | 51.5 | 1133 | 265.2 |
| 1277 | 314.8 | 1305 | 16.8 |
| 1423 | $< 0.1$ | 1411 | 1.4 |
| 1837 | 275.4 | 1798 | 332.8 |
| 3042 | 60.2 | 3128 | 31.4 |
| 3825 | 87.8 | 3756 | 81.4 |

Table A.4: MP2/aug-cc-pVQZ geometry of the *anti*- and *syn*-formic acid-fluoride complexes. (Note: the acidic hydrogen was abstracted in the case of both acidic appended minima)

| Atom | *anti*-FA acidic H appeneded | | | *syn*-FA acidic H appended | | | *syn*-FA formyl H appended | | |
|---|---|---|---|---|---|---|---|---|---|
| | X | Y | Z | X | Y | Z | X | Y | Z |
| C | 0.852784 | -0.249683 | 0.000000 | -1.149569 | 0.315151 | 0.000000 | 0.390544 | -0.136701 | 0.000002 |
| O | -0.041596 | 0.659668 | 0.000000 | 0.000000 | 0.859969 | 0.000000 | 0.985761 | 1.105469 | 0.000000 |
| H | -1.329007 | 0.160923 | 0.000000 | 1.231146 | 0.092383 | 0.000000 | 1.933355 | 0.903053 | -0.000002 |
| O | 2.083002 | -0.107909 | 0.000000 | -1.452830 | -0.886460 | 0.000000 | 1.108267 | -1.120891 | -0.000001 |
| H | 0.451674 | -1.287217 | 0.000000 | -1.984995 | 1.052904 | 0.000000 | -0.769665 | -0.077107 | 0.000004 |
| $F^-$ | -2.285624 | -0.198854 | 0.000000 | 2.141545 | -0.313807 | 0.000000 | -2.251020 | 0.013070 | -0.000001 |



Table A.5: Energies of the *anti*- and *syn*-formic acid-fluoride complexes. (Note: zero-point energy calculated at MP2/aug-cc-pVQZ)

| Fluoride Complexes | ZPE | corrected ZPE | MP2 | | | CCSD(T) | | | |
|---|---|---|---|---|---|---|---|---|---|
| | (kJ/mol) | (kJ/mol) | Q | 5 | CBS | D | T | Q | CBS |
| *anti*-FA acidic H appended | 86.25 | 3.54 | -289.400524 | -289.430725 | -289.458305 | -289.106644 | -289.353141 | -289.430410 | -289.474432 |
| *syn*-FA acidic H appended | 86.91 | 3.51 | -289.398066 | -289.428320 | -289.455944 | -289.104206 | -289.350720 | -289.428076 | -289.424504 |
| *syn*-FA formyl H appended | 87.22 | 4.03 | -289.349159 | -289.379506 | -289.407252 | -289.0605480 | -289.303299 | -289.380491 | -289.472131 |

Table A.6: MP2/aug-cc-pV(Q+d)Z geometry of the *anti*- and *syn*-formic acid-chloride complexes.

| Atom | *anti*-FA acidic H appeneded | | | *syn*-FA acidic H appended | | | *syn*-FA formyl H appended | | |
|---|---|---|---|---|---|---|---|---|---|
| | X | Y | Z | X | Y | Z | X | Y | Z |
| C | -1.055133 | 0.467383 | 0.000000 | -1.055133 | 0.467383 | 0.000000 | -1.055133 | 0.467383 | 0.000000 |
| O | -1.902346 | -0.595215 | 0.000000 | -1.902346 | -0.595215 | 0.000000 | -1.902346 | -0.595215 | 0.000000 |
| H | -2.785697 | -0.200043 | 0.000000 | -2.785697 | -0.200043 | 0.000000 | -2.785697 | -0.200043 | 0.000000 |
| O | -1.475064 | 1.603703 | 0.000000 | -1.475064 | 1.603703 | 0.000000 | -1.475064 | 1.603703 | 0.000000 |
| H | 0.000000 | 0.141653 | 0.000000 | 0.000000 | 0.141653 | 0.000000 | 0.000000 | 0.141653 | 0.000000 |
| $Cl^-$ | 2.125634 | -0.636107 | 0.000000 | 2.125634 | -0.636107 | 0.000000 | 2.125634 | -0.636107 | 0.000000 |

Table A.7: Energies of the *anti*- and *syn*-formic acid-chloride complexes. (Note: zero-point energy calculated at MP2/aug-cc-pVQZ)

| Chloride Complexes | ZPE | corrected ZPE | MP2 | | | CCSD(T) | | | |
|---|---|---|---|---|---|---|---|---|---|
| | (kJ/mol) | (kJ/mol) | Q | 5 | CBS | D | T | Q | CBS |
| *anti*-FA acidic H appended | 89.54 | 3.20 | -649.388367 | -649.416296 | -649.442679 | -649.141607 | -649.368479 | -649.439649 | -649.480808 |
| *syn*-FA acidic H appended | 87.43 | 3.28 | -649.379654 | -649.407572 | -649.433946 | -649.132803 | -649.359563 | -649.430700 | -649.471850 |
| *syn*-FA formyl H appended | 90.39 | 2.35 | -649.361727 | -649.389636 | -649.415990 | -649.118022 | -649.343094 | -649.414364 | -649.455554 |

Table A.8: MP2/aug-cc-pVQZ-PP geometry of the *anti*- and *syn*-formic acid-bromide complexes.

| Atom | *anti*-FA acidic H appeneded | | | *syn*-FA acidic H appended | | | *syn*-FA formyl H appended | | |
|---|---|---|---|---|---|---|---|---|---|
| | X | Y | Z | X | Y | Z | X | Y | Z |
| C | 1.882945 | 0.886596 | 0.000000 | 1.565350 | 1.909306 | 0.000000 | 0.191873 | 1.895603 | 0.000000 |
| O | 0.719453 | 1.505178 | 0.000000 | 0.269688 | 1.704761 | 0.000000 | 1.523273 | 2.160339 | 0.000000 |
| H | 0.000000 | 0.789568 | 0.000000 | 0.000000 | 0.714418 | 0.000000 | 1.579525 | 3.126392 | 0.000000 |
| O | 2.956217 | 1.457055 | 0.000000 | 2.462356 | 1.092562 | 0.000000 | -0.628907 | 2.785712 | 0.000000 |
| H | 1.785229 | -0.206841 | 0.000000 | 1.767270 | 2.991477 | 0.000000 | 0.000000 | 0.809680 | 0.000000 |
| $Br^-$ | -1.213950 | -0.845719 | 0.000000 | -0.943306 | -1.072581 | 0.000000 | -0.282448 | -1.567946 | 0.000000 |

Table A.9: Energies of the *anti*- and *syn*-formic acid-bromide complexes. (Note: zero-point energy calculated at MP2/aug-cc-pVTZ-PP)

| Bromide Complexes | ZPE | corrected ZPE | MP2 | | | CCSD(T) |
|---|---|---|---|---|---|---|
| | (kJ/mol) | (kJ/mol) | Q | 5 | CBS | T |
| *anti*-FA acidic H appended | 89.72 | 2.89 | -605.479181 | -605.585514 | -605.694484 | -605.39417 |
| *syn*-FA acidic H appended | 87.88 | 2.89 | -605.470420 | -605.576785 | -605.685794 | -605.385351 |
| *syn*-FA formyl H appended | 90.29 | 3.48 | -605.454505 | -605.560980 | -605.670087 | -605.371641 |

Table A.10: MP2/aug-cc-pVQZ-PP geometry of the *anti*- and *syn*-formic acid-iodide complexes.

| Atom | *anti*-FA acidic H appeneded | | | *syn*-FA acidic H appended | | | *syn*-FA formyl H appended | | |
|---|---|---|---|---|---|---|---|---|---|
| | X | Y | Z | X | Y | Z | X | Y | Z |
| C | -0.349857 | -2.541520 | 0.000000 | -0.080039 | -2.989215 | 0.000000 | -0.152528 | -2.473730 | 0.000000 |
| O | 0.848412 | -1.980843 | 0.000000 | -0.930499 | -1.983926 | 0.000000 | 1.117323 | -2.945028 | 0.000000 |
| H | 0.712011 | -0.987847 | 0.000000 | -0.479315 | -1.080489 | 0.000000 | 1.023803 | -3.908138 | 0.000000 |
| O | -0.529376 | -3.741128 | 0.000000 | 1.130068 | -2.950028 | 0.000000 | -1.110272 | -3.212416 | 0.000000 |
| H | -1.165156 | -1.807212 | 0.000000 | -0.637002 | -3.937064 | 0.000000 | -0.165046 | -1.375213 | 0.000000 |
| $I^-$ | 0.000000 | 1.204150 | 0.000000 | 0.000000 | 1.177820 | 0.000000 | 0.000000 | 1.309156 | 0.000000 |



Table A.11: Energies of the *anti*- and *syn*-formic acid-iodide complexes. (Note: zero-point energy calculated at MP2/aug-cc-pVTZ-PP)

| Iodide Complexes | ZPE | corrected ZPE | MP2 | | | CCSD(T) |
|---|---|---|---|---|---|---|
| | (kJ/mol) | (kJ/mol) | Q | 5 | CBS | T |
| *anti*-FA acidic H appended | 89.98 | 2.57 | -484.622177 | -484.702110 | -484.783423 | -484.534013 |
| *syn*-FA acidic H appended | 88.47 | 2.47 | -484.613740 | -484.693701 | -484.775044 | -484.525698 |
| *syn*-FA formyl H appended | 90.22 | 1.75 | -484.601309 | -484.680951 | -484.761943 | -484.514757 |

Table A.12: Vibrational frequencies of the *anti*- and *syn*-formic acid-fluoride complexes calculated at MP2/aug-cc-pVQZ.

| *anti*-FA acidic H appended | | *syn*-FA acidic H appended | | *syn*-FA formyl H appended | |
|---|---|---|---|---|---|
| Frequency ($cm^{-1}$) | Intensity (km/mol) | Frequency ($cm^{-1}$) | Intensity (km/mol) | Frequency ($cm^{-1}$) | Intensity (km/mol) |
| 112 | 2.5 | 94 | 2.2 | 138 | 3.9 |
| 120 | 17.9 | 142 | 8.2 | 264 | 0.8 |
| 359 | 104.5 | 351 | 66.5 | 271 | 179.5 |
| 783 | 47.5 | 740 | 15.6 | 617 | 133.1 |
| 1065 | 0.4 | 1056 | 3.7 | 689 | 110.0 |
| 1205 | 68.3 | 1142 | 77.9 | 992 | 507.6 |
| 1279 | 0.4 | 1164 | 43.8 | 1244 | 27.2 |
| 1365 | 349.6 | 1351 | 222.7 | 1293 | 7.7 |
| 1406 | $<$0.1 | 1401 | 5.1 | 1491 | 142.0 |
| 1661 | 1428.0 | 1663 | 964.3 | 1660 | 572.3 |
| 2198 | 2672.9 | 2590 | 3063.3 | 2200 | 1369.0 |
| 2867 | 291.3 | 2837 | 134.7 | 3724 | 12.6 |

Table A.13: Vibrational frequencies of the *anti*- and *syn*-formic acid-chloride complexes calculated at MP2/aug-cc-pV(Q+d)Z.

| *anti*-FA acidic H appended | | *syn*-FA acidic H appended | | *syn*-FA formyl H appended | |
|---|---|---|---|---|---|
| Frequency ($cm^{-1}$) | Intensity (km/mol) | Frequency ($cm^{-1}$) | Intensity (km/mol) | Frequency ($cm^{-1}$) | Intensity (km/mol) |
| 111 | 9.1 | 106 | 1.6 | 87 | 3.3 |
| 167 | 31.8 | 179 | 5.2 | 135 | 31.0 |
| 257 | 64.2 | 263 | 106.2 | 171 | 0.7 |
| 503 | 12.2 | 694 | 38.4 | 627 | 65.0 |
| 1005 | 27.5 | 1013 | 21.7 | 683 | 116.3 |
| 1080 | 0.4 | 1104 | 16.7 | 1087 | 331.0 |
| 1245 | 131.9 | 1253 | 289.5 | 1153 | 2.1 |
| 1414 | 15.0 | 1361 | 14.2 | 1277 | 10.6 |
| 1456 | 142.4 | 1421 | 39.5 | 1442 | 16.9 |
| 1761 | 670.8 | 1744 | 628.8 | 1742 | 364.4 |
| 2722 | 2619 | 2487 | 3408.4 | 2955 | 369.8 |
| 3047 | 75.7 | 2992 | 100.1 | 3754 | 32.9 |

Table A.14: Vibrational frequencies of the *anti*- and *syn*-formic acid-bromide complexes calculated at MP2/aug-cc-pVQZ-PP.

| *anti*-FA acidic H appended | | *syn*-FA acidic H appended | | *syn*-FA formyl H appended | |
|---|---|---|---|---|---|
| Frequency ($cm^{-1}$) | Intensity (km/mol) | Frequency ($cm^{-1}$) | Intensity (km/mol) | Frequency ($cm^{-1}$) | Intensity (km/mol) |
| 100 | 4.3 | 94 | 4.9 | 79 | 2.6 |
| 167 | 28.0 | 160 | 30.3 | 107 | 9.1 |
| 215 | 26.7 | 190 | 24.9 | 168 | 0.2 |
| 700 | 7.1 | 679 | 4.4 | 627 | 65.0 |
| 965 | 20.2 | 915 | 25.1 | 682 | 114.4 |
| 1080 | <0.1 | 1059 | <0.1 | 1092 | 320.6 |
| 1234 | 137.7 | 1204 | 133.2 | 1149 | 1.4 |
| 1416 | 16.2 | 1397 | 12.3 | 1279 | 11.9 |
| 1438 | 129.0 | 1424 | 143.6 | 1438 | 16.7 |
| 1767 | 647.8 | 1745 | 575.3 | 1747 | 359.7 |
| 2868 | 2458.4 | 2976 | 2133.5 | 2973 | 320.5 |
| 3051 | 94.4 | 3071 | 135.7 | 3755 | 35.0 |

Table A.15: Vibrational frequencies of the *anti*- and *syn*-formic acid-iodide complexes calculated at MP2/aug-cc-pVQZ-PP.

| *anti*-FA acidic H appended | | *syn*-FA acidic H appended | | *syn*-FA formyl H appended | |
|---|---|---|---|---|---|
| Frequency ($cm^{-1}$) | Intensity (km/mol) | Frequency ($cm^{-1}$) | Intensity (km/mol) | Frequency ($cm^{-1}$) | Intensity (km/mol) |
| 87 | 3.0 | 75 | 0.3 | 68 | 2.5 |
| 162 | 27.0 | 160 | 6.2 | 86 | 3.0 |
| 181 | 14.1 | 178 | 25.1 | 139 | >0.1 |
| 694 | 2.7 | 670 | 55.7 | 627 | 63.3 |
| 890 | 15.8 | 908 | 24.4 | 681 | 113.3 |
| 1078 | 0.0 | 1076 | 2.1 | 1101 | 299.7 |
| 1216 | 135.4 | 1209 | 290.4 | 1126 | 1.0 |
| 1407 | 102.3 | 1340 | 15.5 | 1284 | 13.8 |
| 1416 | 37.3 | 1425 | 20.2 | 1428 | 15.3 |
| 1776 | 204.2 | 1765 | 462.1 | 1755 | 347.5 |
| 3051 | 204.2 | 2955 | 2758.6 | 3031 | 184.2 |
| 3086 | 1986.3 | 3031 | 95.0 | 3758 | 41.2 |

Table A.16: MP2/aug-cc-pVQZ geometry of the *anti*-formic acid-fluorine complexes.

| Atom | *anti*-FA carbonyl appended hydroxyl side | | | *anti*-FA carbonyl appended non-hydroxyl side | | |
|---|---|---|---|---|---|---|
| | X | Y | Z | X | Y | Z |
| C | -1.047138 | 0.424969 | 0.000000 | 0.000000 | 0.631070 | 0.000000 |
| O | -1.125207 | -0.920093 | 0.000000 | -0.492060 | 1.884809 | 0.000000 |
| H | -2.051868 | -1.183327 | 0.000000 | 0.239879 | 2.511186 | 0.000000 |
| O | 0.000000 | 1.005017 | 0.000000 | -0.711360 | -0.332574 | 0.000000 |
| H | -2.023741 | 0.925835 | 0.000000 | 1.096075 | 0.581418 | 0.000000 |
| F | 2.151122 | -0.330190 | 0.000000 | 0.921268 | -2.144100 | 0.000000 |

Table A.17: MP2/aug-cc-pV(Q+d)Z geometry of the *anti*-formic acid-chlorine complexes.

| Atom | *anti*-FA carbonyl appended hydroxyl side | | | *anti*-FA carbonyl appended non-hydroxyl side | | |
|---|---|---|---|---|---|---|
| | X | Y | Z | X | Y | Z |
| C | 1.192794 | 1.086499 | 0.000000 | 1.089276 | 0.392873 | 0.000000 |
| O | 1.785623 | -0.118772 | 0.000000 | 2.211421 | 1.128357 | 0.000000 |
| H | 2.742370 | -0.004007 | 0.000000 | 2.975745 | 0.541358 | 0.000000 |
| O | 0.000000 | 1.214271 | 0.000000 | 0.000000 | 0.900027 | 0.000000 |
| H | 1.891868 | 1.931874 | 0.000000 | 1.253448 | -0.691033 | 0.000000 |
| Cl | -1.533881 | -1.012403 | 0.000000 | -1.673895 | -1.084390 | 0.000000 |
| Atom | *anti*-FA acidic H appended | | | *anti*-FA out of plane | | |
| | X | Y | Z | X | Y | Z |
| C | -1.610861 | -0.290417 | 0.000024 | 1.753687 | 0.144237 | 0.152576 |
| O | -0.915617 | 0.863734 | 0.000005 | 0.690696 | 0.908745 | -0.191824 |
| H | 0.028229 | 0.659012 | 0.000048 | 0.839729 | 1.816131 | 0.096991 |
| O | -2.807336 | -0.322607 | -0.000027 | 1.796787 | -1.025407 | -0.085306 |
| H | -0.973087 | -1.184656 | 0.000090 | 2.549149 | 0.704795 | 0.659997 |
| Cl | 2.376097 | -0.121228 | -0.000006 | -1.988874 | -0.144297 | 0.032035 |

Table A.18: MP2/aug-cc-pVQZ-PP geometry of the *anti*-formic acid-bromine complexes.

| Atom | *anti*-FA carbonyl appended hydroxyl side | | | *anti*-FA carbonyl appended non-hydroxyl side | | |
|---|---|---|---|---|---|---|
| | X | Y | Z | X | Y | Z |
| C | -0.243422 | -2.188527 | 0.000000 | 1.201635 | 1.358400 | 0.000000 |
| O | 1.084243 | -1.991549 | 0.000000 | 1.931134 | 2.483579 | 0.000000 |
| H | 1.534663 | -2.843497 | 0.000000 | 2.867429 | 2.255187 | 0.000000 |
| O | -1.025519 | -1.278139 | 0.000000 | 0.000000 | 1.382899 | 0.000000 |
| H | -0.543925 | -3.243278 | 0.000000 | 1.787952 | 0.431911 | 0.000000 |
| Br | 0.000000 | 1.296441 | 0.000000 | -0.780408 | -1.193409 | 0.000000 |

Table A.19: MP2/aug-cc-pVQZ-PP geometry of the *anti*-formic acid-iodine complexes.

| Atom | *anti*-FA carbonyl appended hydroxyl side | | | *anti*-FA carbonyl appended non-hydroxyl side | | | *anti*-FA acidic H appended | | |
|---|---|---|---|---|---|---|---|---|---|
| | X | Y | Z | X | Y | Z | X | Y | Z |
| C | -0.247081 | -2.626935 | 0.000000 | 0.262859 | -2.260856 | 0.000000 | -0.367437 | -2.808257 | 0.000000 |
| O | 1.082523 | -2.444113 | 0.000000 | 0.253792 | -3.601416 | 0.000000 | 0.841243 | -2.215275 | 0.000000 |
| H | 1.525084 | -3.300233 | 0.000000 | 1.161469 | -3.925463 | 0.000000 | 0.713984 | -1.255365 | 0.000000 |
| O | -1.017917 | -1.706842 | 0.000000 | -0.753915 | -1.620046 | 0.000000 | -0.504626 | -3.997973 | 0.000000 |
| H | -0.559450 | -3.678118 | 0.000000 | 1.262368 | -1.809355 | 0.000000 | -1.202297 | -2.094326 | 0.000000 |
| Br | 0.000000 | 1.055615 | 0.000000 | 0.000000 | 1.152295 | 0.000000 | 0.000000 | 1.318966 | 0.000000 |

Table A.20: Energies of the *anti*-formic acid-fluorine complexes. (Note: zero-point energy calculated at MP2/aug-cc-pVQZ)

| *anti*-FA-fluorine Complexes | ZPE (kJ/mol) | corrected ZPE (kJ/mol) | MP2 | | | CCSD(T) | | | |
|---|---|---|---|---|---|---|---|---|---|
| | | | Q | 5 | CBS | D | T | Q | CBS |
| *anti*-FA carbonyl appended hydroxyl side | 89.37 | 1.02 | -289.174073 | -289.20354 | -289.230184 | -288.902205 | -289.142190 | -289.217158 | -289.259300 |
| *anti*-FA carbonyl appended hydroxyl side | 89.74 | 1.07 | -289.174668 | -289.204112 | -289.230738 | -288.903659 | -289.143490 | -289.218448 | -289.260576 |

Table A.21: Energies of the *anti*-formic acid-chlorine complexes. (Note: zero-point energy calculated at MP2/aug-cc-pV(Q+d)Z)

| *anti*-FA-chlorine Complexes | ZPE (kJ/mol) | corrected ZPE (kJ/mol) | MP2 | | | CCSD(T) | | | |
|---|---|---|---|---|---|---|---|---|---|
| | | | Q | 5 | CBS | D | T | Q | CBS |
| *anti*-FA carbonyl appended hydroxyl side | 89.72 | 1.32 | -649.204829 | -649.231516 | -649.256512 | -648.971879 | -649.193827 | -649.261929 | -649.300746 |
| *anti*-FA carbonyl appended hydroxyl side | 90.27 | 1.67 | -649.205874 | -649.23259 | -649.257621 | -648.973140 | -649.194950 | -649.263137 | -649.301987 |
| *anti*-FA acidic H appended | 89.50 | 1.10 | -649.203586 | -649.230145 | -649.255015 | -648.970588 | -649.192671 | -649.260291 | -649.298855 |
| *anti*-FA out of plane | 88.78 | 0.76 | -649.203060 | -649.229712 | -649.254667 | -648.969995 | -649.192010 | -649.259934 | -649.298672 |

Table A.22: Energies of the *anti*-formic acid-bromine complexes. (Note: zero-point energy calculated at MP2/aug-cc-pVTZ-PP)

| *anti*-FA-bromine Complexes | ZPE (kJ/mol) | corrected ZPE (kJ/mol) | MP2 Q | MP2 5 | MP2 CBS | CCSD(T) T |
|---|---|---|---|---|---|---|
| *anti*-FA carbonyl appended hydroxyl side | 89.46 | 1.31 | -605.307102 | -605.412162 | -605.519701 | -605.230517 |
| *anti*-FA carbonyl appended hydroxyl side | 89.90 | 1.57 | -605.308164 | -605.413177 | -605.520665 | -605.231540 |



Table A.23: Energies of the *anti*-formic acid-iodine complexes. (Note: zero-point energy calculated at MP2/aug-cc-pVTZ-PP)

| *anti*-FA-iodine Complexes | ZPE (kJ/mol) | corrected ZPE (kJ/mol) | MP2 Q | MP2 5 | MP2 CBS | CCSD(T) T |
|---|---|---|---|---|---|---|
| *anti*-FA carbonyl appended hydroxyl side | 89.33 | 1.18 | -484.463439 | -484.541421 | -484.620565 | -484.382819 |
| *anti*-FA carbonyl appended hydroxyl side | 89.72 | 1.42 | -484.464336 | -484.542306 | -484.621432 | -484.383653 |
| *anti*-FA acidic H appended | 89.24 | 1.23 | -484.462447 | -484.540286 | -484.619293 | -484.382397 |

Table A.24: Vibrational frequencies of the *anti*-formic acid-fluorine complexes calculated at MP2/aug-cc-pVQZ.

| *anti*-FA carbonyl appended hydroxyl side | | *anti*-FA carbonyl appended non-hydroxyl side | |
|---|---|---|---|
| Frequency ($cm^{-1}$) | Intensity (km/mol) | Frequency ($cm^{-1}$) | Intensity (km/mol) |
| 35 | 5.0 | 51 | 22.0 |
| 39 | 56.1 | 67 | 5.9 |
| 96 | 6.6 | 100 | 12.9 |
| 537 | 84.1 | 539 | 84.2 |
| 661 | 11.7 | 664 | 9.0 |
| 1040 | 0.1 | 1043 | 0.1 |
| 1128 | 42.8 | 1131 | 47.2 |
| 1279 | 313.9 | 1281 | 340.5 |
| 1423 | <0.1 | 1423.5 | 0.2 |
| 1831 | 289.3 | 1827 | 309.6 |
| 3048 | 59.8 | 3054 | 45.6 |
| 3824 | 88.3 | 3824 | 90.2 |

Table A.25: Vibrational frequencies of the *anti*-formic acid-chlorine complexes calculated at MP2/aug-cc-pV(Q+d)Z.

| *anti*-FA carbonyl appended hydroxyl side | | *anti*-FA carbonyl appended non-hydroxyl side | | *anti*-FA acidic H appended | | *anti*-FA out of plane | |
|---|---|---|---|---|---|---|---|
| Frequency ($cm^{-1}$) | Intensity (km/mol) | Frequency ($cm^{-1}$) | Intensity (km/mol) | Frequency ($cm^{-1}$) | Intensity (km/mol) | Frequency ($cm^{-1}$) | Intensity (km/mol) |
| 54 | 53.5 | 71 | 21.1 | 35 | 5.8 | 19 | 37.3 |
| 55 | 3.6 | 85 | 0.9 | 58 | 46.8 | 22 | 13.9 |
| 111 | 17.4 | 123 | 39.4 | 92 | 3.5 | 85 | 2.8 |
| 543 | 84.1 | 547 | 84.3 | 572 | 62.8 | 526 | 81.0 |
| 663 | 14.4 | 669 | 7.2 | 665 | 5.8 | 658 | 9.1 |
| 1041 | 0.1 | 1048 | 0.1 | 1043 | $<$0.1 | 1035 | 0.3 |
| 1137 | 29.4 | 1146 | 37.8 | 1134 | 77.3 | 1107 | 71.8 |
| 1279 | 303.9 | 1285 | 389.1 | 1298 | 252.9 | 1269 | 307.6 |
| 1421 | 0.5 | 1423 | 0.8 | 1423 | 0.7 | 1419 | 0.2 |
| 1819 | 317.9 | 1809 | 404.1 | 1832 | 324.8 | 1835 | 252.3 |
| 3056 | 61.2 | 3066 | 29.2 | 3039 | 58.8 | 3050 | 55.9 |
| 3821 | 99.2 | 3819 | 105.0 | 3773 | 299.6 | 3817 | 88.4 |

Table A.26: Vibrational frequencies of the *anti*-formic acid-bromine complexes calculated at MP2/aug-cc-pVTZ-PP.

| *anti*-FA carbonyl appended hydroxyl side | | *anti*-FA carbonyl appended non-hydroxyl side | |
|---|---|---|---|
| Frequency ($cm^{-1}$) | Intensity (km/mol) | Frequency ($cm^{-1}$) | Intensity (km/mol) |
| 52 | 3.6 | 72 | 21.5 |
| 59 | 52.2 | 77 | 1.8 |
| 109 | 17.8 | 115 | 35.0 |
| 539 | 83.6 | 543 | 82.8 |
| 658 | 15.4 | 664 | 7.0 |
| 1039 | 0.2 | 1047 | 0.2 |
| 1135 | 27.2 | 1143 | 40.0 |
| 1276 | 295.9 | 1282 | 393.0 |
| 1416 | 0.6 | 1418 | 1.0 |
| 1812 | 312.7 | 1805 | 391.3 |
| 3056 | 61.6 | 3063 | 27.1 |
| 3804 | 98.1 | 3803 | 103.2 |

Table A.27: Vibrational frequencies of the *anti*-formic acid-iodine complexes calculated at MP2/aug-cc-pVTZ-PP.

| *anti*-FA carbonyl appended hydroxyl side | | *anti*-FA carbonyl appended non-hydroxyl side | | *anti*-FA acidic H appended | |
|---|---|---|---|---|---|
| Frequency ($cm^{-1}$) | Intensity (km/mol) | Frequency ($cm^{-1}$) | Intensity (km/mol) | Frequency ($cm^{-1}$) | Intensity (km/mol) |
| 48 | 3.8 | 67 | 20.7 | 35 | 4.3 |
| 52 | 50.2 | 69 | 2.2 | 76 | 39.5 |
| 98 | 17.3 | 100 | 32.9 | 93 | 4.1 |
| 539 | 83.0 | 543 | 82.3 | 596 | 47.5 |
| 658 | 16.6 | 663 | 6.5 | 663 | 4.6 |
| 1039 | 0.2 | 1047 | 0.1 | 1040 | 0.1 |
| 1134 | 26.0 | 1142 | 43.8 | 1134 | 93.3 |
| 1276 | 287.8 | 1282 | 405.3 | 1302 | 214.7 |
| 1417 | 0.5 | 1420 | 1.6 | 1417 | 1.3 |
| 1812 | 302.7 | 1807 | 376.4 | 1823 | 366.5 |
| 3057 | 64.1 | 3057 | 26.7 | 3034 | 57.2 |
| 3804 | 99.6 | 3803 | 104.5 | 3705 | 475.1 |

Table A.28: MP2/aug-cc-pVQZ geometry of the *syn*-formic acid-fluorine complexes.

| Atom | *syn*-FA double appended | | | *syn*-FA hydroxyl appended | | | *syn*-FA carbonyl appended | | |
|---|---|---|---|---|---|---|---|---|---|
| | X | Y | Z | X | Y | Z | X | Y | Z |
| C | -1.005858 | 0.413016 | 0.000000 | 0.865277 | -0.335354 | -0.000143 | 0.000000 | 0.659334 | 0.000000 |
| O | -1.046797 | -0.922820 | 0.000000 | -0.017691 | 0.679525 | -0.000130 | -0.508278 | 1.899352 | 0.000000 |
| H | -0.127430 | -1.231673 | 0.000000 | 0.498995 | 1.498764 | 0.000178 | -1.472350 | 1.805384 | 0.000000 |
| O | 0.000000 | 1.078869 | 0.000000 | 2.059831 | -0.206735 | 0.000172 | -0.652963 | -0.352415 | 0.000000 |
| H | -2.017568 | 0.822230 | 0.000000 | 0.331446 | -1.287453 | -0.000481 | 1.090402 | 0.699693 | 0.000000 |
| F | 1.839391 | -0.368561 | 0.000000 | -2.484357 | -0.220168 | 0.000091 | 1.074653 | -2.092952 | 0.000000 |

Table A.29: MP2/aug-cc-pV(Q+d)Z geometry of the *syn*-formic acid-chlorine complexes.

| Atom | *syn*-FA double appended | | | *syn*-FA hydroxyl appended | | |
|---|---|---|---|---|---|---|
| | X | Y | Z | X | Y | Z |
| C | 1.178463 | 0.933096 | 0.000000 | 1.451532 | -0.338424 | 0.000191 |
| O | 1.671918 | -0.295837 | 0.000000 | 0.594818 | 0.701741 | 0.000179 |
| H | 0.912994 | -0.909370 | 0.000000 | 1.131573 | 1.508438 | -0.000244 |
| O | 0.000000 | 1.225910 | 0.000000 | 2.648113 | -0.239193 | -0.000241 |
| H | 1.976093 | 1.677294 | 0.000000 | 0.891300 | -1.275395 | 0.000650 |
| Cl | -1.372660 | -0.812182 | 0.000000 | -2.157383 | -0.111935 | -0.000062 |
| Atom | *syn*-FA carbonyl appended | | | *syn*-FA acidic H appended | | |
| | X | Y | Z | X | Y | Z |
| C | 1.114771 | 0.405375 | 0.000000 | -1.873251 | 0.644468 | 0.000000 |
| O | 2.237683 | 1.128596 | 0.000000 | -0.710657 | 1.312881 | 0.000000 |
| H | 1.974004 | 2.060959 | 0.000000 | 0.000000 | 0.650951 | 0.000000 |
| O | 0.000000 | 0.869503 | 0.000000 | -1.984959 | -0.553358 | 0.000000 |
| H | 1.343903 | -0.660873 | 0.000000 | -2.706383 | 1.350651 | 0.000000 |
| Cl | -1.641647 | -1.165713 | 0.000000 | 2.088872 | -0.702623 | 0.000000 |

Table A.30: MP2/aug-cc-pVQZ-PP geometry of the *syn*-formic acid-bromine complexes.

| Atom | *syn*-FA double appended | | | *syn*-FA hydroxyl appended | | | *syn*-FA carbonyl appended | | |
|---|---|---|---|---|---|---|---|---|---|
| | X | Y | Z | X | Y | Z | X | Y | Z |
| C | -0.197999 | -2.052646 | 0.000000 | 2.096643 | -0.330472 | 0.000012 | 1.207858 | 1.386709 | 0.000000 |
| O | 1.108423 | -1.829295 | 0.000000 | 1.292823 | 0.752548 | 0.000010 | 1.952403 | 2.494608 | 0.000000 |
| H | 1.232943 | -0.859949 | 0.000000 | 1.868355 | 1.532161 | -0.000016 | 1.341453 | 3.246705 | 0.000000 |
| O | -1.062452 | -1.200712 | 0.000000 | 3.296297 | -0.290750 | -0.000015 | 0.000000 | 1.372055 | 0.000000 |
| H | -0.412724 | -3.122277 | 0.000000 | 1.487905 | -1.236838 | 0.000041 | 1.838733 | 0.496979 | 0.000000 |
| Br | 0.000000 | 1.158233 | 0.000000 | -1.504259 | -0.057339 | -0.000002 | -0.744187 | -1.228493 | 0.000000 |

Table A.31: MP2/aug-cc-pVQZ-PP geometry of the *syn*-formic acid-iodine complexes.

| Atom | *syn*-FA double appended | | | *syn*-FA hydroxyl appended | | |
|---|---|---|---|---|---|---|
| | X | Y | Z | X | Y | Z |
| C | -0.203054 | -2.495572 | 0.000000 | -0.410659 | -2.550082 | 0.000000 |
| O | 1.108121 | -2.282137 | 0.000000 | 0.702424 | -1.786991 | 0.000000 |
| H | 1.247693 | -1.315858 | 0.000000 | 1.459198 | -2.392520 | 0.000000 |
| O | -1.059320 | -1.638176 | 0.000000 | -0.415108 | -3.750180 | 0.000000 |
| H | -0.419778 | -3.565062 | 0.000000 | -1.293768 | -1.907953 | 0.000000 |
| I | 0.000000 | 0.966356 | 0.000000 | 0.000000 | 1.205629 | 0.000000 |
| Atom | *syn*-FA carbonyl appended | | | *syn*-FA acidic H appended | | |
| | X | Y | Z | X | Y | Z |
| C | -0.317701 | -2.286795 | 0.000000 | 0.01096 | -0.000001 | 0.00859 |
| O | -0.365218 | -3.620383 | 0.000000 | -0.02220 | 0.000002 | 1.34833 |
| H | 0.550748 | -3.936595 | 0.000000 | 0.900005 | 0.000008 | 1.66043 |
| O | 0.700098 | -1.636205 | 0.000000 | 1.00976 | 0.000005 | -0.66275 |
| H | -1.323587 | -1.864432 | 0.000000 | -1.00727 | -0.000008 | -0.38722 |
| I | 0.000000 | 1.161783 | 0.000000 | 3.33016 | 0.000002 | 2.80585 |

Table A.32: Energies of the *syn*-formic acid-fluorine complexes. (Note: zero-point energy calculated at MP2/aug-cc-pVQZ)

| *syn*-FA-fluorine Complexes | ZPE | corrected ZPE | MP2 | | | CCSD(T) | | | |
|---|---|---|---|---|---|---|---|---|---|
| | (kJ/mol) | (kJ/mol) | Q | 5 | CBS | D | T | Q | CBS |
| *syn*-FA double appended | 91.40 | 1.92 | -289.18235 | -289.211757 | -289.238373 | -288.913386 | -289.153172 | -289.228118 | -289.270242 |
| *syn*-FAhydroxyl appended | 89.79 | 0.75 | -289.180235 | -289.209706 | -289.236350 | -288.907779 | -289.147838 | Not converged | Not available |
| *syn*-FA carbonyl appended | 90.48 | 1.22 | -289.181285 | -289.210754 | -289.237407 | -288.9100871 | -289.149944 | -289.224916 | -289.267072 |



Table A.33: Energies of the *syn*-formic acid-chlorine complexes. (Note: zero-point energy calculated at MP2/aug-cc-pV(Q+d)Z)

| *syn*-FA-chlorine Complexes | ZPE | corrected ZPE | MP2 | | | CCSD(T) | | | |
|---|---|---|---|---|---|---|---|---|---|
| | (kJ/mol) | (kJ/mol) | Q | 5 | CBS | D | T | Q | CBS |
| *syn*-FA double appended | 91.96 | 2.82 | -649.214885 | -649.241672 | -649.266784 | -648.982235 | -649.204665 | -649.273049 | -649.312010 |
| *syn*-FA hydroxyl appended | 89.65 | 0.79 | -649.209814 | -649.236479 | -649.261447 | -648.976741 | -649.198688 | Not converged | Not available |
| *syn*-FA carbonyl appended | 90.90 | 154 | -649.212273 | -649.239007 | -649.2640532 | -648.979494 | -649.201324 | -649.269506 | -649.308374 |
| *syn*-FA acidic H appended | 90.28 | 1.22 | -649.209637 | -649.236221 | -649.261118 | -648.976572 | -649.198688 | -649.266316 | -649.304901 |

Table A.34: Energies of the *syn*-formic acid-bromine complexes. (Note: zero-point energy calculated at MP2/aug-cc-pVTZ-PP)

| *syn*-FA-bromine Complexes | ZPE (kJ/mol) | corrected ZPE (kJ/mol) | MP2 Q | MP2 5 | MP2 CBS | CCSD(T) T |
|---|---|---|---|---|---|---|
| *syn*-FA double appended | 91.38 | 2.48 | -605.317728 | -605.422698 | -605.530152 | -605.241255 |
| *syn*-FA hydroxyl appended | 89.36 | 0.81 | -605.311831 | -605.416851 | -605.524344 | -605.235167 |
| *syn*-FA carbonyl appended | 90.57 | 1.45 | -605.314508 | -605.419558 | -605.527084 | -605.237863 |



Table A.35: Energies of the *syn*-formic acid-iodine complexes. (Note: zero-point energy calculated at MP2/aug-cc-pVTZ-PP)

| *syn*-FA-iodine Complexes | ZPE (kJ/mol) | corrected ZPE (kJ/mol) | MP2 Q | MP2 5 | MP2 CBS | CCSD(T) T |
|---|---|---|---|---|---|---|
| *syn*-FA double appended | 91.29 | 2.32 | -484.473525 | -484.551547 | -484.630738 | -484.392557 |
| *syn*-FA hydroxyl appended | 89.40 | 0.87 | -484.467890 | -484.545854 | -484.624981 | -484.387458 |
| *syn*-FA carbonyl appended | 90.57 | 1.45 | -484.470623 | -484.548631 | -484.627799 | -484.389931 |
| *syn*-FA acidic H appended | 90.10 | 1.42 | -484.468021 | -484.545831 | -484.624810 | -484.387979 |

Table A.36: Vibrational frequencies of the *syn*-formic acid-fluorine complexes calculated at MP2/aug-cc-pVQZ.

| *syn*-FA double appended | | *syn*-FA hydroxyl appended | | *syn*-FA carbonyl appended | |
|---|---|---|---|---|---|
| Frequency ($cm^{-1}$) | Intensity (km/mol) | Frequency ($cm^{-1}$) | Intensity (km/mol) | Frequency ($cm^{-1}$) | Intensity (km/mol) |
| 89 | 2.5 | 14 | 1.2 | 46 | 0.1 |
| 99 | 0.9 | 31 | 1.0 | 60 | 0.8 |
| 133 | 9.8 | 81 | 0.3 | 98 | 3.9 |
| 646 | 40.7 | 628 | 40.0 | 633 | 49.1 |
| 712 | 124.0 | 674 | 134.4 | 684 | 134.8 |
| 1065 | 3.6 | 1061 | 3.4 | 1065 | 3.6 |
| 1155 | 246.3 | 1130 | 268.0 | 1140 | 271.6 |
| 1322 | 12.8 | 1298 | 15.6 | 1311 | 20.7 |
| 1414 | 0.5 | 1411 | 1.7 | 1410 | 2.0 |
| 1779 | 357.5 | 1800 | 339.0 | 1789 | 374.7 |
| 3132 | 32.2 | 3131 | 27.4 | 3136 | 23.0 |
| 3735 | 106.6 | 3755 | 86.1 | 3754 | 88.6 |

Table A.37: Vibrational frequencies of the *syn*-formic acid-chlorine complexes calculated at MP2/aug-cc-pV(Q+d)Z.

| *syn*-FA double appended | | *syn*-FA hydroxyl appended | | *syn*-FA carbonyl appended | | *syn*-FA acidic H appended | |
|---|---|---|---|---|---|---|---|
| Frequency ($cm^{-1}$) | Intensity (km/mol) | Frequency ($cm^{-1}$) | Intensity (km/mol) | Frequency ($cm^{-1}$) | Intensity (km/mol) | Frequency ($cm^{-1}$) | Intensity (km/mol) |
| 118 | 9.3 | 12 | 1.3 | 62 | 0.2 | 36 | 1.0 |
| 155 | 2.2 | 39 | 1.3 | 78 | 0.2 | 77 | 1.1 |
| 199 | 35.7 | 81 | 1.3 | 118 | 15.5 | 91 | 3.8 |
| 665 | 38.8 | 626 | 36.9 | 638 | 60.1 | 635 | 42.2 |
| 752 | 93.3 | 666 | 130.9 | 688 | 133.0 | 703 | 103.0 |
| 1066 | 3.5 | 1060 | 3.2 | 1069 | 3.7 | 1064 | 3.2 |
| 1187 | 207.8 | 1124 | 267.3 | 1150 | 284.2 | 1143 | 259.8 |
| 1333 | 4.8 | 1291 | 15.9 | 1319 | 25.7 | 1314 | 18.1 |
| 1413 | 1.4 | 1410 | 2.2 | 1408 | 3.4 | 1414 | 3.8 |
| 1738 | 442.6 | 1801 | 355.5 | 1772 | 483.4 | 1794 | 309.8 |
| 3137 | 29.9 | 3130 | 24.8 | 3144 | 14.1 | 3121 | 42.7 |
| 3611 | 133.2 | 3749 | 91.5 | 3750 | 104.0 | 3701 | 304.6 |

Table A.38: Vibrational frequencies of the *syn*-formic acid-bromine complexes calculated at MP2/aug-cc-pVTZ-PP.

| *syn*-FA double appended | | *syn*-FA hydroxyl appended | | *syn*-FA carbonyl appended | |
|---|---|---|---|---|---|
| Frequency ($cm^{-1}$) | Intensity (km/mol) | Frequency ($cm^{-1}$) | Intensity (km/mol) | Frequency ($cm^{-1}$) | Intensity (km/mol) |
| 102 | 3.4 | 17 | 1.1 | 62 | 0.2 |
| 144 | 2.6 | 41 | 1.2 | 70 | 0.1 |
| 169 | 26.5 | 77 | 1.6 | 110 | 12.6 |
| 660 | 32.7 | 623 | 35.5 | 635 | 59.8 |
| 741 | 83.9 | 659 | 128.3 | 684 | 130.5 |
| 1065 | 3.4 | 1057 | 3.2 | 1068 | 3.8 |
| 1178 | 202.3 | 1119 | 261.8 | 1148 | 289.0 |
| 1331 | 8.9 | 1285 | 13.7 | 1316 | 25.9 |
| 1413 | 1.4 | 1405 | 3.0 | 1405 | 3.7 |
| 1746 | 382.9 | 1797 | 360.1 | 1769 | 476.6 |
| 3131 | 35.6 | 3126 | 24.3 | 3139 | 13.0 |
| 3597 | 193.4 | 3733 | 90.23 | 3735 | 101.9 |

Table A.39: Vibrational frequencies of the *syn*-formic acid-iodine complexes calculated at MP2/aug-cc-pVTZ-PP

| *syn*-FA double appended | | *syn*-FA hydroxyl appended | | *syn*-FA carbonyl appended | | *syn*-FA acidic H appended | |
|---|---|---|---|---|---|---|---|
| Frequency ($cm^{-1}$) | Intensity (km/mol) | Frequency ($cm^{-1}$) | Intensity (km/mol) | Frequency ($cm^{-1}$) | Intensity (km/mol) | Frequency ($cm^{-1}$) | Intensity (km/mol) |
| 88 | 2.3 | 28 | 1.1 | 58 | 0.3 | 37 | 1.1 |
| 123 | 2.6 | 46 | 1.2 | 64 | 0.2 | 97 | 4.7 |
| 140 | 23.1 | 72 | 1.8 | 97 | 11.2 | 105 | 2.6 |
| 655 | 29.4 | 622 | 34.2 | 634 | 60.2 | 635 | 43.8 |
| 726 | 74.9 | 660 | 125.1 | 684 | 128.2 | 718 | 79.5 |
| 1065 | 2.9 | 1057 | 3.0 | 1068 | 3.6 | 1063 | 2.7 |
| 1170 | 194.0 | 1117 | 254.9 | 1148 | 300.3 | 1145 | 257.9 |
| 1326 | 21.1 | 1285 | 11.6 | 1316 | 27.8 | 1314 | 19.3 |
| 1414 | 1.4 | 1406 | 4.4 | 1406 | 4.7 | 1412 | 6.1 |
| 1755 | 339.7 | 1797 | 369.0 | 1771 | 467.7 | 1787 | 289.7 |
| 3128 | 42.9 | 3124 | 25.7 | 3135 | 12.9 | 3114 | 52.2 |
| 3602 | 260.7 | 3732 | 90.2 | 3735 | 102.6 | 3637 | 487.2 |

Table A.40: MP2/aug-cc-pVQZ geometry of the formate anion and radical.

| Atom | Formate anion | | | Formate radical | | |
|---|---|---|---|---|---|---|
| | X | Y | Z | X | Y | Z |
| C | 0.000000 | 0.319043 | 0.000000 | 0.000000 | 0.000000 | 0.187009 |
| O | 1.138080 | -0.209934 | 0.000000 | 0.000000 | 1.170677 | -0.155351 |
| O | -1.138080 | -0.209934 | 0.000000 | 0.000000 | -1.170677 | -0.155351 |
| H | 0.000000 | 1.444689 | 0.000000 | 0.000000 | 0.000000 | 1.363557 |



Table A.41: Energetics of the formate anion and radical. (Note: zero-point energy calculated at MP2/aug-cc-pVQZ)

| Formate | ZPE | MP2 | | | CCSD(T) | | | |
|---|---|---|---|---|---|---|---|---|
| | (kJ/mol) | Q | 5 | CBS | D | T | Q | CBS |
| Anion | 52.99 | -188.984915 | -189.004639 | -189.022885 | -188.797452 | -188.957388 | -189.007268 | -189.035788 |
| Radical | 53.36 | -188.8500071 | -188.868907 | -188.886251 | -188.668696 | -188.825254 | -188.873689 | -188.901150 |

Table A.42: MP2/aug-cc-pVQZ vibrational frequencies of the formate anion and radical.

| Formate anion | | Formate radical | |
|---|---|---|---|
| Frequency ($cm^{-1}$) | Intensity (km/mol) | Frequency ($cm^{-1}$) | Intensity (km/mol) |
| 741 | 17.5 | 660 | 29.3 |
| 1048 | 0.0 | 815 | <0.1 |
| 1337 | 97.6 | 1190 | 3.3 |
| 1380 | 5.6 | 1480 | 107.7 |
| 1651 | 882.1 | 2164 | 29.4 |
| 2701 | 481.3 | 2596 | 6831.0 |



Table A.43: HF molecule summary, frequency and geometry optimised at MP2/aug-cc-pVQZ.

| Formate | ZPE | MP2 | | | CCSD(T) | | | |
|---|---|---|---|---|---|---|---|---|
| | (kJ/mol) | Q | 5 | CBS | D | T | Q | CBS |
| HF | 24.75 | -100.3697608 | -100.3805586 | -100.3901123597 | -100.2636092 | -100.3495709 | -100.3773829 | -100.3930266606 |
| Bond length | 0.9187 | Frequency | Intensity | | | | | |
| | | 4137 | 122.5 | | | | | |

# Appendix B

# Timing Diagram

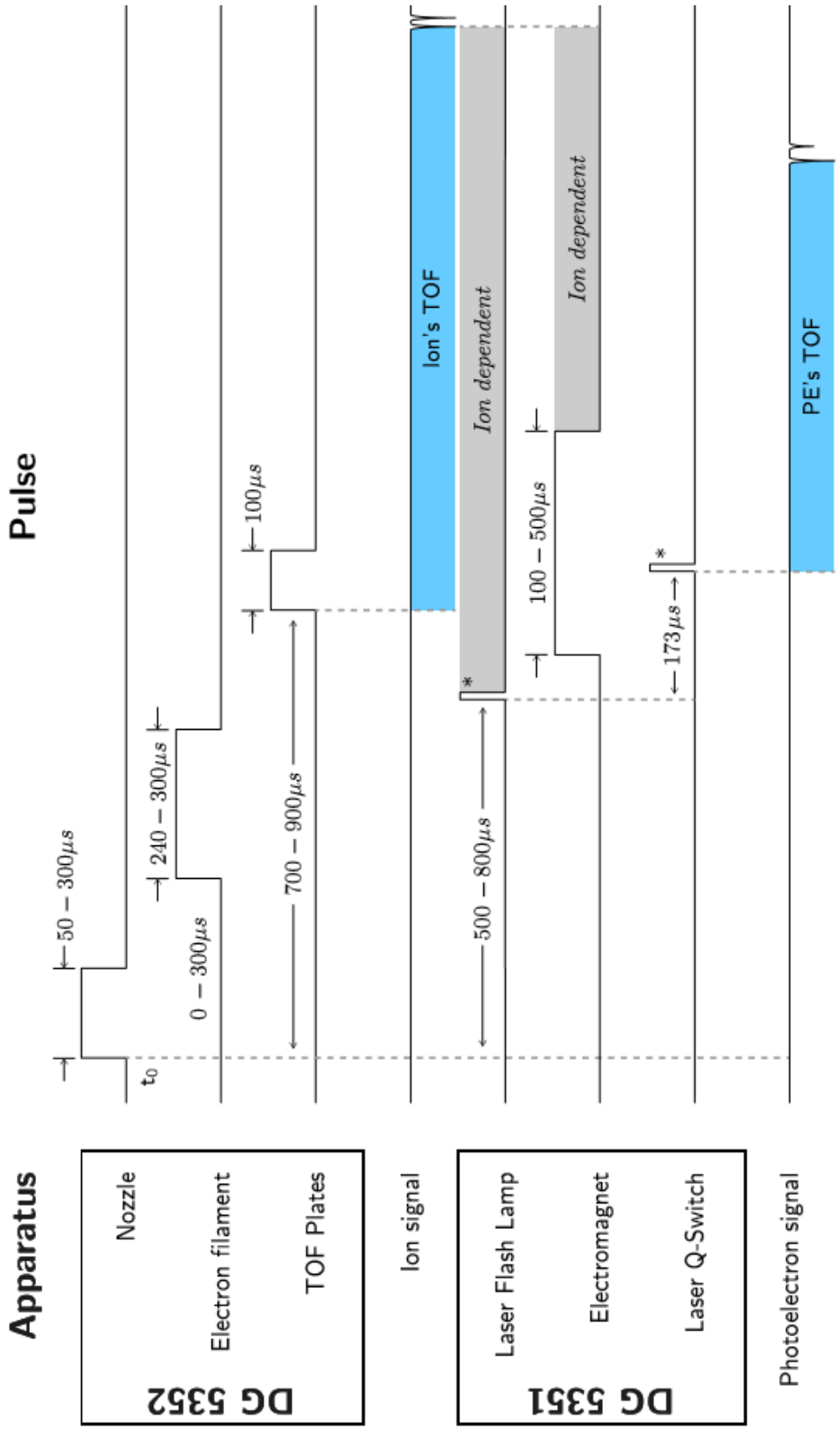


Figure B.1: Graphical representation of the experimental timing.[41]

# Appendix C

# Formic Acid Multipole Expansion Data

The *anti*-formic acid dipole, quadrupole and octupole tensors can be seen as well as the polariziabiliy:

$$\mu_i = \begin{bmatrix} -3.1916 \\ 3.0273 \\ 0 \end{bmatrix} \tag{C.1}$$

$$\Theta_{ij} = \begin{bmatrix} -17.2434 & -1.5905 & 0 \\ -1.5905 & -16.1628 & 0 \\ 0 & 0 & -17.0127 \end{bmatrix} \tag{C.2}$$

$$\Omega_{ijk} = \begin{bmatrix} \begin{bmatrix} -14.6397 & 3.2632 & 0 \\ 3.2632 & -0.8028 & 0 \\ 0 & 0 & -0.2591 \end{bmatrix} \\ \begin{bmatrix} 3.2632 & -0.8028 & 0 \\ -0.8028 & 1.9391 & 0 \\ 0 & 0 & -0.0333 \end{bmatrix} \\ \begin{bmatrix} 0 & 0 & -02591 \\ 0 & 0 & -0.0333 \\ -0.2591 & -0.0333 & 0 \end{bmatrix} \end{bmatrix} \tag{C.3}$$

$$\alpha_{ij} \begin{bmatrix} 4.4614 & -0.2466 & 0 \\ -0.2466 & 3.3305 & 0 \\ 0 & 0 & 2.4497 \end{bmatrix} \tag{C.4}$$

The *syn*-formic acid dipole, quadrupole and octupole tensors can be seen as well as the polariziabiliy:

$$\mu_i = \begin{bmatrix} -1.7283 \\ -0.0816 \\ 0 \end{bmatrix} \tag{C.5}$$

$$\Theta_{ij} = \begin{bmatrix} -22.6801 & -0.2581 & 0 \\ -0.2581 & -12.4652 & 0 \\ 0 & 0 & -16.9989 \end{bmatrix} \tag{C.6}$$

$$\Omega_{ijk} = \begin{bmatrix} \begin{bmatrix} -1.8126 & -0.2581 & 0 \\ -0.7200 & 0 & 0 \\ 0 & 0 & -0.0844 \end{bmatrix} \\ \begin{bmatrix} -0.7200 & -3.3404 & 0 \\ -3.3404 & 4.6019 & 0 \\ 0 & 0 & -0.3027 \end{bmatrix} \\ \begin{bmatrix} 0 & 0 & -0.0844 \\ 0 & 0 & -0.3027 \\ -0.0844 & -0.3027 & 0 \end{bmatrix} \end{bmatrix} \tag{C.7}$$

$$\alpha_{ij} \begin{bmatrix} 4.103 & -0.1080 & 0 \\ -0.1080 & 3.5040 & 0 \\ 0 & 0 & 2.4090 \end{bmatrix} \tag{C.8}$$